AN ABSTRACT OF THE THESIS OF

Xuerong (Sherry) Zhang for the degree of Doctor of Philosophy in Chemistry presented in May 6, 1999. Title: Synthesis and Structural Characterization of Graphite Intercalation Compounds (GICs) with Fluoroanions.

Redacted for Privacy

Abstract approved: _____

Michael M. Lerner

The graphite intercalation compounds $C_xC_8F_{17}SO_3 \cdot yF$ ($x \cong 18$, $y \cong 4$) are prepared in 48% aqueous hydrofluoric acid, using the oxidant $K_2MnF_6$. The product compositions are evaluated by mass uptake, TGA, and elemental analysis. The stable product is obtained after 50 h at room temperature or 1 h at 50 °C. Bragg (*00l*) reflections and peakwidth analyses indicate that the product is comprised of a random solid solution of stage 2 and 3. The addition of up to 83 vol. % conc. $HNO_3$ or 17 % fuming $H_2SO_4$ produces a stage 2 intercalation compound within hours.

Graphite intercalation compounds (GICs) with other oxidatively stable fluoroanions such as bis(trifluoromethanesulfonyl) imide $N(CF_3SO_2)_2^-$ bis(pentafluoroethanesulfonyl) imide $N(CF_3CF_2SO_2)_2^-$, trifluoromethanesulfonyl-*n*-nona-fluorobutanesulfonyl imide $N(CF_3SO_2)(CF_3(CF_2)_3SO_2)^-$, and tris(trifluoromethane-sulfonyl) methide $C(CF_3SO_2)_3^-$, are prepared in 48% aqu. HF. The intercalation of $N(CF_3SO_2)_2^-$ into graphite is very rapid a stage 2 $C_xN(CF_3SO_2)_2$ ($x = 37$) is obtained

within 15 minutes under ambient conditions. The products are evaluated by powder X-ray diffraction (PXRD), thermal gravimetric analysis (TGA), differential scanning calorimetry (DSC), and elemental analyses. One-dimensional structural refinement provides the $N(CF_3SO_2)_2^-$ anion orientation inside the graphite gallery. Larger anions containing $-SO_2C_nF_{2n+1}$ substituents, however, have dramatically slower intercalation rate and the products obtained contain unreacted graphite.

The moisture stabilities of GICs containing the anions $HF_2^-$, $NO_3^-$, $HSO_4^-$, $C_8F_{17}SO_3^-$, $N(CF_3SO_2)_2^-$, or $N(CF_2CF_3SO_2)_2^-$ are evaluated under ambient conditions at 20 °C, at 50 °C and 100 % relative humidity, and in liquid water. The GICs from large perfluoroanions are more stable than GICs with bifluoride, nitrate, or sulfate, with a slower rate of decomposition by approximately three orders of magnitude. A passive surface can be generated by reaction of larger perfluoroanions with $C_xHF_2 \cdot \delta HF$ and much improved stabilities achieved.

The one-dimensional structural refinements of $C_xC_8F_{17}SO_3$ prepared in 48% aqu. HF and mixed acids are reported. The $C_8F_{17}SO_3^-$ anion geometry is provided by ab initio calculations and a helical structure is obtained with the F-C-C-F twist angle of approximately 20°. The twist angle decreases to 16° when the anions are intercalated into graphite. One-dimensional staging disorder is analyzed for $C_xC_8F_{17}SO_3$ through Bragg (*00l*) peak positions and magnitude of peakwidth oscillation.

Semi-empirical and ab initio calculations are performed on $N(CF_3SO_2)_2^-$, $N(CF_3CF_2SO_2)_2^-$, $N(CF_3SO_2)(CF_3(CF_2)_3SO_2)^-$ and $C(CF_3SO_2)_3^-$, and the rotational barriers are determined to be approx. 8 kJ/mol or less for the three $N(RSO_2)_2^-$ anions. The minimum and maximum energy conformations are also reported. The possible anion

conformations and orientations inside graphite galleries are identified and the large differences in intercalation rates for these anions are discussed in terms of diffusion, charge density, and anion rearrangement.

# Synthesis and Structural Characterization of Graphite Intercalation Compounds (GICs) with Fluoroanions

by

Xuerong (Sherry) Zhang

A Thesis Submitted
to
Oregon State University

In Partial Fulfillment of
the requirements for the
degree of

Doctor of Philosophy

Completed May 6, 1999
Commencement June 1999

Doctor of Philosophy thesis of Xuerong (Sherry) Zhang presented on May 6, 1999.

Approved:

Redacted for Privacy

Major Professor, representing Chemistry

Redacted for Privacy

Chair of Department of Chemistry

Redacted for Privacy

Dean of Graduate School

I understand that my thesis will become part of the permanent collection of Oregon State University libraries. My signature below authorizes release of my thesis to any reader upon request.

Redacted for Privacy

Xuerong (Sherry) Zhang

## ACKNOWLEDGEMENT

First and foremost I wish to thank my major professor, mentor, friend and thesis advisor, Dr. Michael M. Lerner for his great patience, broad knowledge, enthusiasm for science, and unlimited supply of keen and constructive ideas. He provided by example the perfect role model. I owe all my success to him. I must also thank Dr. Arthur Sleight who introduced me to the DIFFaX software and provided me with the computing power for my structural refinement calculations. Dr. Douglas Keszler was a constant source of knowledge, whose suggestions have helped me a great deal on structural refinement. I also wish to thank my committee members: Dr. Carrol Dekock, Dr. Wei Kong and Dr. John Wager for their time and support. I would like to thank all past and former members of the Lerner groups, Dr. Victor Koch, Dr. Christopher Oriakhi, Dr. Rick Nafshun, Nipaka Sukpirom, Ravi Krishnamurthy, Henry Li and Wei Yan for their friendship. I would also like to thank Juzhou Tao for his helpful discussions and Engelene Chrysostom for her true friendship.

Finally, a special thanks goes to my boyfriend Dr. James K. Pugh who has taught me a great deal of computational chemistry and gave me constant encouragement. At last, I could not have come to where I am without the financial and spiritual support from my loving parents, Qiongguang Zhang and Yingtong Deng, and my dear brother Michael Zhang. They are all my best friends.

## TABLE OF CONTENTS

## TABLE OF CONTENTS (continued)

**Page**

TABLE OF CONTENTS (continued)

**Page**

## TABLE OF CONTENTS (continued)

## LIST OF FIGURES

## LIST OF FIGURES (Continued)

**Figure** **pages**

## LIST OF FIGURES (Continued)

## LIST OF FIGURES (Continued)

## LIST OF FIGURES (Continued)

## LIST OF FIGURES (Continued)

**Figure** **pages**

## LIST OF TABLES

## LIST OF TABLES (continued)

# Synthesis and Structural Characterization of Graphite Intercalation Compounds (GICs) with Fluoroanions

## Chapter 1

## Introduction

### 1.1 General Introduction

The term " intercalation" indicates the insertion of guest species into a layered host structure with maintenance of the host's structural features. Two-dimensional hosts exhibit strong intralayer bonding but weaker interlayer forces of attraction. Since a large number of layered host materials are available, the intercalation of neutral or ionic species is probably the most common type of insertion chemistry.

The hexagonal graphite structure consists of planes of carbon atoms (graphene layers) stacked parallel to each other in the repeat sequence $(AB)_n$. Within each graphene layer, carbon atoms are covalently bonded, with a bond distance of 1.42 Å. The $\sigma$ bonds within the sheets are formed from the overlap of $sp^2$ hybrid orbitals, and the additional p orbitals, one contributed by each carbon atom, overlap to form delocalized $\pi$ bonds that extend over the plane. The carbon sheets are separated from each other at a distance of 3.354 Å , which indicates that they interact by weak van der Waals forces.

Graphite is the only electroactive structure known to undergo a broad chemistry for both oxidative and reductive intercalation. [1] Therefore, the graphene sheets may be oxidized and intercalate anions (forming acceptor-type compounds) or be reduced and intercalate cations (forming donor-type compounds). Examples of the anions that can be

intercalated in acceptor-type graphite intercalation compounds (GICs) include oxoanions (ex. $SO_4^{2-}$, $ClO_4^-$, and $NO_3^-$), fluoride, bifluoride, hexafluorometallates, and some chlorometallate anions. One significant obstacle to the formation of GICs is the relatively high potential required to oxidize the carbon sheets (> 4.0V vs the $Li/Li^+$ redox couple). The high potential requires that intercalated anions be stable against oxidation and also significantly limits the selection of solvents and electrolytes. In the preparation of donor type GICs, a potential as low as 0.1V vs $Li/Li^+$ is needed to obtain stage 1 $C_xLi$ ($x \sim 6$). At such potentials, many organic electrolytes will be reduced, and successful reactions often require the formation of a passive surface on graphite.

The intercalation of graphite usually proceeds by way of ordered stages, in which, for stage n GICs, intercalated galleries are separated by n carbon layers, as indicated in Figure 1.1. The symbol $I_c$ is used to denote the unit cell repeat distance along the stacking direction, and $d_i$ is the gallery height, or distance along the c axis between carbon plane centers encasing an intercalant gallery. The relationship between $I_c$, $d_i$ and n is then:

$$I_c = d_i + 3.354\ \text{Å} * (n - 1) \qquad (1.1)$$

Daumas and Herold first proposed that staged GICs actually consist of microscopic domains. [2] Within a single domain the GIC is ordered into stages as described above, but in different domains the intercalant occupies galleries between different pairs of host layers, see Figure 1.2. This model provides a mechanism for stage transitions without the need for guest species to "tunnel" through the carbon layers. Transmission electron

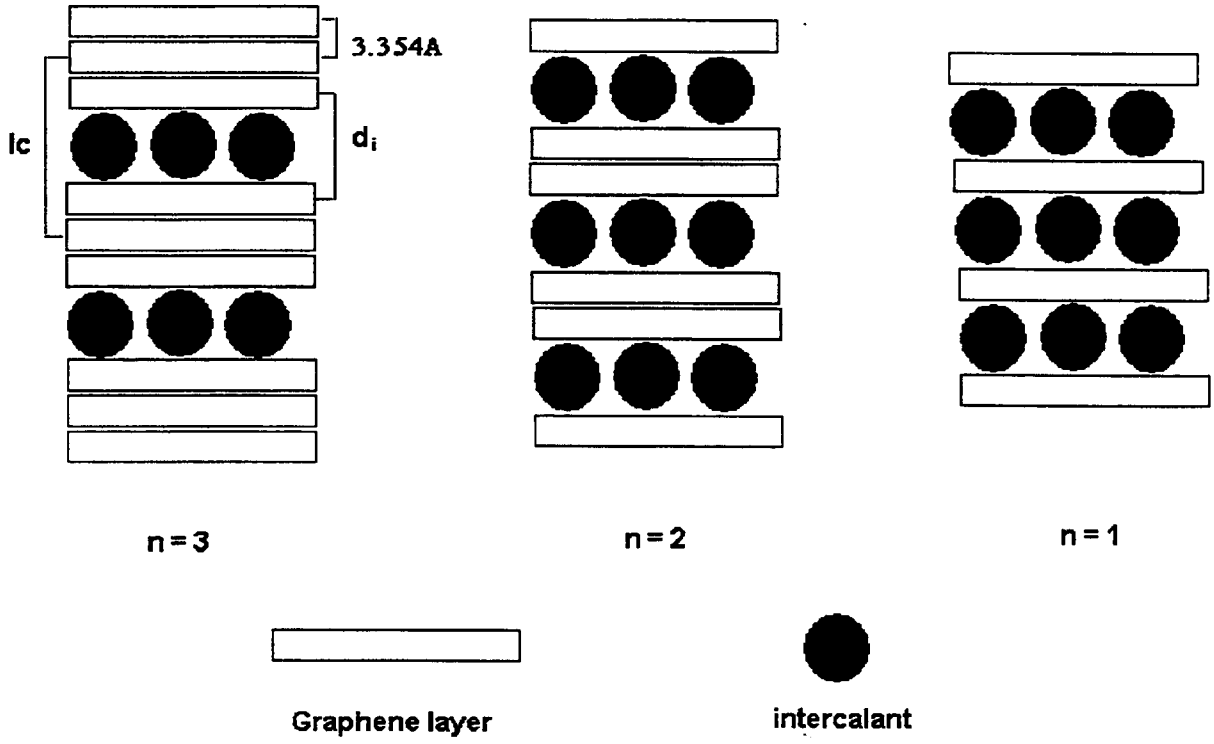


**Figure 1.1** Illustration of staging in graphite intercalation compounds.

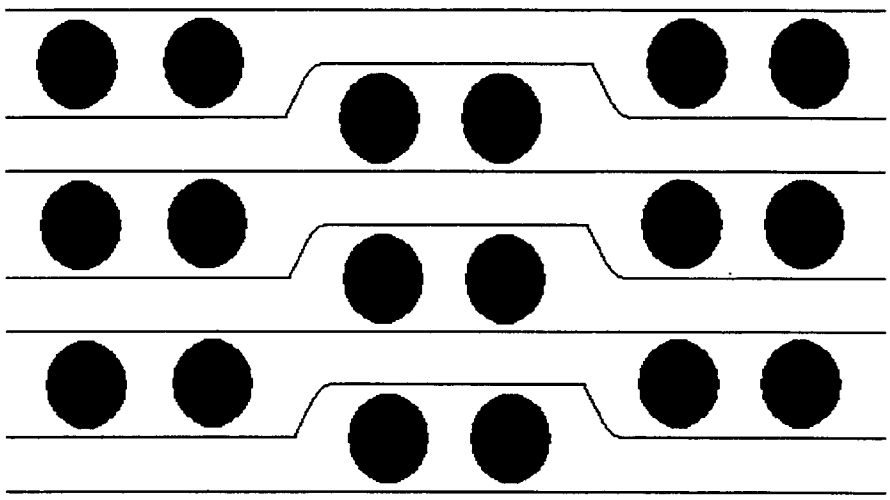

**Figure 1.2** Daumas-Herold domain model for a stage 2 GIC.

micrographs of $C_xFeCl_{3+y}$ have provided direct evidence for the Daumas-Herold staging model. [3]

GICs with fractional stages, n/m, contain an ordered arrangement of n carbon layers in the repeating unit and m galleries occupied by intercalant. Such ordering is not common, but stage 3/2 and 4/3 have been reported for the donor type compounds $C_xK$ [5] and $C_xK{\cdot}\delta THF$ [4]. Figure 1.3 shows the ordering for a fractional stage of 4/3.

Staging disorder is more commonly reported and has been described for many GICs including $C_xK$, $C_xFeCl_4{\cdot}\delta FeCl_3$ and $C_xCo_cM_{1-c}Cl_2$ GICs (M = Mn, Ni). [6-8] Hendricks-Teller theory for one-dimensional disordered crystal lattice diffraction has been used to provide detailed analyses of the disorder and to generate structural models for GICs. [9] From PXRD data, the disordering is characterized by (*00l*) peak shifts and additional peak broadening relative to that predicted for ordered stage GICs. More details on analysis of staging disorder of GICs containing graphite perfluorooctanesulfonate $C_xC_8F_{17}SO_3{\cdot}4F$ ($C_8F_{17}SO_3^-$ is denoted as PFOS from here on) will be presented in Chapters 2 and 5 of this thesis.

Graphite and its compounds are currently employed in many applications and have chemical and physical properties that suggest additional uses. Graphite is used as the anode material in lithium ion batteries due to its low weight and the high charge density for $C_xLi$, and the polycarbon fluorides, $(C_yF)_n$, y = 1 or 2, are used as cathode materials in primary lithium cells. GICs are also effective catalysts or reducing agents in many organic syntheses. [10] The electronic conductivity of $C_xSbF_6{\cdot}\delta SbF_5$ and $C_xAsF_6{\cdot}\delta AsF_5$ is as high as $10^8$ S/m (higher than that of metallic copper) and such compounds have therefore been proposed as conductive components in many

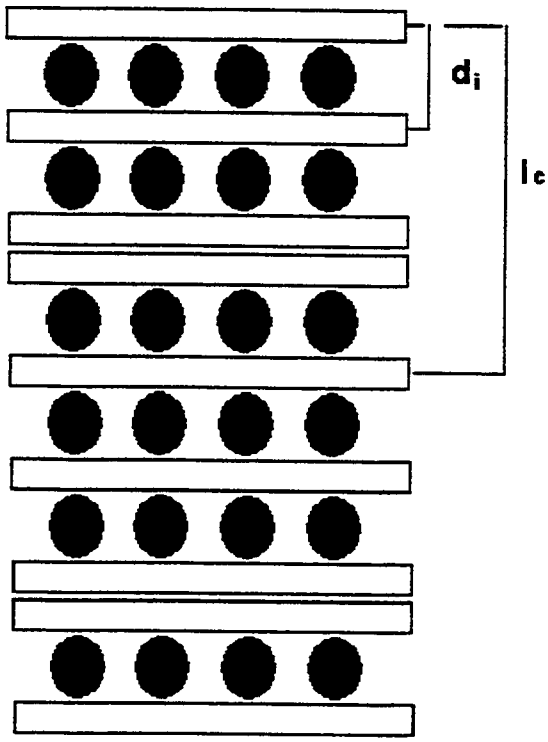


**Figure 1.3** Fractional stage 4/3 GIC.

applications. Thermally expanded graphite, discussed in more details in Section 1.5, is used commercially to form high temperature sealant and gaskets. Most of the GICs, however, are very unstable in air, which constitutes a significant obstacle to their practical use. In Chapter 4, we will discuss the methods to improve environmental stability of acceptor-type GICs .

This thesis work is centered around the development of simple chemical routes to new acceptor-type GICs. Chapter 2 reports a bench-top chemical route to prepare a pillared GIC containing $C_xPFOS$ anions in 48% aqueous HF (aqu. HF will be used to denote this solution through out this chapter) or a mixed solution of aqu. HF and concentrated nitric or sulfuric acid. The new synthetic technique was subsequently tested with other perfluoroanions such as $N(CF_3SO_2)_2^-$, $N(CF_3CF_3SO_2)_2^-$ and $C(CF_3SO_2)_3^-$, and novel GICs were obtained. During characterization of these new materials, they were found to be unusually air-stable. Chapter 4 describes detailed studies on the air stability of these GICs and indicates methods to improve air stability of other GICs by surface protection with perfluoroanions. Chapter 5 contains a detailed structural refinement of the $C_xPFOS$ unit cell structure and analysis of one-dimensional stage disorder. Chapter 6 reports electronic structure calculations of selected perfluoroanions by Gaussian calculations.

In order to provide additional background, the rest of this chapter will focus on acceptor-type GICs, including both ionic (Sec.1.2) and covalent types (Sec.1.3). A review of recent developments in complex graphite and graphite oxide compounds is presented in Sec. 1.4. Sec. 1.5 discusses the syntheses and application of thermally

expanded graphite. Finally, the experimental details of one-dimensional structural refinement are described in Sec 1.6.

## 1.2 Ionic Acceptor-Type GICs

### 1.2.1 GICs containing Oxoanions

The oxidation of graphite in mineral acid solutions generally results in the intercalation of the conjugate anions along with neutral acid inside graphite gallery. Bartlett et al. concluded that, using suitable oxidants, all strong acids should be intercalated into graphite, except, perhaps, the very bulky ones. [1] Stage 1 GICs can be prepared using $KMnO_4$ or $K_2Cr_2O_7$ in many concentrated acids. Experimental data [11] for most stage 1 GICs with oxoanions show $I_c$ values close to 7.9 Å, which is consistent with close packing of a single layer of bisulfate or perchlorate tetrahedra in a gallery. Stoichiometries of $C_{24}HSO_4 \cdot 2.5H_2SO_4$ [12] and $C_{24}ClO_4 \cdot 2HClO_4$ [12] have been reported. The GICs compositions will be given as $C_xI \cdot \delta N$ (I is the ion intercalant, and N is a neutral cointercalant, and x is thus a measure of the charge on carbon) throughout this chapter. For GIC containing the planar nitrate, $I_c$=7.8 Å may indicate double layers of planar $NO_3^-$, as was proposed by Touzain [13] for a stoichiometry of $C_{25.8}NO_3 \cdot 5HNO_3$. In these GICs, the neutral molecules act as dielectric spacers for the anions, and form hydrogen bonds within the intercalant gallery.

The neutral co-intercalants can be removed by evacuation in most cases. Stage 1 $C_{16}F \cdot \delta 4.3HF$ loses HF under evacuation and forms a stage 2 GIC of composition $C_{16}HF_2$. [19] Neutral organic molecules intercalated can be removed by evacuation as well. For

example, $C_xPFOS \cdot \delta CH_3NO_2$ loses nitromethane from the intercalant galleries to form $C_xPFOS$ after 12 hours of evacuation at room temperature. Graphite nitrate with $d_i$ = 6.55 Å can be obtained from a GIC with $d_i$ = 7.8 Å compound by evacuation to remove $HNO_3$. The smaller gallery height is only consistent with a structural model where $NO_3^-$ anions lie parallel to graphene layers at the center of the gallery. The stoichiometry of this material is $C_{8n}NO_3^- \cdot \delta HNO_3$ ($x < 1$). [1] The gallery height for a stage 2 graphite sulfate is smaller (7.65 Å) when the chemical oxidation is carried out in aqu. HF. That is explained by the intercalation of HF as the neutral species in place of $H_2SO_4$, see Chapter 4. The exact content of neutral species cannot be determined by coulommetry and will vary with preparative conditions.

GICs containing oxoanions can be prepared using a chemical oxidant, or by electrochemical oxidation in concentrated acids. Chemical methods provide for rapid and large-scale synthesis, but electrochemistry allows the reaction to be monitored by the potential charge curve, and the degree of oxidation to be controlled more easily. An idealized potential-charge plot is shown in Figure 1.4. The potential plateaus occur with the presence of two phases, a higher stage being converted to lower stage at constant potential during electro-oxidation. By slow oxidation to point J in Figure 1.4, a homogeneous stage 1 GIC, $C_xAn \cdot \delta HAn$, is derived. [14] Further oxidation will generate a graphite oxide containing C-O covalent bonds. This structure type is discussed further in Section 1.3.

Kang et al. have synthesized stage 3 to 5 GICs from natural graphite (0.3 mm particle diameter) and formic acid by the electrochemical method, where formic acid served as both electrolyte and intercalant source. Since $HCO_2H$ can be oxidized at

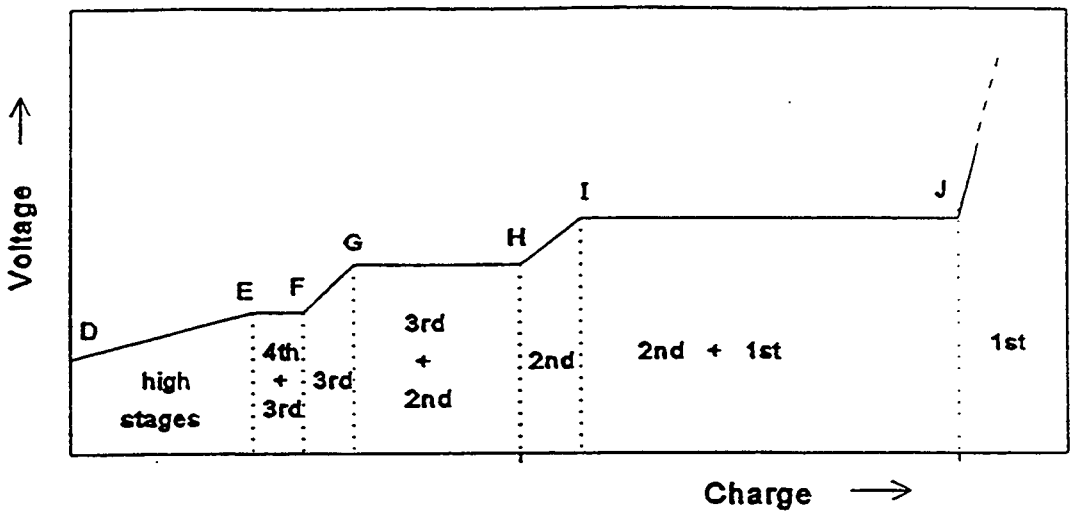


**Figure 1.4** Ideal potential-charge curve for the electrochemical intercalation of graphite.

potentials less than those required for graphite oxidation, a side-reaction during the intercalation process was the oxidation of formic acid to form $CO_2$. The GIC obtained was shown to be a good precursor to thermally expanded graphite. The self-exfoliation of graphite at room temperature was also observed in this study at higher potentials. Section 1.5 will further describe graphite exfoliation.

### 1.2.2 GICs containing Fluoroanions

It is well known that $F_2$ does not intercalate into graphite by direct reaction at room temperature. According to Hooley [15], fluoride ions formed at the opening to a gallery become fixed at edge sites and cannot move forward into the galleries. This model is consistent with the small size and high charge density of $F^-$. In the presence of liquid or gaseous HF at room temperature, graphite bifluoride is produced. Graphite bifluoride can also be prepared by electrochemical oxidation of graphite in anhydrous HF, with a gallery height of about 6 ~ 6.5 Å. [17-19] Further oxidation beyond the stage 1 graphite bifluoride results in the formation of semi-covalent planar-sheet graphite fluoride, which will be discussed in Section 1.3. A stage 2 graphite bifluoride salt ($d_i$ = 6.48 Å) can also be prepared from aqu. HF by chemical oxidation using $K_2MnF_6$ as an oxidant. [16] The bifluoride anion does not become fixed at the graphene layer surface, and has a high rate of insertion between graphite layers. Stage 2 $C_xHF_2$ is formed in minutes from SP-1 graphite (100 um particle diameter), and this GIC decomposs back to graphite within an hour in air (see chapter 4). In the presence of large fluoroanions such as PFOS, $HF_2^-$ is displaced and GICs with more expanded galleries are derived. The

development of a simple chemical synthesis of $C_xPFOS$ and $C_xN(CF_3SO_2)_2$, is discussed in Chapters 2 and 3.

There are a few synthetic methods to obtain GICs with fluoroanions. Strongly oxidizing metal fluorides such as $AsF_5$ and $SbF_5$ react spontaneously with graphite. For example:

$$2\,x\,C + (3+2\delta)\,AsF_5 \rightarrow 2\,C_xAsF_6{\cdot}\delta AsF_5 + AsF_3 \qquad (1.2)$$

Weaker oxidants, like $PF_5$, can be intercalated to make GICs in the presence of $F_2$.

$$2\,x\,C + 2\,(1+\delta)\,PF_5 + F_2 \rightarrow 2\,C_xPF_6{\cdot}\delta PF_5 \qquad (1.3)$$

GIC with fluoroanions can also be made by electrochemical oxidation of graphite in anhydrous HF or other oxidatively stable organic solvents. For example, $C_xPF6$ can be made in nitromethane ($CH_3NO_2$) containing $LiPF_6$ by the electrochemical method. [20] All these GICs with tetra- or hexa-fluorometallate anions have a similar gallery height of ~ 8Å.

### 1.2.3 GICs containing Chloroanions

Many of the GICs containing chloroanions derive from the reaction of graphite with a metal chlorides such as $AlCl_3$, $SbCl_5$ or $FeCl_3$ by reaction of metal chloride in a $Cl_2$ atmosphere, such as:

$$x\,C + \tfrac{1}{2}\,Cl_2 + (1+\delta)\,AlCl_3 \rightarrow C_xAlCl_4\cdot\delta AlCl_3 \qquad (1.4)$$

The gallery heights for these GICs are approximate 9.5Å, indicating that galleries contain a single layer of chloroanions. It is clear that from stoichiometric and other data such as Mossbauer and electron excitation studies that the neutral molecules as well as chloroanions are intercalated. [21-23] The graphite metal chloride compounds can be quite stable in air, though very contradictory results on the environmental stabilities have been found by different research groups. [24] This will be discussed in more detail in the introduction to Chapter 4.

There are some other halogen compounds, such as IBr, ICl, $Br_2$, which can react to form GICs. In some cases, these have been reported as very stable in air or even under severe conditions such as boiling water. [25] Both these graphite salts and the graphite chlorometallates can be highly conductive, with electronic conductivities reaching $10^6$ to $10^7$ S/m. [24] The environmental stability in addition to the high conductivity may provide a definite advantage to the development of practical uses such as conductive additives and /or antistatic coatings.

## 1.3 Covalent-Type GIC Structures

### 1.3.1 Polycarbon Fluorides and Planar-sheet Graphite Fluorides

There are two classes of solids containing carbon sheets and intercalated fluoride, one is the polycarbon fluorides, $(C_yF)_n$, and the other is planar sheet graphite fluoride,

$C_xF$ ($x \geq 1.3$). The polycarbon fluorides are white or gray insulators with the fluorides covalently bonded to the puckered carbon sheets, and hence the carbon atoms are $sp^3$ hybridized. These can be obtained by reacting graphite with fluorine gas at 400 –600°C. [26] The carbon - fluorine interaction in the planar-sheet graphite fluorides has been described as semi-covalent and the compounds are black or gray semiconductors. [27] Stage 1 GICs of these materials, $C_xF{\cdot}\delta HF$ ($2 < x < 6$) can be prepared by chemical or electrooxidation of a stage 1 graphite bifluoride salt, $C_xHF_2{\cdot}nHF$, $x \approx 12$. [17-19] The planar-sheet graphite fluorides lose HF much more slowly than graphite bifluoride, and a stage 1 $C_xF{\cdot}\delta HF$ remains as stage 1 under prolonged evacuation, while $C_xHF_2{\cdot}\delta HF$ loses sufficient HF to go to a higher stage. The gallery heights for the planar-sheet graphite fluoride range from 5.5 – 6.0 Å after evacuation [19], which is smaller than those observed for graphite bifluorides (6.1 Å - 6.5Å) [17-19]. Stage 2 $C_xF$ ($x = 14$) has also been prepared by electrochemical oxidation of graphite in aqu. HF. [19]

Planar-sheet graphite fluorides can also be prepared by chemical oxidation of graphite in anhydrous HF, using $F_2$ or transition metal fluorides as oxidants at room temperature. [16] When $K_2MnF_6$ was employed in sufficient quantity, a graphite bifluoride $C_{28}HF_2{\cdot}\delta HF$ was converted to a graphite fluoride $C_xF$ ($x > 5$).

### 1.3.2 Graphite Oxide

Graphite oxide can be prepared by several chemical methods including (1) the oxidation of graphite by $KClO_3$ in fuming nitric acid (the Brodie method) [28], (2) the addition of graphite to a concentrated mixture of sulfuric and fuming nitric acids (the

Staudenmaier method) [29], and (3) the reaction of graphite with $KMnO_4$ or $K_2Cr_2O_7$ in concentrated sulfuric acid [30]. An ideal composition of $C_4OOH$ was proposed for the products from all these synthetic methods. [31] However, the best structural model for graphite oxide has been an ongoing debate.[31-33] The generally accepted structure indicates the presence of hydroxyl groups C-OH, 1-3 epoxy bridges C-O-C and C=C double bonds. [31] The material is very hygroscopic and readily takes up moisture from atmosphere. Hence, gallery height may vary from 6 to 11.3 Å, depending on the amount of water present in the intercalant galleries.

## 1.4 Complex Graphite Compounds

### 1.4.1 Pillar Type Graphite Salts

#### *1.4.1.1. Previous work*

Boehm and coworkers first described the intercalation of perfluoroalkylsulfonate anions into graphite [34-37]. The products were prepared by galvanostatic oxidation of graphite in the corresponding molten acids or propylene carbonate with the addition of an alkali metal salt. The GICs obtained were characterized by X-ray diffraction.

GICs with greatly expanded galleries were obtained when intercalated with $C_nF_{2n+1}SO_3^-$ ($n \geq 4$). The gallery height with perfluorobutanesulfonate was 17.7Å, and for PFOS $\cong$ 34 Å , which strongly suggested a bilayer intercalant structure. [35-37] The bilayer arrangement is a common intercalant orientation upon exchange of smectite clays [38] or other layered metal oxides or sulfides when intercalated with surfactant-like cations, [39] but had not been previously observed for GICs. There was, however, very

limited structural information and characterization in these initial reports. Nevertheless, they demonstrated for the first time that graphite could form intercalation compounds with galleries larger than 10 Å, and provided the first example of an anionic bilayer intercalant structure in a GIC. The same research group also did similar experiments on alkanesulfonic acids and alkylsulfuric acids and obtained dramatic swelling of graphite, although no new GIC structures could be identified.

Our group subsequently reported electrochemical synthesis of stage 2 graphite perfluorooctanesulfonate in $LiC_8F_{17}SO_3$/ $CH_3NO_2$ at ambient temperature. [40] The gallery height was found to be 25 – 26 Å for stages 2-7, with $x \approx 17$ for stage 2.

### *1.4.1.2 Chemical Preparation of GICs using Strong Oxidants*

A simple chemical synthesis for $C_x$PFOS in aqu. HF is introduced in Chapter 2, which, unlike the two earlier methods, allows the preparation of bulk quantities of the GIC in a short time. The crucial step in this chemical synthesis is the selection of a suitable oxidant for graphite, one that is compatible with an oxidatively stable, but convenient, solvent.

Different oxidants were tested in the GICs synthesis. In aqu. HF solution, $K_2MnF_6$ was found to be the best candidate. $K_2MnF_6$ powder forms a bright yellow stable solution in 48% HF at ambient conditions, with only 25 mol% decomposition observed in two months. At 50 °C, however, the solution decomposes at a faster rate (Figure 1.5) [42]. $K_2MnF_6$ is not stable in some other concentrated acids such as sulfuric

acid and nitric acid. These solutions can be stabilized, however, by addition of a small amount of aqu. HF. [41]

$KMnO_4$ and $K_2Cr_2O_7$ are both strong oxidants used in synthesis of stage 1 graphite sulfate and graphite nitrate in concentrated acids. $KMnO_4$ has a standard potential of 1.51 V on reduction to $Mn^{2+}$, and the standard potential for reduction of $Cr^{+6}$ to $Cr^{+3}$ is 1.33V:

$$5\,e + MnO_4^- + 8H^+ \rightarrow Mn^{2+} + 4\,H_2O \qquad E_{1/2} = 1.51V \qquad (1.5)$$

$$6\,e + Cr_2O_7^{2-} + 14\,H^+ \rightarrow 2\,Cr^{3+} + 7\,H_2O \qquad E_{1/2} = 1.33V \qquad (1.6)$$

$KMnO_4$, however, can oxidize $H_2O$ to $O_2$ in aqu. HF at ambient temperature at a significant rate. The purple solution turns brown in a few hours, which indicates the formation of a $Mn^{3+}$ complex. When permanganate was used as the oxidant, the intercalation process was slower than with $K_2MnF_6$, and only stage 3 or higher stage GICs were obtained. Similarly, the orange colored $K_2Cr_2O_7$ solution in aqu. HF turned green due to $Cr^{3+}$ complex formation within two hours. Consequently, stage 4 or higher GICs were the only products observed using dichromate as the oxidant.

$PbO_2$ and $NaBiO_3$ can oxidize graphite and form low stage GIC with PFOS in aqu. HF.

$$2\,e + PbO_2 + 4\,H^+ \rightarrow Pb\,(II) + 2\,H_2O \qquad E_{1/2} = 1.46\,V \qquad (1.7)$$

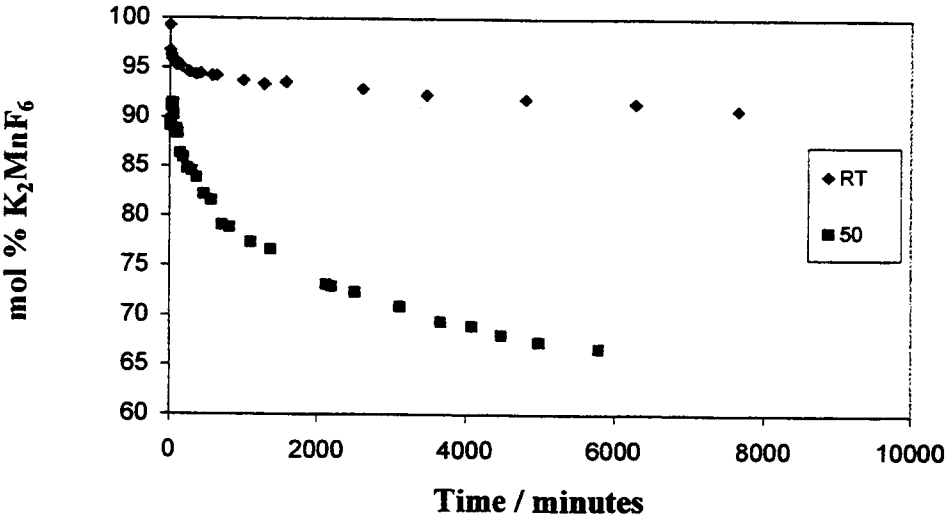


**Figure 1.5** Decomposition of $K_2MnF_6$ in aqu. HF at room temperature and 50 °C.

$$NaBiO_3 + 4\,HF \rightarrow BiF_3 + H_2O + NaF + O_2 \qquad E_{1/2} \cong 2\,V \qquad (1.8)$$

However, relatively insoluble $PbO_2$ or $BiF_3$ are mixed in with the resulting GIC products. Warm concentrated sulfuric acid can dissolve $PbO_2$, but during this workup step, PFOS was displaced by sulfate and $C_xHSO_4 \cdot \delta H_2SO_4$ was obtained after this wash. Using $PbO_2$ as an oxidant, an impure $C_x$PFOS was also synthesized in conc. $HNO_3$ solution. [41] Ozone gas was tested as oxidant in aqu. HF, but no graphite intercalation was observed.

The pH, or for concentrated acids, Hammett acidity function, $H_0$, of the aqueous media is strongly related to the water oxidation potential. $H_0$ is defined as:

$$H_0 = - \log 10 \, (\alpha_{H+} * \gamma_B / \gamma_{BH+}) \qquad (1.9)$$

where $\alpha_{H+}$ is the activity of hydrogen ions, and $\gamma_B$ and $\gamma_{BH+}$ are the activity coefficients for an electrically neutral weak base B (the indicator) and its protonation product $BH^+$:

$$B + H^+ \Leftrightarrow BH^+ \qquad (1.10)$$

The $H_0$ values measured for aqu. HF [43] are provided in Figure 1.6.

The oxidation potential required for graphite is greater than 4.0 V vs $Li/Li^+$, and as the potential increases, higher intercalant content (lower stage) GICs are obtained. The formation of GICs in neutral water or basic solution is not likely due to the low water oxidation potential. First stage GICs, however, can be obtained in concentrated sulfuric

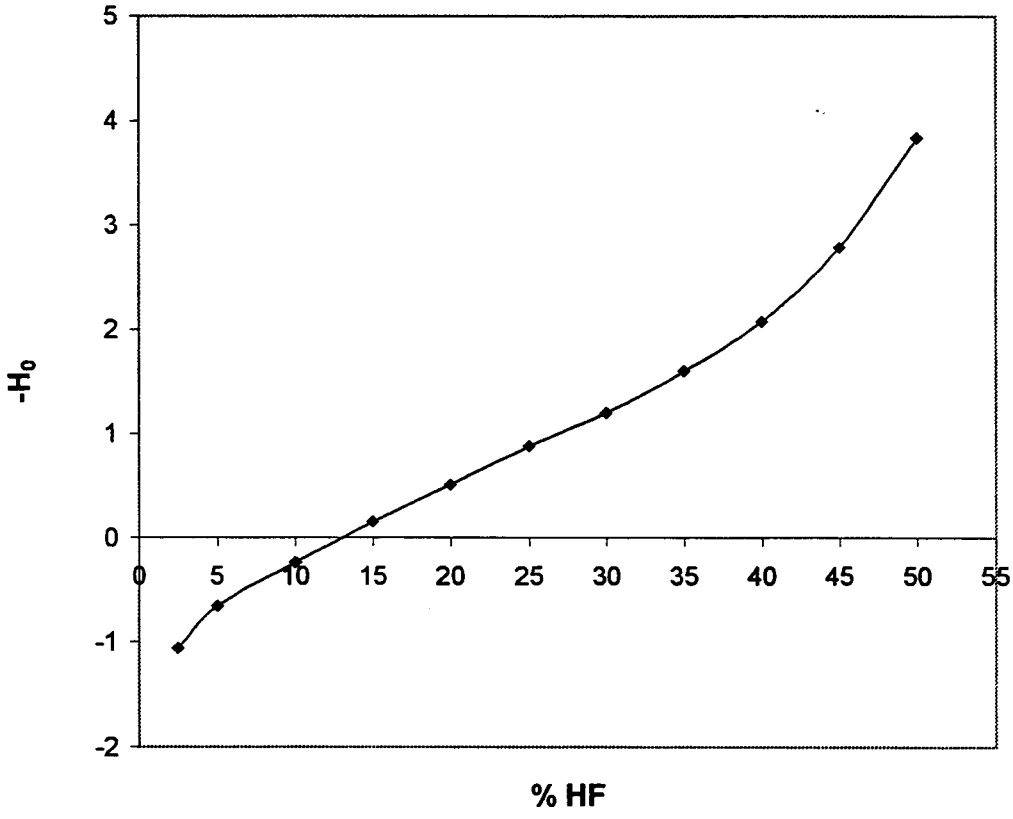


**Figure 1.6** Hammett acidity function for aqu. HF. The percent HF is v/v with water.

acid and 97 % $HNO_3$. As the water activity increases in the acid solution, only higher stage products will be derived. It is shown that solid solution of 79 % 2nd and 21 % 3rd staging of $C_x$PFOS is obtained in 48 % aqu. HF, which has an $H_0$ = -3.4 [43]. By adding 17 % (v/v) of 69 % $HNO_3$ ( $H_0 \approx$ -3.95 [43]) to aqu. HF, a pure stage 2 GIC is obtained. In contrast, higher stage GICs are derived when a more diluted hydrofluoric acid solution is used and therefore the intercalant content inside the graphite galleries decreases. Figure 1.7 shows observed intercalant content of $C_x$PFOS changes with Hammett acidity function $H_0$ of aqu. HF solution. The intercalant contents are calculated assuming 100% for a stage 2 GIC and then using the equation

$$\text{intercalant content \%} = 100 * 2 / n \qquad (1.11)$$

where n is the stage number. The intercalant content of the $C_x$PFOS synthesized using this chemical method are derived from the refinement method described in Chapter 5.

It should be pointed out that the intercalation process in aqu. HF represents a dynamic state: oxidation of graphite and reduction of GICs by water occur simultaneously. The GIC is not stable in aqu. HF without the presence of an oxidant. The data points obtained in Figure 1.7 therefore represent products from a kinetic equilibrium rather than the true thermodynamic limit of oxidation at that acidity.

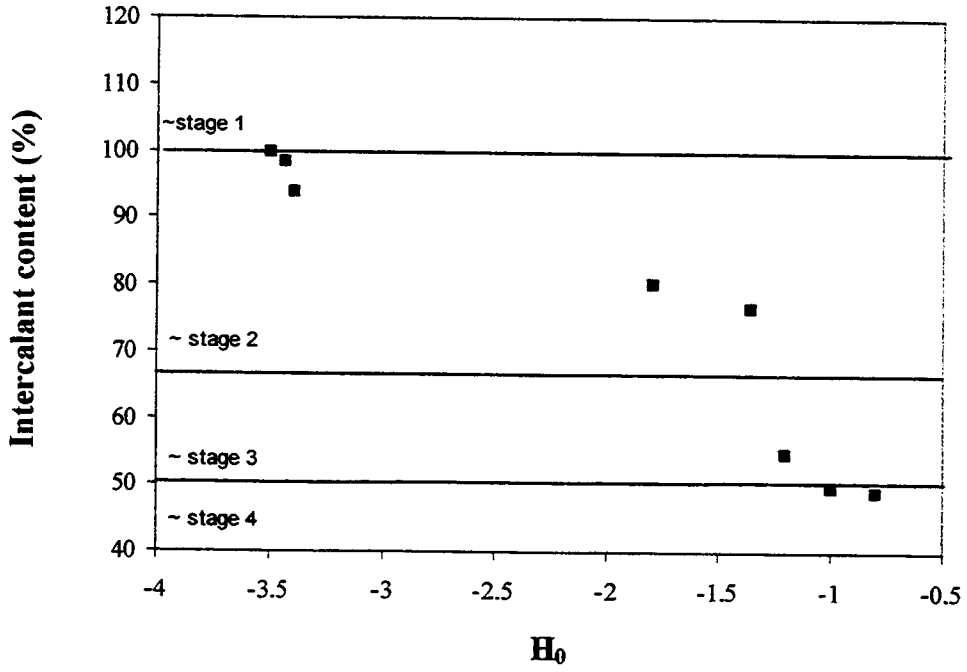


**Figure 1.7** Intercalant content and staging for $C_x$PFOS in various concentrations of hydrofluoric acid.

### 1.4.2. Intercalation of Graphite Oxide with surfactants and polymers

GICs containing mononuclear metal anion complexes (ie. $MF_n^-$, $MCl_n^-$, $MO_n$) have gallery heights of 10 Å or less. Attempts to exfoliate graphite to form a colloidal suspension of single graphite sheets have not yet succeeded, and no strong evidence of polymer or oligomer intercalation has been reported until very recently [44]. The binding energy between carbon layers in graphite is approximately 1.5 kcal/mole carbon, but the non-polar surface does not interact strongly with molecular species. In contrast, the lamellar structure of graphite oxide (GO), with a surface containing charged alkoxyl groups or carboxyl functions can disperse in basic solution.

GO has a polar surface and can incorporate n-alkyl-ammonium cations through ion exchange. The dried GIC has a gallery height ranging from 14.5 to 15.9Å for $C_{14}$ to $C_{18}$ chain intercalants, which is consistent with double layers of n-alkylammonium with the carbon chains oriented parallel to the GO layers. [46] These materials were observed to swell in organic solvents of various polarities (ethanol, toluene, cyclohexane, and n-heptane) and their binary mixtures. A gallery height as large as 45 Å was observed. This large expansion corresponded to the rearrangement to a bilayer orientation of the cations, with a chain tilt angle of 56° relative to the GO planes. The basal spacing for this structural was calculated using:

$$I_c = 2 * (1.27\, n_c + 2.8) * \sin 56^\circ + 6.1\ \text{Å} \qquad (1.12)$$

where $n_c$ is the number of carbon atoms in the cations. The degree of swelling was also observed to be a function of the polarity of the solvent.

Matsuo et al. recently reported intercalation of the high molecular weight polymers poly(ethylene oxide) (PEO) and poly(vinyl alcohol) (PVA) into graphite oxide. [45] GO was dispersed in a 0.1 M NaOH and added to a aqueous PEO solution. The product was found to have a GO-PEO nanocomposite structure containing a single layer of PEO between the GO sheets. PXRD of this material showed broad intercalation peaks and the repeat distance, $I_c$, was 12.3Å - 13.4Å. PVA and a $Cu(OH)_2$-PVA complex were intercalated into graphite oxide by a similar method. Depending on the amount of intercalated PVA, $I_c$ values of GO-PVA nanocomposites was either 13.2 or 22.1 Å, corresponding to the incorporation of single and double layers of PVA, respectively.

## 1.5 Thermally Exfoliated Graphite

Thermally exfoliated graphites (TEGs) are widely used in high temperature sealants and gaskets due their flexibility and thermal stability. These materials are usually prepared by the rapid thermal treatment (up to 1200°C [47]) of GICs resulting in a large volume expansion (up to 300 times). SEM shows a porous honeycomb microstructure after the processing. [47] The lamella thickness is 0.5 μm, corresponding to approx. $10^3$ graphene layers.

Most TEG precursors are made by oxidation of graphite in concentrated sulfuric acid. [58,59] Various oxidants have been examined, for example $KMnO_4$ [48], $K_2Cr_2O_7$ [50], $HNO_3$ [50], and $H_2O_2$ [49]. The bulk density of the TEG obtained was found to be dependent on the amount of oxidant used, the concentration of the sulfuric acid, and the particle size of graphite source. [48] The major disadvantages for the current methods

are the release of large amounts of environmental polluting gases, $SO_2$ and $SO_3$, in the exfoliation process, and the presence of corrosive sulfur residuals.

Efforts have been made to reduce the sulfur content, or to produce totally sulfur-free TEGs by substituting other GICs as precursors. Alternate precursors proposed have included: (1) GICs containing other oxoanions, $C_xClO_4 \cdot \delta HClO_4$ or $C_xNO_3 \cdot \delta HNO_3$ [51,52], (2) GICs containing chlorometallates such as $FeCl_4^-$, $SbCl_6^-$ and $ZnCl_3^-$ [24], (3) donor type GICs with co-intercalated solvent, such as $C_xK \cdot \delta THF$ [24,50], (4) GICs electrochemically derived from acetic acid [54] or $H_2O_2$ [53] / $H_2SO_4$, and (5) GICs derived in organic acids such as formic acid [53]. Many of the above reactions will introduce new difficulties, such as releasing environmentally polluting $Cl_2$ and $NO_x$ gases, or have the potential for incorporating residual metals in the TEG. The last two methods are appealing but it is likely that a process based on conventional chemical oxidation will be required to achieve commercial liability.

The exfoliation of graphite at room temperature has been observed during electrochemical oxidation of graphite in organic acids that do not have high oxidative stabilities, such as formic acid. When graphite was electrochemically oxidized in pure trifluoroacetic acid, mixtures of stage 2 and higher stage GICs were obtained, with $I_c$ = 11.48 Å for the stage 2 GIC. [56,57] Exfoliation of the GIC, along with oxidation of the trifluoroacetate, occurred during the reaction at room temperature. [57] Analysis of the gases evolved during the intercalation process indicate $C_2F_6$ and $CO_2$, which suggests the oxidation of trifluoroacetate, corresponding to the Kolbe reaction, as shown in equations (1.10) and (1.11):

$$CF_3COO^- \rightarrow \cdot CF_3 + CO_2 + e^- \quad (1.13)$$

$$2 \cdot CF_3 \rightarrow C_2F_6 \quad (1.14)$$

It was proposed that this process occurs both on the carbon surface as well as within the GIC galleries, and that gas generated within the galleries causes the exfoliation.

Graphite electrodes are known to partially delaminate when intercalated with $Li^+$ in some organic electrolytes, such as propylene carbonate, due to the cointercalation and decomposition of solvent molecules [61]. A similar observation was made for the reduction of $C_xFeCl_{3+y}$ in an aprotic medium (mixture of ethylene carbonate and diethylcarbonate) containing $LiClO_4$ [60]. The product was found to be a nanocomposite of Fe and exfoliated graphite, which was examined for catalytic applications where a supported metal is required.

When PFOS was electrochemically intercalated into graphite at ambient temperature, the graphite electrode was observed to swell dramatically and exfoliate if oxidation continued beyond stage 2. [40] To allow a faster reaction, co-intercalation of sulfate or perchlorate with PFOS was also investigated. When $C_{70}SO_4 \cdot \delta H_2SO_4$ was oxidized in LiPFOS / $CH_3NO_2$, the GIC exfoliated after incorporation of small amount of PFOS. SEM images showed that the exfoliated product consisted of 1μm thick platelets, comparable to those in conventional TEG materials. [47]

When heating $C_x$PFOS prepared from highly-oriented pyrolytic graphite (HOPG) to 200 °C in $N_2$ atmosphere, an accordion-like reversible expansion along the C direction was observed. [40] The chip (original thickness is $t_0$) was expanded to ~$100t_0$ on the c direction and upon cooling to RT the material contracted to ~ $10t_0$. The expansion and

contraction between $10t_0$ and $100t_0$ was found to last for more than 20 cycles upon temperature cycling. A similar reversible expansion has been reported for $C_xBr$. [41]

## 1.6 Structural Characterization

### 1.6.1 Powder X-ray Diffraction

PXRD data were collected on a Siemens D5000 powder diffractometer, using Ni-filtered CuKα radiation, with 0.02 ° 2θ steps, between 1.5 and 60 degrees. Collection times varied from 0.1 s / step for routine analyses to 1.0 s / step for data used in structural modeling. The GIC powder was pressed onto a flat sample holder with a diameter of 15 mm. The measurement was done in a variable slit mode to maintain a 6 mm irradiation diameter, the detector slit width was 0.2mm.

### 1.6.2. Structural Refinement for Stage 2 $C_xPFOS$

One-dimensional electron density calculations were generated for the proposed model (calculated) and from the PXRD (observed), the details of the calculations will be discussed in Chapter 2 and 3. The PXRD data were collected using a variable slit and converted to a fixed-slit intensity data set using D5000 "New Eva" software. The peak intensities were obtained by integration of peaks and corrected by the Lorentz-polarization factor. The assigned phase of the observed structure factor was kept the

same as that for the corresponding calculated $F_{00l}$, which assumes the initial proposed model is a reasonable approximation of the correct structure.

The intercalant anion geometry employed for PFOS was the optimized structural minimum obtained using Gaussian 94, [64] Details of the energy calculations are discussed below in Sec.1.6.5. The stage 2 GICs were fit using a centrosymmetric unit cell. Structure factors and the electron density maps were then calculated in an MS Excel worksheet according to the following equations:

$$F_{calc}(00l) = \Sigma\, 2\, f_i \cos(2\pi\, l\, z_i) \qquad (1.15)$$

$$\rho(z) = (1/c)\,[F_0 + 2\ \Sigma F_{00l} \cos(2\pi\, l\, z)\,] \qquad (1.16)$$

where f refers to atomic scattering from reference 2.17.

The comparison of 1-D electron density maps for the observed and calculated data set can provide an instructive means to further refine the structural model. If the initial phase assignments are not correct, however, the calculated electron density map can be very misleading. Nevertheless, the reliability factor R, which was used to optimize structural refinement, is not affected by phase assignments and was calculated by:

$$R = \Sigma\, ||F_{obs}(00l)| - k\,|F_{cal}(00l)|| \,/\, \Sigma\, |F_{obs}(00l)| \qquad (1.17)$$

PXRD patterns of the optimized structural model were simulated using the DIFFaX program (v1.76). [62]

### 1.6.3 Introduction to DIFFaX

Crystal lattices can generally be described by the repeat stacking of unit cells. With the DIFFaX method, lattices are described in terms of layered structural units and a set of stacking operations that occur with defined probabilities. DIFFaX can use either "explicit" or "recursive" methods to generate the layer sequencing in the lattice. The explicit method requires the input of the fixed sequence of layers. The recursive method calculates diffraction intensities for a statistical ensemble of crystallites, each with a distinct stacking sequence and weighted by the calculated probabilities that such a sequence will occur. [62] In addition, DIFFaX can also automatically generate and calculate diffraction intensities from a random sequence of layers.

The scattered wavefunction from a lattice centered on any layer is equivalent to the scattering contribution from that layer plus the scattered wavefunction from a displaced lattice centered on the next layer:

$$\Psi(u) = F(u) + \exp(-2\pi i u R)\Psi(u) \qquad (1.18)$$

where $\Psi(u)$ is the scattered wavefunction at reciprocal lattice vector u, F(u) is the scattering contribution from the layer at the origin, and R is the shift between the two origins.

When a lattice contains planar defects, multiple layers types can be employed. For simplicity, two types of layers are considered here. When a probability factor, $\alpha_{ij}$, is

introduced to describe the transition probability between layers, the scattered wavefunction becomes:

$$\Psi_i(u) = F_i(u) + \Sigma \alpha_{ij} \exp(-2\pi i u R_{ij}) \Psi_j(u) \qquad (1.19)$$

A pictorial representation of this recursive model is shown in Figure 1.8. The diffraction intensities are calculated as the incoherent sum of scattered intensities over an ensemble of crystallites.

The recursive method was used for all structure calculations. For observed staging disorders in GICs, the two layer types were used to generate a solid solution of two stages. For example, to constitute stage 2 + 3 sequence, the method is schematically shown in Figure 1.9. A sample DIFFaX input file is provided in Appendix A 2, which constructs the model of a GIC containing a random solid solution with 67% $2^{nd}$ and 33% $3^{rd}$ staging of graphene layers. A ordered stage 2 GIC diffraction pattern can also be calculated from DIFFaX using only layer type 1 in Figure 1.9. Pseudo-Voigt diffraction peak profiles were used for all calculations.

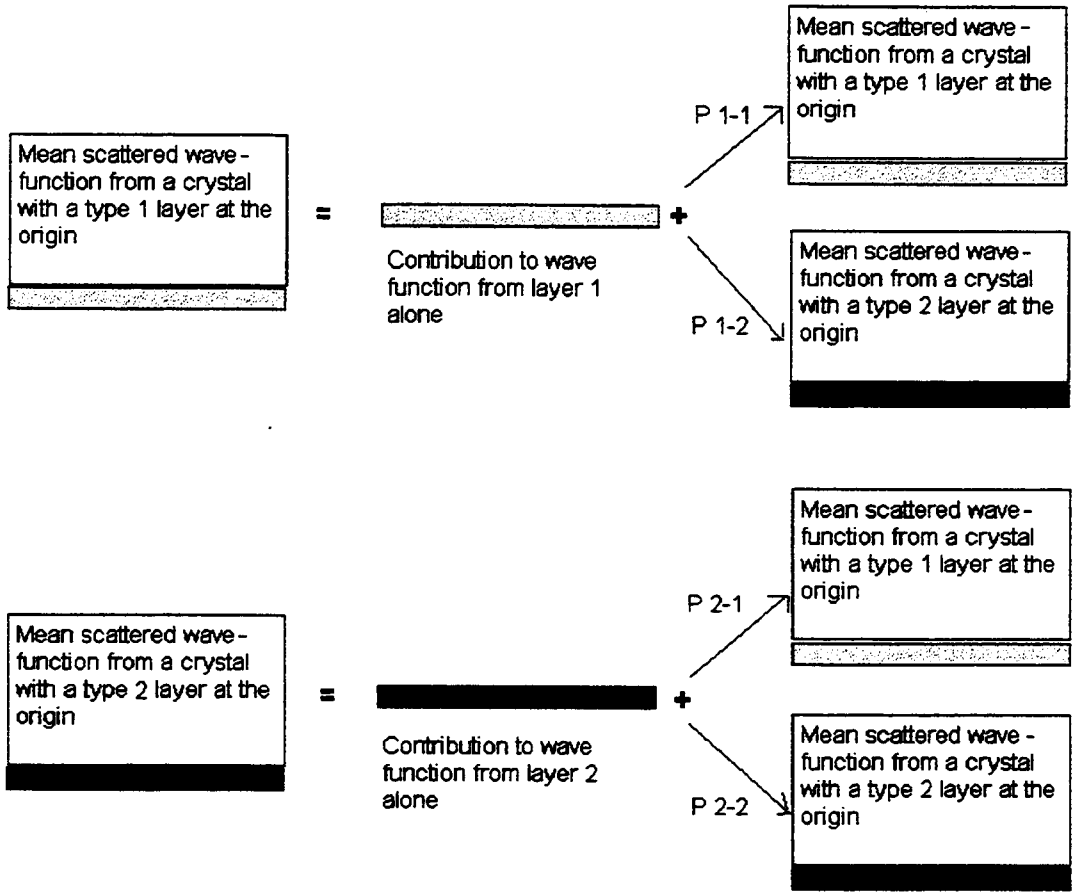


**Figure 1.8** Illustration of recursion in randomly faulted periodic objects (Figure is taken from DIFFaX manu). P 1-1, P 1-2, P 2-1, and P 2-2 are the probabilities for type 1 layer followed by type 1 layer, type 1 layer followed by type 2 layer, type 2 layer followed by type 1 layer, and type 2 layer followed by type 2 layer, respectively.

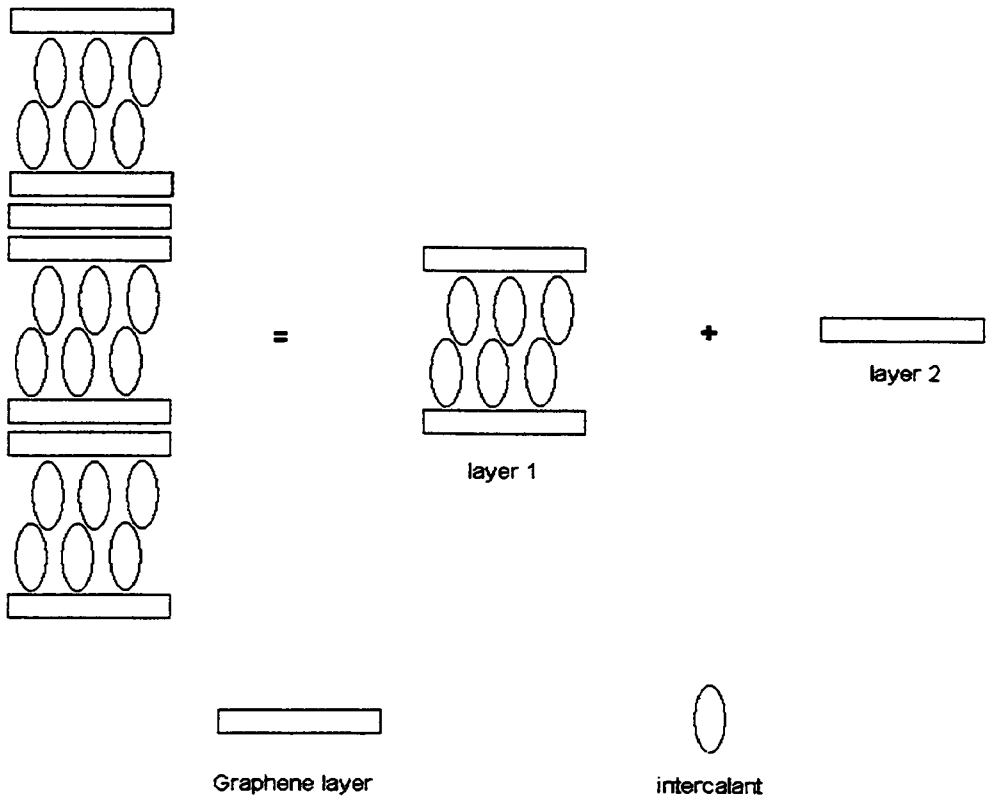


**Figure 1.9** Solid solution structure of a 2nd and 3rd staging $C_x$PFOS generated by a combination of moieties for stage 2 (layer 1) and a graphene layer (layer 2).

### 1.6.4 Peak Broadening and Williamson-Hall relationship

PXRD peakwidths for $C_xPFOS$ were analyzed considering strain and domain size as factors for broadening, according to the Williamson-Hall relation: [63]:

$$FWHM * \cos\theta = (4 \sin\theta)(\xi / 2) + (\lambda / t) \quad (1.20)$$

where FWHM is the peak full width (in radians) at half maximum, $\xi$ is related to the lattice strain distribution, $\lambda = 1.5418$ Å, and t is the coherent domain size. If FWHM is plotted vs 4sin $\theta$, the best-fit line slope and intercept can be used to determine the strain and particle size. For most materials, the Williamson-Hall plot provides a fairly linear relationship. The sinusoidal shape of the obtained curve for $C_xFPSO$ made in aqu. HF is due to the stage disorder, which is further discussed in Chapter 5. The peakwidths and peak positions were obtained through the 'profile' window functions in the Siemens D5000 software, and all peakwidths were evaluated using a Gaussian profile function.

## 1.7. Molecular Structural Calculations

### 1.7.1 Molecular Mechanics Method

The molecular mechanics method can be used to rapidly perform energy calculations of large molecular systems. This calculation model uses the laws of classical physics and considers atoms as spheres and bonds as springs, a very different approach

than using quantum mechanics. The energy is thus calculated based on bond stretching, bending, twisting, and also the non-bonded interactions as follows:

$$\text{Energy} = \text{Stretching Energy} + \text{Bending Energy} + \text{Torsion Energy} + \text{Non-Bonded Interaction Energy.} \quad (1.21)$$

Atoms not directly bonding can also interact through van der Waals attractions, steric repulsions, or long range electrostatic forces.

### 1.7.2. Electronic Structure Method

The electronic structure method uses quantum mechanics which is based on Schrodinger's equation:

$$H\Psi = E\Psi \quad (1.22)$$

where H is the Hamiltonian operator, $\Psi$ is the wavefunction and E is the energy. Schrodinger's equation can only be solved approximately for molecular systems. The type of approximations made in constructing the molecular Hamiltonian defines each electronic structure method.

Semi-empirical methods, such as AM1 and PM3, use mostly experimental data to estimate some of the time-consuming terms in Schrodinger's equation, with the benefit of reduction of the calculation time at a cost of some inaccuracy of results. Nevertheless, this often gives a valuable starting geometry for higher-level calculations.

Ab-initio models use no experimental parameters, and rely solely upon the laws of quantum mechanics. The Hamiltonian for a molecule can be simplified into four terms: electron kinetic energy, electron-nucleus attractions, electron-electron repulsions,

and nucleus-nucleus repulsions. In non-correlated methods, each electron is assumed to move in an average energy field of all others, which underestimates the electron-electron repulsive term, and therefore results in a reported energy that is too high. Correlated models tie the movements of the electrons together and can return a more accurate energy.

The structural calculations for PFOS and $N(CF_3SO_2)_2^-$ anions used the correlated ab initio method. The initial anion geometries were obtained using the AM1 semi-empirical module included in the Spartan 5.0 [61] suite of programs. Structures were then exported to Gaussian 94 and full geometry optimizations were carried out using Density Functional Theory (DFT). The method employed was Becke's three parameter hybrid functional with non-local correlation provided by the correlation functional of Lee, Yang and Parr (B3LYP). This method has been found to provide accurate geometrical data when combined with a reasonable basis set. For this work, the split valence basis set 6-31G(d) [61] was used. Final geometry are reported by B3LYP/6-31G(d) calculations. Geometries were characterized as mimina by performing frequency calculations. These optimized structures provided the initial model for structural refinements of the GICs, see Chapter 5.

## 1.8 References


1. Bartlett, N.; McQuillan, B. in *Intercalation Chemistry*; Whittingham, S.; Jacobson, A., Eds.; Acad. Press: New York, **1982**.

2. Daumas, N.; Herold, A. *C.R. Acad. Sci., Ser. C* **1969**, *268*, 373.

3. Scholz, W.; Boehm, H.B. *Z. Anorg. Allg. Chem.* **1969**, *369*, 327.

4. Marcus, B.; Touzain, P. *Synth. Met.* **1988**, *23*, 13.

5. Fuerst, C.; Fischer, J.; Axe, J.; Hastings, J.; McWhan, D. *Phys. Rev. Lett.* **1983**, *50*, 357.

6. Fischer, J.E.; Fuerst, C.D; Woo, K. C. *Phys. Rev. B* **1989**, *39*, 4374.

7. Hohlwein, D.; Metz, W. *Z. Kristallogr.* **1974**, *139*, 279.

8. Suzuki, I. S.; Suzuki, M. *J. Phys. Condens. Matter.* **1991**, *3*, 8825.

9. Hendricks, S.; Teller, E. *J. Chem. Phys.* **1942**, *10*, 147.

10. Setton, R. *Synth. Met.* **1988**, *23*, 519.

11. Ref. 1, p 36.

12. Rudorff, W.; Hofmann, U. *Z. Phys. Chem.* **1938**, *238*, 1.

13. Touzain, P. *Synth. Met.* **1979**, 1, 3.

14. Zhang, Z.W. *Ph.D Thesis*, Oregon State Univ. **1995**, 11.

15. Hooley, J.G.; in "*Preparation and Crystal Growth of Materials with Layered Structures*: (R.M.A.Lieth, ed.), Reidel Publ., Dordrecht, Netherlands, **1977**, pp. 1-33.

16. Lemmon, J.; Lerner, M. *Carbon* **1993**, *31*, 437.

17. Mallouk, T.; Bartlett, N. *J. Chem. Soc. Chem. Commun.* **1983**, 103.

18. Mallouk, T.; Hawkins, B.L.; Conrad, M.P.; Zilm, K.; Maciel, G.E.; Bartlett, N. *Phil. Tran. R. Soc. Lond* A **1985**, *314*, 179.

19. Takenaka, H.; Kawaguchi, M.; Lerner, M.; Bartlett, N. *J. Chem. Soc., Chem. Commun.* **1987**, 1431.

20. Zhang, Z.W.; Lerner, M.M. *J. Electrochem. Soc.* **1993**, *140*, 742.

21. Bach, B.; Ubbelohde, A.R. *J. Chem. Soc. A* **1971**, 3669.

22. Freeman, A.J. J.C. S. *Chem. Commun.* **1968**, 193.

23. Hooley, G.G.; Bartlett, M.W.; Liengone, B.V; Sams, J.R. *Carbon* **1968**, *6*, 681.

24. Inagaki, M. *J. Mater. Res.* **1989**, *4*, 1560.

25. Inagaki, M.; Wang, Z.D.; Okamoto, Y.; Ohira, M. *Synth. Met.* **1987**, *20*, 9.

26. Ruff, O.; Bretschneider, O.; Ebert, F. *Z. Anorg, Allg. Chem.* **1934**, *217*, 1.

27. Watanabe, N.; Touhara, H.; Nakajima T.; Bartlett, N.; Mallouk, T.; Selig, H. In *Inorganic Solid Fluorides*, Hagenmuller, P. Ed.; Academic Press: New York, **1985**, (pp331-369) and references contained therein.

28. Brodie, B.C. *Ann. Chim. Phys.* **1855**, *45*, 351.

29. Staudenmaier, L. *Ber. Deut. Chem. Ges.* **1898**, *31*, 1481.

30. Hummers, W.S. *U.S. Patent No. 2,798,878*, **1957**.

31. Hamwi, A.; Marchand, V. *J. Phys. Chem. Solids* **1996**, *57*, 867.

32. Nakajima, T.; Matsuo, Y. *Carbon* **1994**, *32*, 3, 469.

33. He, H.; Klinowski, J.; Forster, M.; Lerf, A. *Chem. Phys. Let.* **1998**, *287*, 53.

34. Horn, D.; Boehm, H.P. *Mater. Sci. Eng.* **1977**, *31*, 87.

35. Ruisinger, B; Boehm, H. P. *Angew. Chem. Int. Ed. Engl.* **1987**, *26*, 253

36. Boehm, H.P.; Helle, W.; Ruisinger, B. *Synth. Met.* **1988**, *23*, 395

37. Ruisinger, B.; Boehm, H.P. *Carbon* **1993**, *31*, 7, 1131.

38. Pinnavaia, T. *Science* **1983**, *220*, 365.

39. Jacobson, A. in *Intercalation Chemistry*; Whittingham, S.; Jacobson, A., Eds.; Acad. Press: New York, **1982**.

40. Zhang, Z.; Lerner, M. *Chem. Mater.* **1996**, *8*, 257.

41. Salib, M.S.; Petrou, A.; Chung, D. *Carbon* **1997**, *35*, 5, 709.

42. These data were obtained from Henry Li. The percent of K2MnF6 remained in HF solution was determined by oxidation of excess KI solution, followed by and back titration with $Na_2S_2O_3$.

43. Rochester, C.H. in *Acidity Functions*, Blomquist, A.T. Ed.; Acad. Press: London, New York, **1970**, pp.21-71.

44. Matsuo, Y.; Tahara, K.; Sugie, Y. *Carbon* **1997**, *35*, 113.

45. Matsuo, Y.; Hatase, K.; Sugie, Y. *Chem. Mater.* **1998**, *10*, 2266.

46. Dekany, I; Kruger-Grasser; Weiss, A. *Colloid Polym. Sci.* **1998**, *276*, 570.

47. Frackowiak, E.; Kaiser, W.; Krohn, H.; Beck, F. *Mol. Cryst. Liq. Cryst.* **1994**, *244*, 221.

48. Kuzina, T.A.; Shempel, N.A.; Golipad, P.N.; Kurnevich, G.I. *Zh. Prikladnoi Khim.* **1993**, *66*, 2, 271.

49. Nilol'skaya, I.V.; Fadeeva, V.A.; Semenenko, K.N. *Zh. Obshch. Khim.* **1989**, *59*, 2653.

50. Inagake, M.; Shiwachi, Y. Maeda, Y. *J. Chimie. Phys.* **1984**, *81*, 847.

51. Furdin, G. *Fuel* **1998**, *77*, 6 479.

52. Scharff, P.; Xu, Z-Y.; Stumpp, E.; Barteczko, *Carbon* **1991**, *29*, 31.

53. Kang, F.; Leng, Y.; Zhang, T.-Y. *J. Phys. Chem. Solids* **1996**, *57*, 889.

54. Kang, F.; Zhang, T.Y.; Leng, Y. *Carbon* **1997**, *35*, 1167.

55. Kang, F.; Leng, Y.; Zhang, T.-Y. *Carbon* **1997**, *35*, 1089.

56. Scharff, P. *GFECI 89*, Nantes, France, Mars **1989**, Ext. Abstracts, p81.

57. Bourelle, E.; Douglade, J.; Metrot, A. *Mol. Cryst. Liq. Cryst.* **1994**, *244*, 227.

58. Avdeev, V.V.; Monyakina, L.A.; Nikolskaya, I.V.; Sorokina, N.E.; Semenenko, K.N. *Carbon* **1992**, *30*, 819.

59. Inagaki, M.; Iwashita, N.; Kouno, E. *Carbon* **1990**, *28*, 49.

60. Beguin, F.; Frackowiak, E. *J. Phys. Chem. Solids* **1996**, *57*, 841.

61. Hehre, W.J.; Shusterman, A. J.; Huang, W.W. *A Laboratory Book of Computational Organic Chemistry*, Wavefunction Inc., Irvine, CA, **1996**.

62. Treacy, M. M; Newsam, J. M.; Deem, M. W. *Proc. R. Soc. Lond. A* **1991**, 433, 499.

63. Williamson, G.; Hall, W. *Acta Metallurgica* **1953**, *1*, 22.

64. Frisch, M. J. et. al. Ga*ussian 94*, Revision E.1, Gaussian, Inc., Pittsburgh PA, **1995**.

# Chapter 2

## Chemical Synthesis of Graphite Perfluorooctanesulfonate Using $K_2MnF_6$ in Hydrofluoric Acid or Mixed Acid Solutions

*Xuerong Zhang and Michael M. Lerner,*
*Department of Chemistry and Center for Advanced Materials Research,*
*Oregon State University,*
*Corvallis, OR 97331-4003, USA.*

**submitted to Chem. Mater. for publication in May, 1999**

## 2.1 Abstract

Graphite intercalation compounds (GICs) of nominal composition $C_xC_8F_{17}SO_3 \cdot yF$ are prepared under ambient conditions in 48 % hydrofluoric acid, using the oxidant $K_2MnF_6$. The product compositions are evaluated by mass uptake, TGA, DSC, and elemental analysis. PXRD analysis indicate that the stable product after 3 – 4 day reaction ($x \cong 18$, $y \cong 4$) is a GIC comprised of a solid solution of stage 2 and stage 3. A similar product, although containing a greater graphite fluoride impurity, can be obtained within 1 h. using this method at 50 °C. Longer reactions at elevated temperature lead to product degradation and other impurities. The addition of up to 83 vol. % conc. $HNO_3$ or 17 % fuming $H_2SO_4$ produces a stage 2 intercalation compound within hours. One-dimensional structural modeling for the stage 2 GIC provides refined values for the graphene carbon / intercalant mole ratio, distance between graphene and sulfonate oxygen planes, position of additional intercalated fluoride, and the chain take-off angle. The products obtained by this synthetic method and the observed staging phenomena are related to previous reports on graphite fluorometallates and an energetic model for graphite intercalation.

## 2.2 Introduction

Graphite is the only layered structure to undergo an extensive intercalation chemistry by both oxidative and reductive processes. Graphite intercalation compounds (GICs) are also unusual in the common occurrence of several well-defined stages, i.e. phases with ordered arrangements of occupied and unoccupied galleries. The Daumas-Herold domain model has been widely used to describe this staging phenomenon. [1] A schematic representation of a stage 2 GIC in Figure 2.1, with alternating galleries occupied by intercalant, indicates the relationship between the basal repeat length ($I_c$), gallery height ($d_i$), and stage (n). The integral stage number indicates the number of galleries contained in a repeat sequence where only the first is occupied by intercalant. The relationship between these parameters can also be expressed as:

$$I_c = d_i + (n - 1)(3.354\ \text{Å}) \qquad (2.1)$$

According to this model, fractional stages can also be envisioned, for example stage 3/2 would refer to an occupancy between stage 1 and 2, where the repeat sequence contains 3 galleries, with the first two galleries being occupied.

The combination of extensive staging and broad intercalant chemistry allows a wide range of graphite intercalation reactions and compounds. [2-4] In addition to the basic research interest in GICs and associated chemistry, some of these materials have electrochemical properties that have become important in charge storage devices. [5-7]

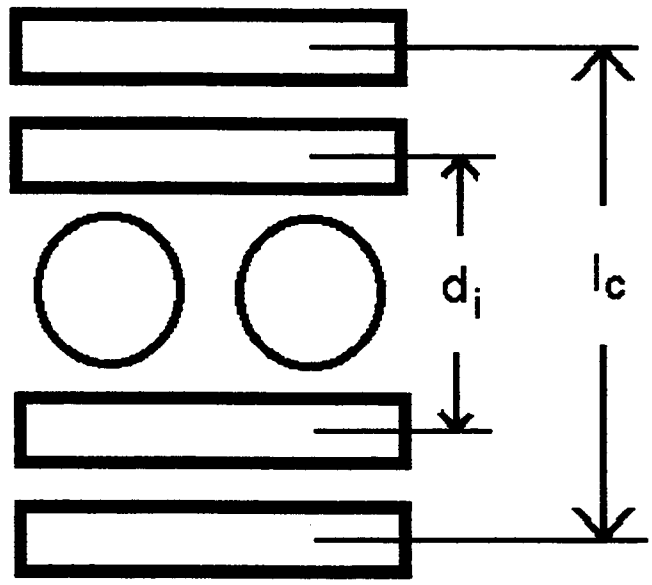


**Figure 2.1** Representation for a stage 2 GIC showing relation of $d_i$ and $l_c$.

GICs are also important as precursors to malleable graphite forms. [8] New practical and scalable synthetic methods need to be developed in order to expand these applications.

Boehm and coworkers first described the intercalation of perfluoroalkylsulfonate anions into graphite, they prepared these compounds by the electrochemical oxidation of graphite in the corresponding acids at elevated temperature. [9] These studies include the significant observation that GICs were formed with greatly expanded galleries when n > 4 in $C_nF_{2n+1}SO_3^-$. The distance between graphene carbon planes encasing intercalated galleries, $d_i$, was found to be approx. 34 Å for the perfluorooctanesulfonate compound, $C_xC_8F_{17}SO_3$ or $C_x$PFOS, which strongly suggested a bilayer intercalant structure. The bilayer arrangement is a common intercalant orientation upon exchange of smectite clays [10] or for other layered metal oxides or sulfides when intercalated with surfactant-like cations. [11] This bilayer arrangement is favorable as it allows increased interaction between the charged sheet surface and oppositely-charged head groups, and also close interaction between non-polar chains at the gallery centers. These reports demonstrated for the first time that graphite could form intercalation compounds with galleries larger than 10 Å, and provided the first example of an amphoteric bilayer intercalant structure in a GIC.

In 1996, our group reported a study on $C_x$PFOS where the target compounds were prepared by the electrochemical oxidation of graphite in $LiC_8F_{17}SO_3$ (sat.) / $CH_3NO_2$ at ambient temperature. [12] Compounds of stages 2 – 7 were obtained, with $d_i \cong 25 - 6$ Å for all the stages, and $x \cong 17$ for the stage 2 product.

In both the above studies, the electrosynthetic reactions are inherently limited by the low charge density required to avoid a large overpotential at the carbon surface,

which would result in electrolyte decomposition and passivation of the graphite surface. In addition, the high potential required for graphite oxidation limits the selection of binders, electrolytes, and current collectors. For these reasons, scalable electrochemical reactions are unlikely to be realized, and it is preferable to find chemical routes for the bulk preparation of such GICs.

In 1993, our group reported on the use of transition metal fluorosalts as oxidants in the formation of graphite bifluoride and planar-sheet graphite fluorides: [13]

$$C_x \xrightarrow[\text{anhyd. HF}]{\text{AMFn}} C_xHF_2 \cdot \delta HF \ (x > 28) \text{ or } C_xF \ (x > 2) \qquad (2.2)$$

$$M = \text{Mn(IV), Ni(IV), Co(III), or Fe(III)}$$

The extent of fluorination was found to be limited by the oxidizing power of the fluoroanion. In particular, Mn(IV), in the form of $MnF_6^{2-}$, was suitable for obtaining $C_xF$ compounds with $x > 5$. A method similar to reaction (2), with the addition of a soluble perfluoroalkanesulfonate and oxidant to the anhydrous solution, could lead to intercalation of these anions, but the necessity of handling anhydrous HF may also tend to limit the practical application of such a method.

In earlier experiments with the oxidant $MnF_6^{2-}$, reaction (2) was also evaluated using aqueous hydrofluoric acid, allowing a simplified synthetic apparatus and procedure [14]. Although $K_2MnF_6$ is very stable in this solvent, no GIC products were recovered. The desired reaction sequence appears to be subverted by the instability of the graphite bifluoride salt intermediate in hydrofluoric acid. Thus, rather than the desired GIC, a

disordered graphite is obtained. The relative stability of $C_x$PFOS, however, suggested that this might be successfully prepared in aqueous acid.

In this report, we describe chemical methods to produce $C_x$PFOS, using a simple and rapid bench-top procedure. In addition, we extend the characterization of this GIC by PXRD, elemental, and thermal analyses.

## 2.3 Experimental

Fuming $H_2SO_4$ (Baker, fuming 30 – 33 oleum %), conc. $HNO_3$ (Mallinckrodt, 69.2 %) and hydrofluoric acid (Mallinckrodt AR, 48 % (w / o)) were used as received. $C_8F_{17}SO_2F$ (3M, experimental product) was treated with excess 20 % KOH solution and refluxed at 120 °C overnight. The white precipitate $KC_8F_{17}SO_3$ was washed with distilled water and dried under vacuum at room temperature. Bright yellow $K_2MnF_6$ powder was synthesized according to a literature method by reduction of $KMnO_4$ (EM Science GR) using $H_2O_2$ (Mallinckrodt AR, 30 % in aqu. soln.) in a KF / hydrofluoric acid solution [15]. Two types of graphite reagent were used; SP-1 powder (Union Carbide, 100 um avg. particle diameter) and natural graphite flakes (Aldrich, 1 - 2 um).

In a typical reaction, the graphite powder (50.0 mg, 4.16 mmole) was added to a stirred hydrofluoric acid solution (15 ml) containing $K_2MnF_6$ (200 mg, 0.8 mmole) and $KC_8F_{17}SO_3$ (200 mg, 0.4 mmole) in a polyethylene flask. The reactions proceeded in air, in a fumehood, at the specified temperatures and times. *Caution – heating hydrofluoric acid produces hazardous vapors and must be carried out under controlled conditions in a fumehood.* Products were filtered and washed briefly with cold hydrofluoric acid, then

briefly rinsed with hexane and dried overnight at 25 °C and a pressure of less than 0.1 torr. The mass uptake for the solid product was obtained after the final drying step.

In some experiments, graphite powders were oxidized in mixed acid solutions, $H_2SO_4$ / HF or $HNO_3$ / HF. *Caution – Hydrofluoric acid was cooled in an ice bath before the addition of the concentrated acids.* The ratios of acids were varied as indicated in the text. Other synthetic steps were as above.

PXRD data were collected on a Siemens D5000 powder diffractometer, using CuKa radiation, with 0.02 ° 2θ steps, between 1.5 and 60 degrees. Collection times varied from 0.1 s / step for routine analyses to 1.0 s / step for data used in structural modeling. Thermal analyses of powdered samples were carried out at 5 °C / min using a Shimadzu TGA-50 and DSC-50Q. The carrier gas for the thermal analyses was purified $N_2$ (< 5 ppm $O_2$) at 25 mL / min, however, the $O_2$ content of the gas is likely to be significantly higher due to outgassing from the instrument. Elemental analyses (C,H,N,S, and F) were performed by Desert Analytics (Tuscon, AZ).

Integration of $^{19}F$ NMR peaks for $-CF_3$ endgroups indicated that the $C_8F_{17}SO_2F$ reagent used contained 70 % linear and 30 % branched isomers, with the predominant branched isomer being $(CF_3)_2C(F)C_5F_{10}SO_2F$. The same isomeric composition of the potassium salt and prepared GIC's were assumed. Energy-minimized structural models for these anions were calculated by the Spartan program (4.1.1), using the semi-empirical AM-1 method.

PXRD peak widths were analyzed according to the Williamson-Hall relation for strain and domain size: [16]

$$\text{FWHM} * \cos\theta = (4 \sin\theta)(\xi / 2) + (\lambda / t) \quad (2.3)$$

where FWHM is the peak full width (in radians) at half maximum, $\xi$ is related to the lattice strain distribution, $\lambda = 1.5418$ Å, and t is the coherent domain size.

One-dimensional electron density maps were generated for centrosymmetric stage 2 cells using either the experimental diffraction data or a proposed structural model. Observed intensity data were used to generate structure factors after correction by a Lorentz-polarization ($L_p$) factor:

$$F_{obs}(00l) = \pm (I / L_p)^{1/2} \quad (2.4)$$

$$L_p = (1 + \cos^2 2\theta) / (\sin^2\theta \cos\theta) \quad (2.5)$$

where I is the integrated peak intensity. The calculated structure factors were obtained using:

$$F_{calc}(00l) = \Sigma\, 2 f_i \cos(2 \pi l z_i) \quad (2.6)$$

where $l$ is the Miller index, $z_i$ the fractional c-axis coordinate of each atom, and $f_i$ the angle-dependent scattering factor obtained from the literature. [17] Electron density maps were then generated for $z = 0 - 1$, at increments of 0.004, using the following relation:

$$\rho(z) = (1/c)\left[F_0 + 2\sum_{l=1}^{4} F_{00l}\cos(2\pi l z)\right] \quad (2.7)$$

where c is the cell dimension, and $F_0$ the zeroth order structure factor. Data collected between 14 and 17.5 ° 2θ were excluded due to small, broad peaks at 5.8 and 5.4 Å, ascribed to a $C_xF$ impurity phase. Structures were refined by minimizing the crystallographic R factor:

$$R = \Sigma \left| k\left|F_{obs}(00l)\right| - \left|F_{cal}(00l)\right|\right| / \Sigma k\left|F_{obs}(00l)\right| \quad (2.8)$$

A powder X-ray diffraction pattern was simulated by the DIFFaX program (v1.76) for the proposed model, and compared with the observed PXRD. The DIFFaX software allows the introduction of probability in the stacking sequence in structural models. [18]

## 2.4 Results and Discussion

### 2.4.1Products from hydrofluoric acid:

When graphite is added to the solution of $K_2MnF_6$ and $KC_8F_{17}SO_3$ in hydrofluoric acid, the structure evolves rapidly through a series of stages or mixtures of stages of a graphite compound containing $C_8F_{17}SO_3$ ($C_xPFOS$). A relatively constant pattern is obtained after

15 – 24 h (Figure 2.2), although a broad peak around 40 ° appears at very long reaction times due to the precipitation of an amorphous Mn-containing phase. With the smaller-particle natural graphite (1 - 2 μm), a similar final diffraction pattern is obtained after a 4 h. reaction. After drying, the low-stage products no longer exhibit a metallic luster as in graphite, and are instead observed to be hydrophobic, electrostatic powders.

Generally, PXRD patterns taken using the flat diffractometer sample orientation show strong preferred orientation of these platy particles, and most or all of the observed peaks are (00*l*) reflections. The PXRD patterns obtained are similar in general appearance to those previously reported by electrochemical oxidation of graphite in electrolytes containing the $C_8F_{17}SO_3^-$ anion, and at first most reflections appear to relate to an $I_c \cong 33 - 36$ Å, with a notable set of 5 strong peaks centered at $d \cong 3.4$ Å.

For the majority of XRD patterns obtained where hydrofluoric acid is used as a solvent, however, a reasonable fit of positions for these strong peaks found between 20 – 30 °2θ cannot be obtained using a single indexing cell parameter. In Figure 2.3 and Table 2.1, comparisons of best-fit data for a representative pattern are provided. As can be seen, the calculated peak positions using indices (008) – (0011) ($I_c$ = 32.92 Å) are too far separated, and those using (009) – (0012) ($I_c$ = 36.53 Å) are too close together. The assignment of these $I_c$ values to stages 2 and 3 will be described later.

In these patterns, a better fit to the observed peak positions can be obtained using a weighted average of the stage 2 and 3 predicted positions. The stages in this fit are constrained to have the same values of $d_i$, such that $I_c$ differs by exactly 3.354 Å for the two stages. Although a slight improvement in the fit can be obtained by allowing the gallery heights to differ, GICs are known to show similar gallery compositions and

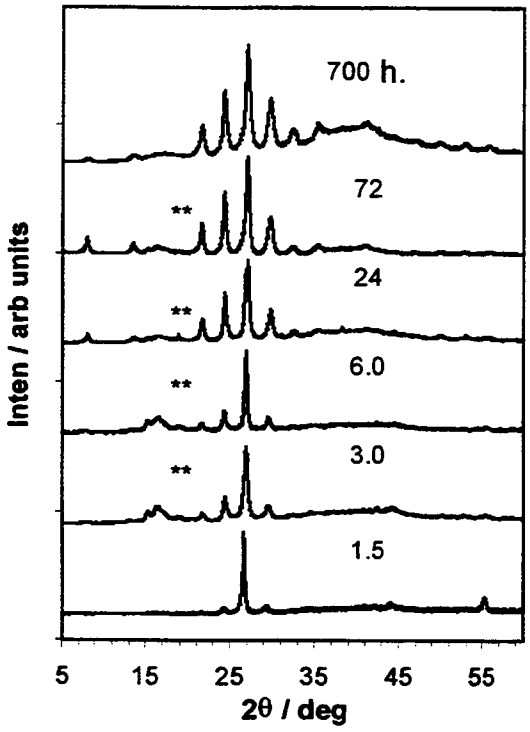


**Figure 2.2** PXRD obtained at various reaction times for $C_xPFOS$ obtained by reaction of SP-1 graphite with a solution of $KC_8F_{17}SO_3$ and $K_2MnF_6$ in 48 % hydrofluoric acid at 20 °C. The starred reflections at approx. 5.8 and 5.5 Å are ascribed to a $C_xF$ impurity.

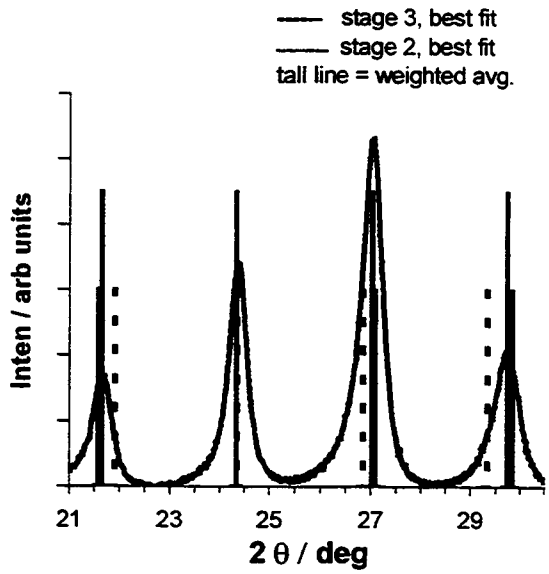


**Figure 2.3** Calculated diffraction peak positions for stage 2, stage 3, and the 0.7 : 0.3 weighted average. The PXRD pattern overlay is that observed for the product after 72 h. reaction using hydrofluoric acid.

**Table 2.1** Peak position fits for stage 2 and stage 3 $C_x$PFOS, and a weighted average. This solid product was prepared after 72 h. reaction in hydrofluoric acid. The calculated root-mean-square deviations and lattice parameters are given for each case.

| | stage 2 | | stage 3 | | stage 2 / 3 |
|---|---|---|---|---|---|
| **d obs / Å** | **index** | **d calc / Å** | **index** | **d calc / Å** | **d calc / Å** |
| | | | | | |
| 4.105 | *(008)* | 4.115 | *(009)* | 4.058 | 4.103 |
| 3.653 | *(009)* | 3.658 | *(0010)* | 3.653 | 3.657 |
| 3.299 | *(0010)* | 3.292 | *(0011)* | 3.321 | 3.298 |
| 3.005 | *(0011)* | 2.993 | *(0012)* | 3.044 | 3.004 |
| | | | | | |
| RMS dev. | | 0.018 | | 0.064 | 0.005 |
| $I_c$ calc | | 32.921 | | 36.526 | 32.971 |

dimensions for stages > 1. In the example given, the best fit was obtained using the combination of 79 mol % stage 2 and 21 mol % stage 3.

Two different structural models can be used to interpret these peak position data. The product may be modeled as containing either (1) a physical mixture of these stages, with overlapping peaks contributing to an averaged position, or (2) a solid solution of 2$^{nd}$ and 3$^{rd}$ staging, viz. a structure where either 2 or 3 graphene layers may separate the intercalated galleries. In the latter case, the staging sequence may exhibit some degree of ordering for the 2 or 3 graphene layers between galleries, or be entirely random. These different models are depicted in Figure 2.4.

In a physical mixture, the calculated weighting factor is approximately the relative abundance of each stage. In the solid solution model, the fractions of 2$^{nd}$ staging and 3$^{rd}$ staging content derived from peak positions will indicate the probability of either 2 or 3 graphene layers, respectively, between occupied galleries in the product. An assumption made in either case is that the overlapping peaks from the different stages have similar intensities. This is only approximately true, but the actual calculated peak intensities from this structural model, described below, can provide a more accurate composition.

Since $d = c / l$ for (00*l*) Bragg reflections of a given stage, the stage (n + 1) phase with the same value of $d_i$ will generate reflections at:

$$d\,'(00l) = (c + 3.354\,\text{Å}) / l \qquad (2.9)$$

The overlap of reflections from these phases can be described by the minimum separation, Δ, between calculated peak positions for the two patterns. This function has

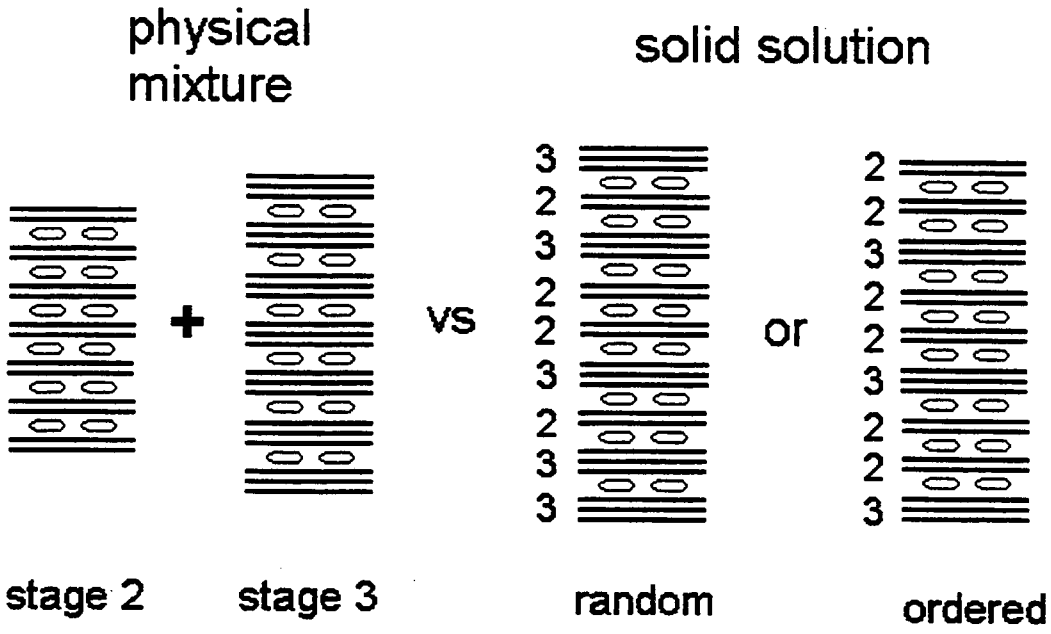


**Figure 2.4** Schematic representations of GICs containing of a physical mixture of stage 2 and 3, and random or ordered solid solutions of 2$^{nd}$ and 3$^{rd}$ staging.

minima at d = 3.35 Å and 1.68 Å in the diffraction region investigated (see Figure 2.5), corresponding in the calculated example to the overlap of stage 2 *(0,0,l)* reflections with stage 3 *(0,0,l + 1)* reflections, and the overlap of stage 2 *(0,0,l)* with stage 3 *(0,0,l + 2)* reflections, respectively. The calculated peak separations at 5 – 15 ° 2θ indicate that the reflections from a physical mixture should be clearly resolvable, with peaks separated 1 – 2 ° 2θ. In each pattern obtained, however, only single reflections occur at low angle (Figure 2.6), indicating that these patterns do not arise from physical mixtures of the stages. These results, in combination with evidence from peak broadening (described below), indicate that these products are solid solutions containing 2$^{nd}$ and 3$^{rd}$ staging.

Two separate effects may be considered for contributing to peak broadening in solid solutions of stacking arrangements, (1) a Williamson-Hall broadening that relates increasing peak width to the finite coherent domain size and lattice strain in the stacking direction, and (2) a broadening due to the disordered presence of the two component sequences (in this case, stage 2 and stage 3). It is expected that each of these may contribute to the overall FWHM for each reflection. The first effect will generate symmetric peak profiles with FWHM increasing as 4 sin θ. The second effect was here evaluated by generating recursive structural models for solid solutions containing 2$^{nd}$ and 3$^{rd}$ staging, and examining peak profiles obtained from the calculated patterns. The broadening calculated for the disordered solution has a similar periodic variation to the function Δ defined above, with minima at d = 3.35 and 1.68 Å, but is of lesser magnitude and generates asymmetric profiles for some peaks.

A Williamson-Hall plot (Figure 2.7) for the $C_x$PFOS product obtained following 72 h. reaction in hydrofluoric acid shows that peak broadening does not follow the simple

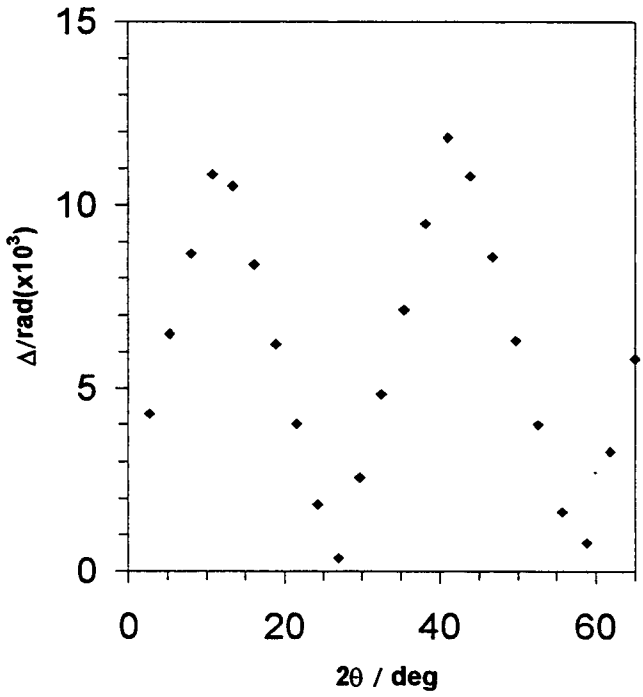


**Figure 2.5** Plot of the minimum separation of peak positions (in radians), Δ, vs. 2θ, where Δ is calculated for diffraction peaks of stage 2 and 3 GIC's with $d_i$ = 33 Å. The minima near 4 sinθ = 1 and 2 arise from the overlap of stage 2 *(0,0,l)* with stage 3 *(0,0,l + 1)*, and stage 2 *(0,0,l)* with stage 3 *(0,0,l + 2)*, respectively.

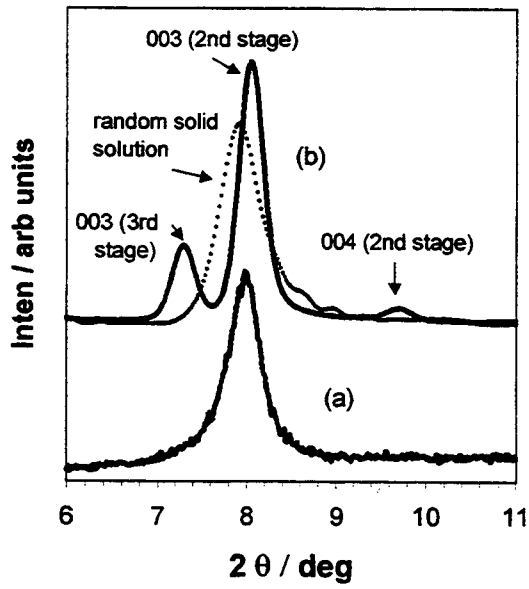


**Figure 2.6** PXRD profiles (a) observed for $C_xPFOS$ after reaction for 72 h. in hydrofluoric acid, and (b) calculated for mixed phase and solid solution models. The solid line in (b) is for a physical mixture of stage 2 (70 %) and stage 3 (30 %), and the dotted line is for a random solid solution with those staging mole percents.

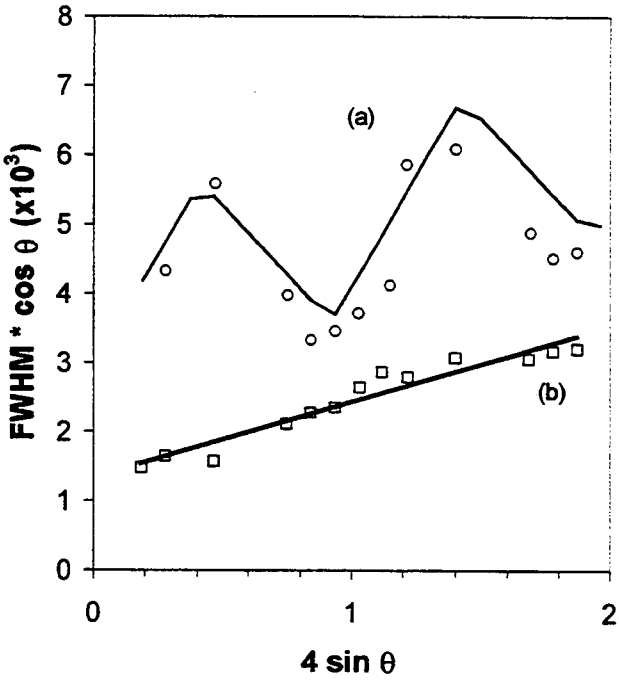


**Figure 2.7** Williamson-Hall plots for two $C_x$PFOS products. In (a), PXRD data (open circles) and the calculated trend (see text) are for a solid solution obtained from hydrofluoric acid . In (b), PXRD data (open squares) and a best-fit line are for a product from hydrofluoric acid / nitric acid (17:83 v / v). FWHM is the full width at half peak maximum expressed in radians.

linear trend from the domain-strain effect. The peakwidths obtained clearly show the periodic variation expected for a solid solution. The experimental values are seen to conform well to a fit using a combination of both broadening effects, a periodic variation overlying a linear increase due to a domain/strain effect, and the fit for this product is obtained using a random sequencing of $2^{nd}$ and $3^{rd}$ staging with a coherent domain size of approx. 1000 Å. In marked contrast, the product obtained from a mixed acid solution (preparation described below), which is satisfactorily indexed as a simple stage 2 GIC, shows a good fit to the Williamson-Hall relation. The peak broadening data thus support a random solid solution model for the products obtained from hydrofluoric acid. Although degree of short-range ordering in the stacking direction might occur for each domain, the fit obtained using a completely random stacking sequence is not significantly improved by allowing such ordering.

After each reaction time studied, the products are best fit as a solid solution containing a random combination of $2^{nd}$ and $3^{rd}$ staging. Using the fitting method described above for peak positions, the fractional mole content for each staging component is obtained, and these, along with the calculated $d_i$ values and mass uptakes, are plotted against reaction time. (Figure 2.8) As can be seen, at 20 °C the $2^{nd}$ staging content increases to a maximum of 80 % after approximately 100 h. No subsequent increase in the $2^{nd}$ staging content occurs even after reaction for 4 weeks, although the product obtained continues to increase in mass.

At 50 °C, the rate of intercalation increases significantly. The maximum intercalant content arises at approx. 1 – 10 h., and PXRD patterns and mass uptakes for this product are similar to those at 20 °C. After 170 h. reaction at 50 °C, a decrease in

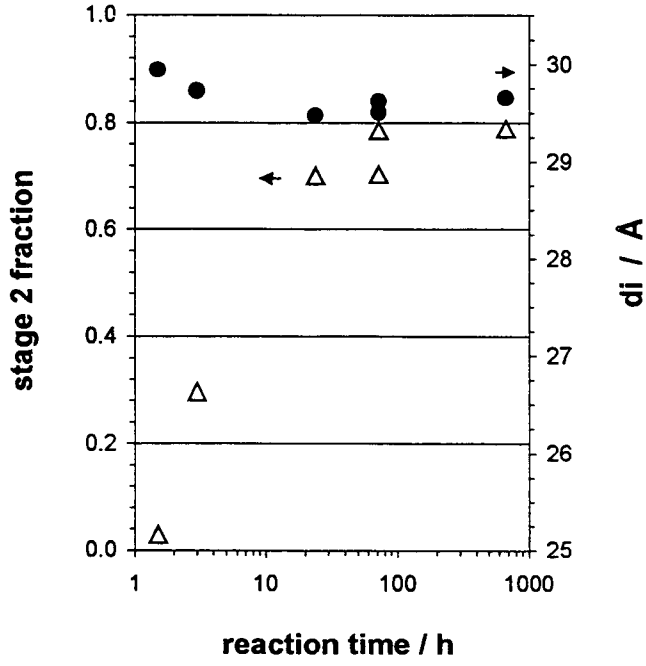


**Figure 2.8** $2^{nd}$ staging content (remainder is $3^{rd}$ staging) and $d_i$ calculated from PXRD peak positions at various reaction times, (a) at 20 °C, and (b) at 50 °C. Mass uptakes for these products ( ■ = 20 °C, O = 50 °) are shown in (c).

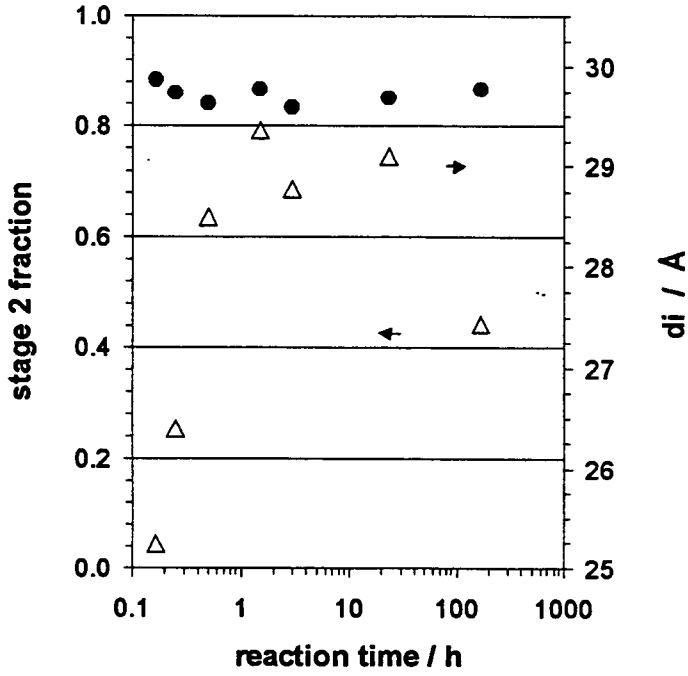
1.0
0.8
0.6
0.4
0.2
0.0
stage 2 fraction
30
29
28
27
26
25
di / A
0.1
1
10
100
1000
reaction time / h

**Figure 2.8 (b)**

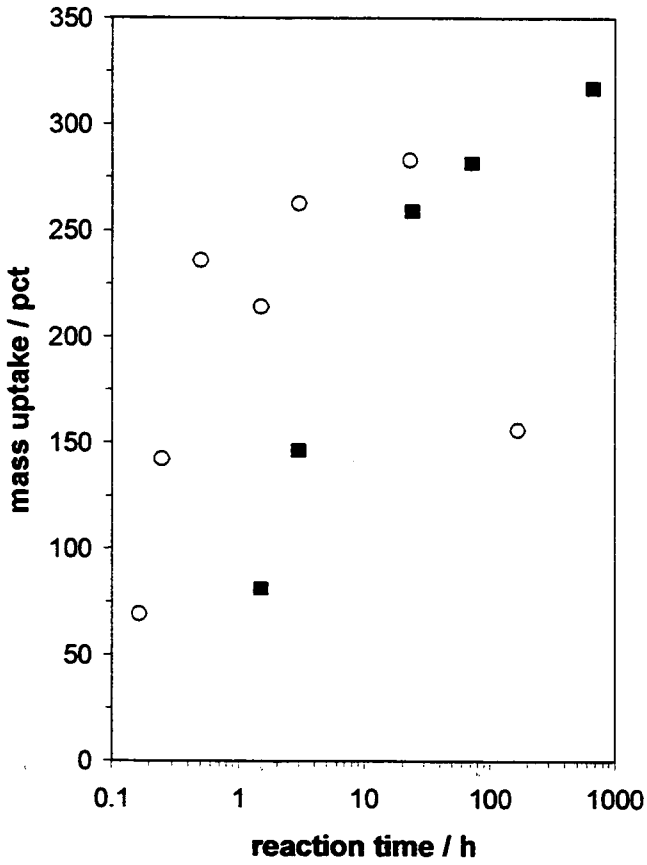
350
300
250
200
150
100
50
0
mass uptake / pct
0.1
1
10
100
1000
reaction time / h

**Figure 2.8 (c)**

both the 2nd staging content and the product mass indicate a loss of intercalant. At 70 °C, similar results are obtained, again with no evidence for the formation of a simple stage 2 $C_x$PFOS.

The loss of intercalant at long reaction times and higher temperatures is related to the instability of the oxidant in hydrofluoric acid at these temperatures. The solution gradually loses the bright yellow color associated with $MnF_6^{2-}$ after the maximum intercalant content is obtained, and an amorphous solid residue containing Mn, is produced. Although $C_x$PFOS is very stable in air over this time period, [19] this is not true in either liquid water or hydrofluoric acid. The air stability most likely originates from the formation of hydrophobic particle surfaces by $C_8F_{17}SO_3$, which can form a low surface energy monolayer and shield the positive graphite sheets effectively from water vapor in air. AFM studies have shown such an organized structure of PFOS forming at a graphite – solution interface. [20] In neat aqueous HF, however, the transition from stage 3 to a high stage will take place within several hours. When $K_2MnF_6$ is added to hydrofluoric acid, $C_x$PFOS is stabilized by re-oxidation, and will remain unchanged while the oxidant is present in solution. The decomposition of $K_2MnF_6$ at elevated temperature will therefore allow GIC reduction to proceed.

All the PXRD patterns show additional reflections at 5.8 and 5.5 Å, which occur in the region typical of (00*l*) reflections from layered graphite fluorides. The relation of peak position in this region to composition has been evaluated previously. [21,22] The peak at 5.8 Å can be identified with an approximate composition of $C_3F$. The peak close to 5.5 Å overlaps with (006) from the $C_x$PFOS phase, but should correspond to a planar-sheet graphite fluoride, $C_xF$, $x \cong 4$. Products obtained using natural graphite (1 μm part.

dia.) have greater intensities for these peaks than those derived from SP-1 graphite (100 μm part. dia.), suggesting that the side products arise at the particle edges. At 20 °C these impurity peaks are somewhat variable in intensity, but are often only a few percent of the total diffracted intensity. At a reaction temperature of 70 °C these peaks become similar in intensity to the strong peaks for $C_xPFOS$ between 20 and 30 ° 2θ. (Figure 2.9)

The use of aqueous media for graphite intercalation is clearly restricted to acidic solutions due to the high potential required for graphite oxidation. Concentrated acids, such as fuming $H_2SO_4$ and 97 % $HNO_3$, have long been used to prepare GICs of their conjugate anions. [2-4,23] Using the Nernst relation for the dependence of the water oxidation on activities of water and hydronium ion, an approximate relation for thermodynamic potential for oxidation of water in concentrated acid is:

$$E \cong 1.23\ V - (0.059\ V) \log H_0 \qquad (2.10)$$

where $H_0$ represents the Hammett acidity function for a given acid solution. Figure 2.10 illustrates these derived potentials in relation to the potential ranges for various stages of $C_xAsF_6$. The potential ranges for stage formation are derived from the quasi-equilibrium galvanostatic oxidation of graphite in anhydrous HF [24]. These potential–stage relations are well-defined for that system, but should be considered only as representative values here because the potentials depend to some extent on the nature of the intercalating anion. Still, it is reasonable to suggest from this relation that 48 % HF ($H_0 \cong -4$) [25] is sufficiently stable towards oxidation to allow formation of stage 2 or higher GICs.

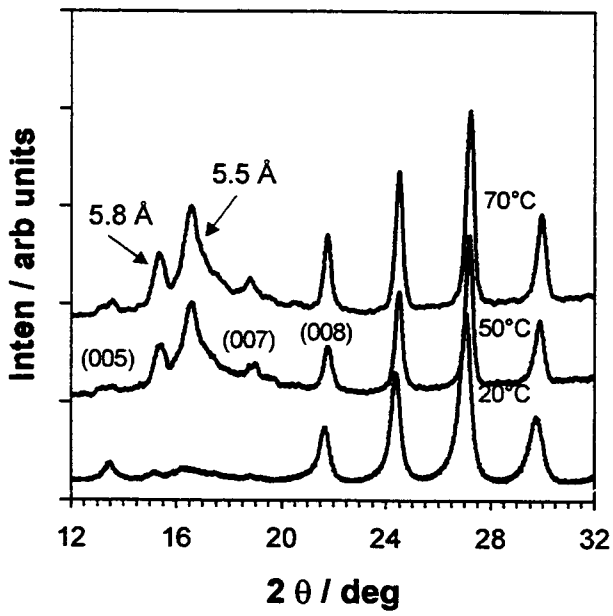


**Figure 2.9** PXRD patterns for solid products obtained in hydrofluoric acid at 20, 50, and 70 °C. Reaction times are 24 h. at 20 °C, and 15 – 30 min. at 50 ° and 70 °C.

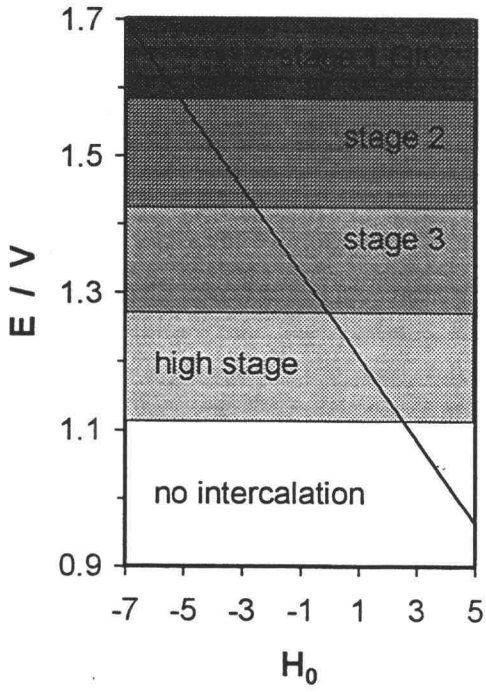


**Figure 2.10** Approximate potential ranges for GIC stages. The solid line indicates the oxidation potential of water vs. $H_0$.

The solid solution of stage 2 and 3 GIC described above is an example of a stable stage disorder, for it represents a product obtained at long reaction time without rearrangement to a simple integral stage or mixture of stages. Evidence for GICs with highly-ordered fractional stages is not common, but there have been such observations for the donor-type GIC $C_xK$. A highly-ordered stage 4/3 (that is, a repeat sequence of three intercalated then one empty gallery) was obtained by electrochemical reduction in THF, [26] and the existence of a 3/2 fractional stage at high pressure was confirmed by PXRD. [27] In these cases, the chemical potential energy of the fractional stages must be sufficiently different to permit the stabilization relative to an integral stage. There are several reports, however, of highly disordered staging for both donor and acceptor-type GICs. For example, Huaw et al reported the coexistence of several phases for single-crystal graphite intercalated with $CuCl_2$, [28] and Thomas et al reported TEM images of disordered staging for a fine natural graphite powder intercalated with $FeCl_3$. [29] In some cases, stage disorder may well result from incomplete reaction kinetics, especially where the experiment involved the use of a highly-crystalline graphite.

The disordered staging observed in these $C_x$PFOS products appears to derive from the limiting oxidative stability of the solvent rather than slow kinetics associated with rearrangement of large anions in these intercalated bilayers. This is supported by the formation of these same solid solution products within several hours at elevated temperature, as well as by the rapid formation of simple stage 2 GIC's in mixed acids solutions described below.

Two energetic factors have been associated of the ordering of GICs into stages, the coulombic repulsion of intercalated galleries and the elastic strain energy required to

mechanically surround the intercalated domains by graphene layers. The unusual bilayer arrangement of anions, and associated large gallery height for $C_xPFOS$, will change the contribution of these terms significantly from that in most acceptor-type GICs. Despite the large volume of the $C_8F_{17}SO_3$ anion, the bilayer arrangement actually allows a relatively high charge density on the graphene layers, as can be gauged in low value of x considering the stage assignments. The correspondingly high positive charge density on the encasing graphene sheets will result in a repulsive term between graphene sheets that can be comparable to that in compounds such as $C_xSO_3F$, where $x \cong 7$ for stage 1. [30] The intercalant bilayers of $C_8F_{17}SO_3$ will likely mitigate coulombic repulsion through the $C_xPFOS$ galleries, but the predominant repulsive energy term that favors staging does not require a long-range interaction of that type. As for the mechanical elastic energies, it is difficult at this point to assess how these are affected, or even if the Daumas-Herold domain model can be employed with such large galleries.

Mass uptake, TGA, and elemental analyses on the products provide information on the product stoichiometries and identity of intercalating species. Four mass loss regions between 25 °C and 900 °C are seen in the TGA traces of GICs prepared in hydrofluoric acid. (Figure 2.11) The first loss, below 120 °C, ranges from 0.5 – 3 mass percent, with longer reaction times associated with a greater mass loss. The PXRD patterns do not significantly change after heating briefly in this temperature range, and the mass loss is ascribed to intercalated or surface-adsorbed $H_2O$ or HF. The next two regions occur between 150 – 200 °C and 400 – 500 °C, with the former accounting for the majority of the mass loss. After heating at 300 °C, the GICs show only a broad reflection due to poorly crystalline graphite, so the ordered GIC structure has disappeared

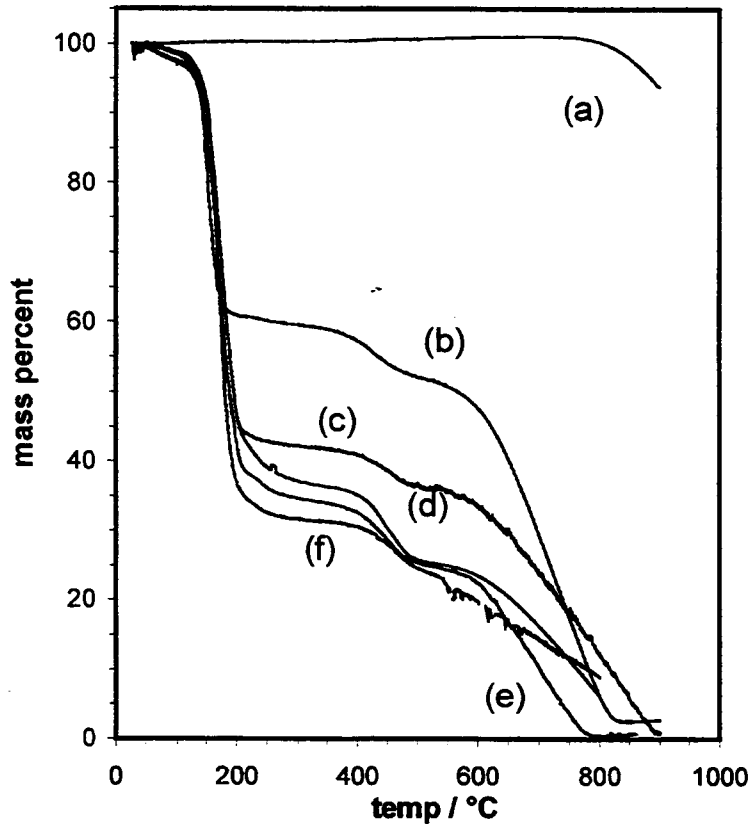


**Figure 2.11** TGA curves (a) graphite, and $C_x$PFOS prepared in hydrofluoric acid after the following reaction times; (b) 1.5, (c) 3, (d) 24, (e) 72, and (f) 700 h.

by this temperature. For comparison, $KC_8F_{17}SO_3(s)$ shows a sharp mass decrease beginning at 420 °C. (Figure 2.12) The remaining carbonaceous material is completely volatilized during the final mass loss beginning at 600 °C. This can be compared to graphite, which under these experimental conditions begins to lose mass at 650 - 800 °C. The presence of a small $O_2$ impurity in the $N_2$ purge gas is responsible for the combustion of graphitic carbon.

DSC analyses on KPFOS (Figure 2.12) show a complex exothermic decomposition for the salt beginning at 420 °C. The $C_x$PFOS samples present several thermal events between ambient and 500 °C. The first is a broad endotherm between approximately 50 and 250 °C, within which occurs a large, relatively sharp, exothermic peak with onset at 130 °C. The endotherm is related to volatilization of species from the first two mass loss events noted above, and the sharp exotherm indicates a decomposition reaction of the GIC in mass loss region 2. The two exotherms observed between 400 and 500 °C are similar to those of KPFOS, and suggest that mass loss in region 3 is related to $C_8F_{17}SO_3^-$ decomposition exterior to the graphite structure. This agrees with the loss of an ordered structure in samples annealed above 300 °C.

The mass uptake data are compared with the combined TGA mass losses below 500 °C in Table 2. The general similarity in mass uptake and loss indicates that these mass losses arise from the degradation of the anions to volatile species, without significant loss of graphene carbon. For this reason, the TGA loss data are taken as an approximate indicator of product stoichiometry, and the calculated mole ratios of graphene C to $C_8F_{17}SO_3^-$ are reported in the Table. An exception occurs after long reaction time at 50 °C, where the precipitation of a manganese-containing byproduct

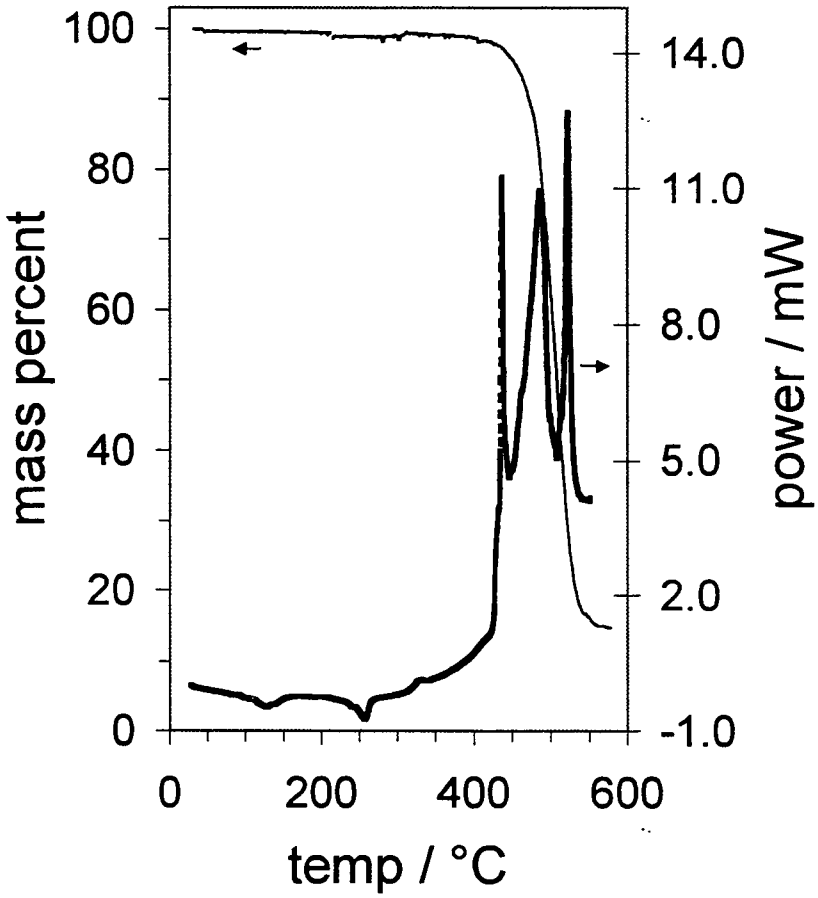


**Figure 2.12** DSC and TGA curves for (a) KPFOS and (b) $C_x$PFOS prepared in hydrofluoric acid (reaction time = 72 h.)

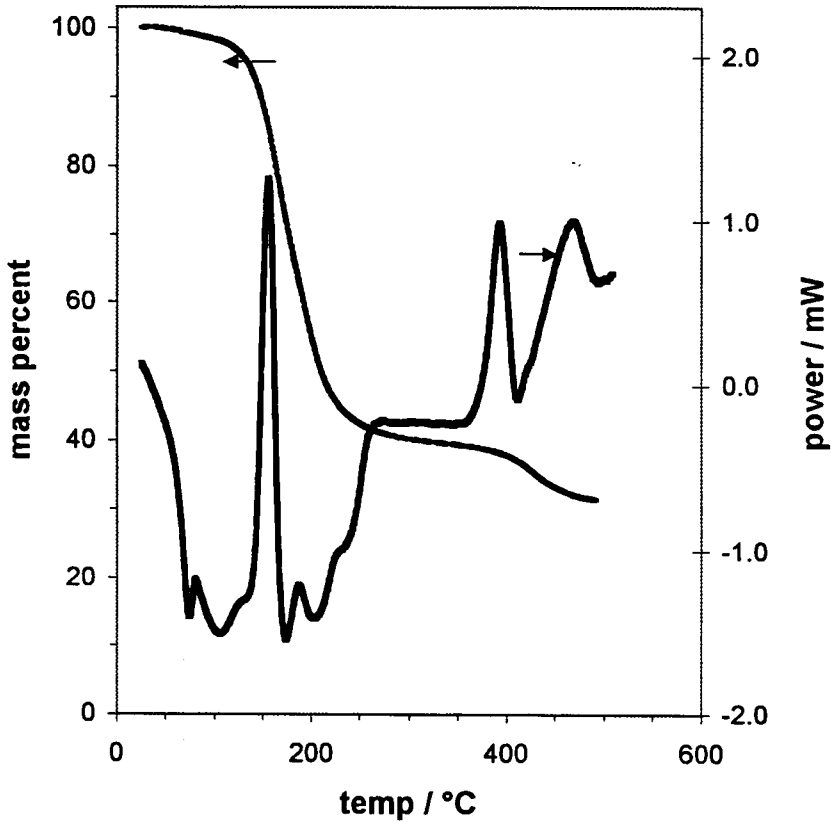
100
80
60
40
20
0
mass percent
2.0
1.0
0.0
-1.0
-2.0
power / mW
0
200
400
600
temp / °C

**Figure 2.12 (b)**

**Table 2.2** Compositional data from mass uptake, TGA, and elemental analyses, for $C_xPFOS$ prepared in hydrofluoric acid or a hydrofluoric acid / nitric acid co-solvent.

| **HF / $HNO_3$ v / v [1]** | **temp. / °C** | **time / h.** | **intercalant / C g / g** | | **C / $C_8F_{17}SO_3$ mol / mol [2]** | **composition [3]** |
|---|---|---|---|---|---|---|
| | | | by mass uptake | by TGA | | by elem. anal. |
| | | | | | | |
| 100 / 0 | 20 | 1.5 | 0.81 | 0.83 | 61.0 | |
| " | " | 3.0 | 1.46 | 1.45 | 33.0 | |
| " | " | 24 | 2.59 | 2.57 | 18.6 | |
| " | " | 72 | 2.82 | 2.56 | 18.7 | $C_{28.2}C_8F_{17}SO_3 \cdot 4.8F$ |
| " | " | 700 | 3.17 | 2.94 | 16.3 | |
| | | | | | | |
| 100 / 0 | 50 | 0.1 | 0.3 | 0.40 | 136 | |
| " | " | 0.3 | 1.42 | 1.87 | 25.6 | |
| " | " | 0.5 | 1.49 | 1.84 | 27.2 | |
| " | " | 1.5 | 2.14 | 2.45 | 19.6 | |
| " | " | 3.0 | 2.15 | 2.25 | 21.3 | |
| " | " | 24 | 2.83 | 2.89 | 16.6 | |
| " | " | 170 | 1.56 | 5.02 | 9.6 | |
| | | | | | | |
| 17 / 83 | 20 | 24 | 2.25 | 2.70 | 17.7 | $C_{22.2}C_8F_{17}SO_3 \cdot 4.0F$ |
| 33 / 66 | " | 24 | 2.63 | 2.66 | 18.0 | |
| 50 / 50 | " | 24 | 2.21 | 2.72 | 17.6 | |
| 87 / 13 | " | 24 | 2.16 | 1.86 | 25.8 | |

1. Indicates relative vol. pct. added of 48 % aqu. HF and 69 % $HNO_3$.
2. Calculated from TGA data as x in $C_xC_8F_{17}SO_3$ A4F.
3. Based on elemental analyses for C, S, N, and F.

leads to a significant overestimate by TGA of the intercalant content. Table 2 includes compositional data from elemental analyses that indicate significant excess of F relative to S in the compounds. There is an impurity of the fluorine-rich phases $C_xF$ ($x \cong 3 - 4$), which accounts for part of the excess fluorine. Structural refinement (see below) also shows excess electron density in intercalated galleries approx. 3 - 4 Å from each graphene carbon plane, which is ascribed to HF, fluoride, or bifluoride. In both analyses, the nominal compositions can be described as $C_xC_8F_{17}SO_3 \cdot yF$, with y ranging from 3 to 5. The calculated values for x, the molar ratio of graphene C to $C_8F_{17}SO_3$, in Table 2, therefore assume y = 4.

The minimum value obtained for x is approximately 16 - 19, which agrees well with the value x = 17 obtained previously for the stage 2 compound prepared by electrochemical oxidation of graphite in $CH_3NO_2$. [12] The GICs obtained by this chemical route have galleries approximately 3 Å smaller than those obtained by the electrochemical method, which suggests a significantly greater anion takeoff angle in the latter GICs. The principal compositional difference between these products is in the lack of excess fluoride in the electrochemical products, which appears to have a pronounced effect on the interaction of anions within the galleries.

The bilayer intercalant structure allows this relatively high intercalant content for the graphite galleries (approx. 1 anion / 10 graphene carbons). Based on the relation between $d_i$ and stage, the intercalant content, and volume (calculated at 344 $Å^3$ for $C_8F_{17}SO_3^-$), the gallery occupancies can be derived for different stage assignments. These are summarized in Table 3 for the pure stages and the solid solution model, and

**Table 2.3** Occupied volume fraction of expanded galleries calculated for different stage assignments. The fractional stage assignments reflect random solid solutions with probabilities of $2^{nd}$ staging : $3^{rd}$ staging :: 0.7 : 0.3.

| **possible stage assignment** | | **occupied volume fraction in gallery** | |
|---|---|---|---|
| integral stage | mixed stage (0.70 : 0.30 relative content) | | |
| 1 | | 0.28 | |
| | 1 / 2 | | 0.40 |
| 2 | | 0.66 | |
| | 2 / 3 | | **0.80** |
| 3 | | 1.13 | |
| | 3 / 4 | | 1.26 |
| 4 | | 1.52 | |

1. The occupied volume fraction is calculated using a composition of $C_{18}C_8F_{17}SO_3 \cdot 4F$, $d_i = 29.6$ Å, vol. $(C_8F_{17}SO_3) = 344$ Å$^3$, vol. (F) = 16 Å$^3$.

demonstrate that the assignment of the solid solution with 2nd and 3rd staging is in best agreement with the compositional data.

### 2.4.2 Products in aqu. HF / $HNO_3$ and aqu. HF / $H_2SO_4$

As noted above, the solvent oxidative stability can limit the extent of intercalation. Stage 1 GICs can be prepared in more highly concentrated acids, and a stage 1 $C_x$PFOS was prepared by electrochemical oxidation using organic solvents. For this reason, the addition of concentated nitric or sulfuric acid to hydrofluoric acid can allow a lower stage product to be obtained.

When we add $K_2MnF_6$ and $KC_8F_{17}SO_3$ to 69 % $HNO_3$ (all other reaction conditions maintained as above), a reddish-brown color, presumed due to Mn(III), is observed immediately in solution, and slowly disappears over several hours to give a colorless solution and amorphous precipitate. The instability of $K_2MnF_6$ in 69 % $HNO_3$ precludes the formation of a low stage GIC in this solvent. [31] PXRD on the solid products obtained from reaction of graphite with the reddish-brown solution show stage 3 graphite nitrate and several broad, unassigned peaks. Heating this product to 900 °C generates crystalline $Mn_3O_4$.

The oxidant $K_2MnF_6$ is stable in nitric acid, however, when hydrofluoric acid is a co-solvent. Table 4 provides a summary of PXRD peak position analyses from reactions containing 13 - 83 % (v / o) hydrofluoric acid in conc. $HNO_3$. In each case, the pattern fits well as a simple stage 2 GIC, with minimal contribution (0 – 6 %) due to other stages. A Williamson-Hall plot indicates a coherent domain length of 1200 Å, or approx.

**Table 2.4** Fractional stage content determined for $C_xPFOS$ prepared in hydrofluoric acid / nitric acid co-solvents. In each case, the products can be fit well by a simple stage 2 model.

| **HF / $HNO_3$ v / v *** | **reaction time** | **fractional content** | | |
|---|---|---|---|---|
| | | **stage 1** | **stage 2** | **stage 3** |
| | | | | |
| 83 / 17 | 24 h. | 0.03 | 0.97 | |
| 66 / 33 | 24 h. | | 1.00 | |
| 50 / 50 | 24 h. | 0.05 | 0.95 | |
| 13 / 87 | 24 h. | | 0.99 | 0.01 |
| 13 / 87 | 1 week | | 0.94 | 0.06 |

1. Indicates relative vol. pct. added of 48 % HF and 69 % $HNO_3$.

35 unit cell repeats, for the product obtained using 17 % HF. (Fig. 2.7b) In addition to the formation of stage 2 GIC rather than the solid solution, the products obtained within this range of solvent compositions are obtained at shorter reaction time than those prepared in hydrofluoric acid. Hence, stage 2 GICs appear within 24 h. at 20 °C.

Elemental analysis for N (< 0.1 %) in these products indicates that $NO_3^-$ (or $HNO_3$) accounts for at most 4 mol % of intercalant species relative to the $C_8F_{17}SO_3$ anion. Since stage 2 or 3 graphite nitrate compounds are obtained within 30 minutes by this method when the $C_8F_{17}SO_3$ salt is not present, the larger anion either prevents intercalation of nitrate, or exchanges for the nitrate anion at longer reaction times. Compositions determined for the products obtained using the acid mixtures are very similar to those obtained in hydrofluoric acid. (Table 2)

A similar phenomenon occurs by the addition of small amounts of $H_2SO_4$ to hydrofluoric acid. With a solvent composition of 17 % (v / o) fuming $H_2SO_4$, a stage 2 $C_xPFOS$ is obtained within 24 h. If the sulfuric acid content is increased, however, the GIC product stage increases and a graphite sulfate phase is observed by PXRD. The stage 1 graphite sulfate compound ($I_c \cong 8.0$ Å) is the only product obtained with the $H_2SO_4$ content above 50 %. For reaction times greater than 24 h., even with the lower $H_2SO_4$ content, the $C_xPFOS$ converts to graphite sulfate. Similarly, stirring a stage 2 $C_xPFOS$ (obtained by other means) in fuming $H_2SO_4$ at ambient temperature results in its conversion to stage 1 graphite sulfate within 30 minutes.

These results are consistent with previous findings that GICs of singly-charged anions are readily converted to graphite sulfate. For example, Avdeev, et. al., have described the exchange reaction to form graphite sulfate from graphite nitrate. [32] It is

likely that the favorable lattice enthalpy associated with sulfate within the intercalant gallery provides the driving energy for this displacement.

Details on the intercalated gallery structure are obtained by refinement of the stage 2 product obtained using 17 % $HNO_3$. As the anion length is approximately 15 Å, the gallery dimensions indicate that a bilayer intercalant structure is most reasonable. [9] The structural model employed places the three oxygens in each anionic $-SO_3$ headgroup in a plane parallel to graphite sheet, with hydrophobic fluorocarbon chains thus oriented towards the center of the gallery, as indicated in Figure 2.13. An initial take-off angle, or angle between anionic chain and graphene carbon plane, of 54 ° is obtained from the S-C-C bond angle for the energy-minimized isolated anion. Subsequent refinement of the PXRD data provides a slightly greater take-off angle of 57 °. This requires the bilayers to nestle into one another by 2 – 3 Å at the gallery center.

A 1D electron density map generated from diffraction data is compared to that calculated from the structural model in Figure 2.14. The greatest electron density, at $z \cong 0.05$ (and 0.95), derives from the graphene carbon planes. The sulfonate groups contribute most of the electron density near $z = 0.15$ (and 0.85), but additional electron density is required to fit the PXRD data. As a simple model, a single plane of F density is included at ≅ 3 - 4 Å above the graphene layers, with the position of this plane found by refinement. The F stoichiometry for the best fit lies in the range of $y = 3 - 5$ for $C_xC_8F_{17}SO_3 \cdot yF$, and $y = 4$ is used for subsequent refinement. Peaks at $z = 0.22$, 0.30, 0.38, and 0.45 arise from successive $-CF_2-$ or $-CF_3$ units along the anionic chains, and these planes of electron density are used to refine both the take-off angle and anion content in the galleries.

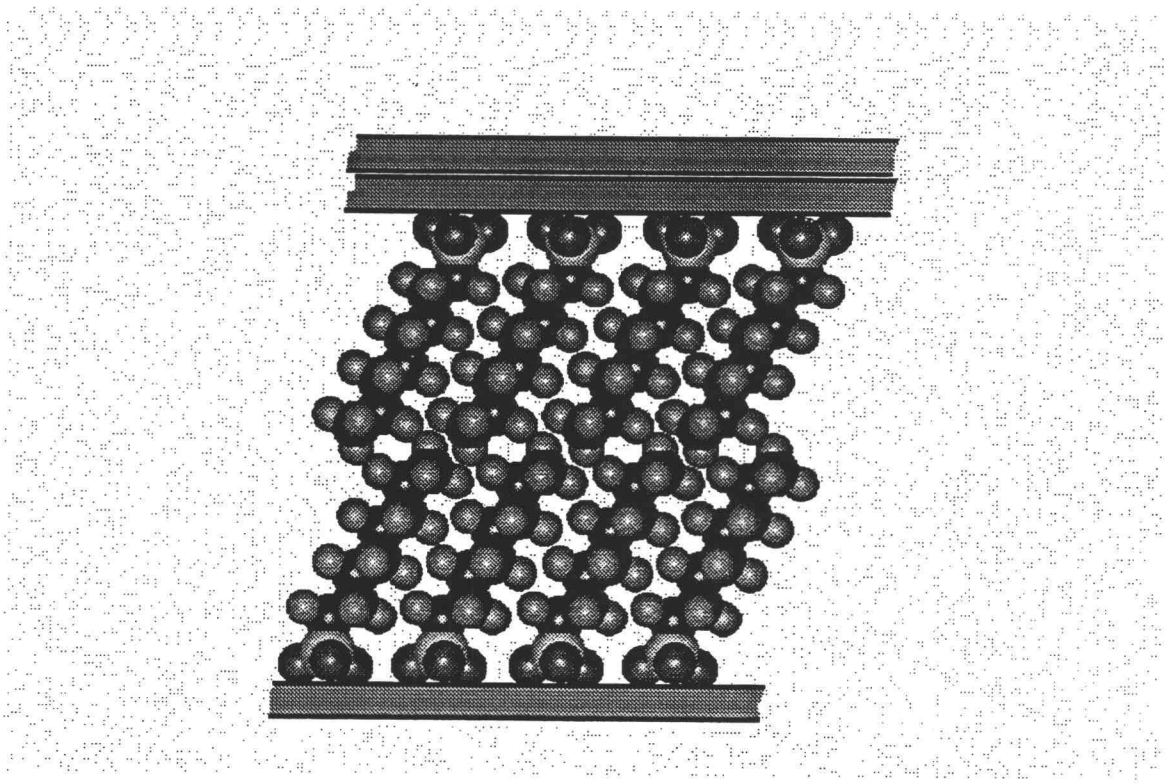

**Figure 2.13** The bilayer intercalant arrangement in $C_x$PFOS.

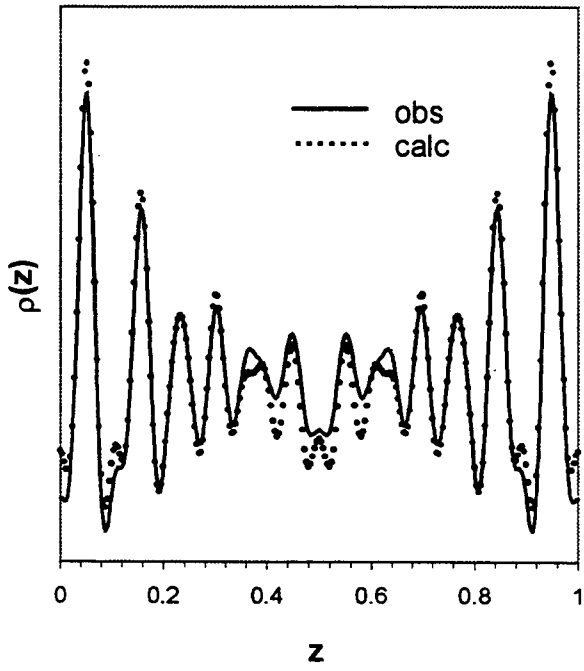


**Figure 2.14** Electron density map derived from PXRD data and calculated for refined structural model of $C_{21.6}C_8F_{17}SO_3 \cdot 4F$.

The electron density peak near z = 0.38 is notably broader than the others due to the inclusion of the branched isomer $(CF_3)_2C(F)C_5F_{10}SO_3^-$. This isomer contains two $-CF_3$ groups in the range $z \cong 0.38 - 0.41$. The isomeric content of the GIC may differ from that in the starting reagent due to selectivity during the intercalation process, and an improved fit to the data can be obtained by decreasing the linear isomer content below 70 %. In the model employed, however, the linear isomer content is maintained at 70 % and not further refined.

The four refined parameters and best fits obtained for the structural model are thus: the chain take-off angle (56.6 °), the graphene plane to sulfonate oxygen plane distance (3.04 Å), the graphene plane to fluoride plane distance (3.8 Å), and the graphene carbon / intercalant molar ratio (x = 21.6). These results provide a reliability factor R = 0.082 for $C_{21.6}C_8F_{17}SO_3 \cdot 4F$. Figure 2.15 shows the observed and calculated PXRD for the product using this structural model.

The value for x obtained agrees reasonably well with those found from gravimetry (x = 18) and elemental analyses (x = 22) (Table 2). The graphene plane - O distance conforms to the anticipated result, in comparison this distance is 3.2 Å for graphite nitrate (stage 2, $I_c$ = 9.9 Å). The graphene plane – F distance (3.8 Å), however, is somewhat larger than observed for other graphite compounds containing fluoride or bifluoride. Stage 1 planar-sheet graphite fluorides, $C_xF$, would have this distance at most in the range of 2.8 – 3.0 Å, assuming a central location of the fluoride in the galleries. [21] Due to the bilayer arrangement of fluoride in $C_xF$, and the semi-covalent nature of the C-F interaction, much smaller values for this distance are likely in the graphite fluorides. [33,34] Stage 2 graphite bifluoride exhibits $I_c$ = 9.83 Å, which can give a maximum

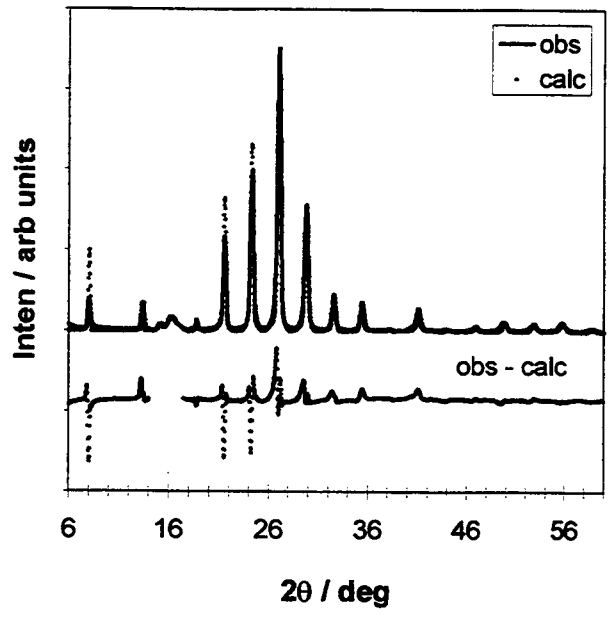


**Figure 2.15** Observed and calculated PXRD patterns for $C_xPFOS$ prepared by 24 h. reaction using 17 % (v / o) $HNO_3$ in hydrofluoric acid. Data between 14 and 17.5 °2θ were excluded due to peaks ascribed to a $C_xF$ impurity phase.

graphene plane – F distance of 3.24 Å. In graphite bifluoride compounds, the location of bifluoride at the gallery center is far more likely due to the less covalent nature of the interaction. The larger distance observed for $C_x$PFOS suggests weaker interaction between the positive graphene carbon sheet and the fluoride-containing species. Since the model employed does not distinguish fluoride from bifluoride (or HF), and there is also the possibility of a distribution of distances in the product, further analysis of the interaction will require additional investigation.

Although a reasonable fit is obtained given the data set and number of refinement parameters employed, there are additional considerations that may significantly improve the structural model. Calculations indicate that energy-minimized perfluorocarbon chains are helical rather than linear, although the twist may be reduced when shorter chains are packed together. [35] The twist angle for these chains, and other parameters, such as the content of branched chain isomer in the GICs, are not refined due to the limited data set obtained using these conditions. Preliminary calculations, however, suggest that these additional parameters should be included in a more sophisticated structural model when a higher-quality PXRD data set can be obtained.

## 2.5 Acknowledgement

The authors gratefully acknowledge support from NSF grant DMR-9419481. $^{19}$F NMR data were obtained at Portland State Univ. through Prof. Gary Gard. The authors also thank Prof. Gard, Prof. Douglas Keszler and Prof. Arthur Sleight at OSU for helpful discussions.

## 2.6 References


1. Daumas, N.; Herold, A. *C.R. Acad. Sci.* **1969**, *C268*, 373.
2. Bartlett, N.; McQuillan, B. in *Intercalation Chemistry*; Whittingham, S.; Jacobson, A., Eds.; Academic Press: New York, **1982**.
3. Zabel, H.; Solin, S. Eds. *Graphite Intercalation Compounds I*; Springer-Verlag: Berlin, **1990**.
4. Watanabe, N.; Touhara, H.; Nakajima, T.; Bartlett, N.; Mallouk, T.; Selig, H. in *Inorganic Solid Fluorides* Hagenmuller, P., Ed. Academic Press: New York, **1985**.
5. Guerard, D.; Herold, A. *Carbon* **1975**, *13*, 337.
6. Ozawa, K. *Sol. St. Ionics* **1994**, *69*, 212.
7. Markovsky, B.; Levi, M.; Aurbach, D. *Electrochim. Acta* **1998**, *43*, 2287.
8. Buckley, J.; Edie, D., Eds. *Carbon-carbon materials and composites.* Noyes Publ.: NJ, 1993.
9. Boehm, H.; Helle, W.; Ruisinger, B. *Synth. Met.* **1988**, *23* ,395.
10. Pinnavaia, T. *Science* **1983**, *220*, 365.
11. Jacobson, A. in *Intercalation Chemistry*; Whittingham, S.; Jacobsen, A., Eds.; Academic Press: New York, **1982**.
12. Zhang, Z.; Lerner, M. *Chem. Mater.* **1996**, *8*, 257.
13. Lemmon, J.; Lerner, M. *Carbon* **1993**, *31*, 437.
14. Lemmon, J.; Lerner, M. ACS National Meeting, San Diego, March, **1994.**
15. Bode, H.; Jenssen, H.; Bandte, F. *Angew. Chem.* **1953**, *65*, 304.

16. Williamson, G.; Hall, W. *Acta Metallurgica* **1953**, *1*, 22.

17. Su, Z.; Coppens, P. *Acta Crys.* **1997**, *A53*, 749.

18. Treacy, M. M; Newsam, J. M.; Deem, M. W. *Proc. R. Soc. Lond. A* **1991**, 433, 499.

19. $C_x$PFOS shows 94 % phase retention after 16 days in humid air. The exceptional air stability of this GIC will be reported separately.

20. Lamont, R.; Ducker, W. *J. Coll. Inter. Sci.* **1997**, *191*, 303.

21. Mallouk, T.; Bartlett, N. *J. Chem. Soc. Chem. Commun.* **1983**, 103.

22. Hagiwara, R.; Lerner, M.; Bartlett, N. *J. Chem. Soc., Chem. Commun.* **1989**, 573.

23. Ubbelohde, A. *Proc. R. Soc. London A* **1968**, *304*, 25.

24. Lerner, M. Ph.D. thesis, UC Berkeley, **1988**.

25. Bell, R.; Bascombe, K.; McCoubrey, J. *J. Chem. Soc.* **1956**, 1286.

26. Marcus, B.; Touzain, P. *Synth. Met.* **1988**, *23*, 13.

27. Fuerst, C.; Fischer, J.; Axe, J.; Hastings, J.; McWhan, D. *Phys. Rev. Lett.* **1983**, *50*, 357.

28. Hauw, C.; Gaultier, J.; Flandrois, S.; Gonzalez, O.; Dorignac, D.; Jagut, R. *Synth. Met.* **1983**, *7*, 313.

29. Thomas, J.; Millward, G.; Schlogl, R.; Boehm, H. *Mat. Res. Bull.* **1980**, *15*, 671.

30. Aubke, F.; Karunanithy, S. *J. Chim. Phys.* **1984**, *81*, 827.

31. If a stable oxidant is used, $C_xC_8F_{17}SO_3$ can be obtained in 69 % $HNO_3$. When graphite, excess $PbO_2$, and $KC_8F_{17}SO_3$ are added to hydrofluoric acid, the solid products contain stage 2 or 3 $C_xC_8F_{17}SO_3$, stage 2 graphite nitrate and $PbO_2$.

Interestingly, the $C_xC_8F_{17}SO_3$ is stable in the acid as long as $PbO_2$(s) is present, but reverts back to graphite within 2 hours in neat 69 % $HNO_3$.

32. Avdeev, V.; Sorokina, N.; Nikolskaya, I.; Monyakina, L.; Voronkina, A. *Inorg. Mater.* **1997**, *33*, 699.

33. Mallouk, T. Bartlett, N. *Phil Trans. R.. Soc. Lond.* **1985**, *A314*, 179.

34. Matsuo, Y.; Segawa, M.; Sugie, M. *J. Fluo. Chem.* **1998**, *87*, 145.

35. Knochenhauer, G.; Reiche, J.; Brehmer, L.; Barberka, T.; Woolley, M.; Tredgold, R.; Hodge, P. *J. Chem. Soc., Chem. Commun.* **1995**, 1619.

# Chapter 3

## Graphite Intercalation of Bis-(trifluoromethanesulfonyl) Imide and Related Anions Containing Perfluoroalkanesulfonyl Substituents

Xuerong Zhang, Nipaka Sukpirom and Michael M. Lerner,*
*Department of Chemistry and Center for Advanced Materials Research,*
*Oregon State University,*
*Corvallis, OR 97331-4003, USA.*

**Submitted to Mater.Res.Bull. for publication in 1999**

## 3.1 Abstract

Graphite intercalation compounds (GICs) containing the bis(trifluoromethanesulfonyl) imide anion, $C_xN(SO_2CF_3)_2$, were prepared under ambient conditions in 48% hydrofluoric acid, using the oxidant $K_2MnF_6$. Within seconds, the graphite phase was no longer observed, and a stable, stage 2 product with $x = 37$ and $d_i = 8.1$ Å was obtained in 15 minutes. Product compositions were evaluated by powder X-ray diffraction (PXRD), thermogravimetric analysis (TGA), differential scanning calorimetry (DSC) and elemental analyses. One-dimensional structural refinement for the stage 2 product provided values for the graphene carbon/intercalant molar ratio, distance between graphene and sulfonate oxygen planes, and the anion orientation within the intercalated galleries. Intercalation reactions with the larger fluoroanions bis(pentafluoroethanesulfonyl) imide $(CF_3CF_2SO_2)_2N^-$, trifluoromethanesulfonyl-*n*-nona-fluorobutanesulfonyl imide $(CF_3SO_2)(CF_3(CF_2)_3SO_2)N^-$, and tris(trifluoromethanesulfonyl) methide $(CF_3SO_2)_3C^-$ occurred but were dramatically slower. For each product, stages and $d_i$ were determined for the mixed phase products. In all cases with the larger anions, the products obtained also contained unreacted graphite.

## 3.2 Introduction

Graphite can undergo intercalation chemistry by either oxidation or reduction of the carbon layers and concomitant insertion of anions or cations between graphene sheets. A wide range of graphite intercalation reactions and compounds have been studied [1,2]. In addition to the basic research interest in GICs and their associated chemistry, some of these compounds have electrochemical properties that have been evaluated or commercialized in charge storage devices [3-5]. GICs are also important as precursors to malleable graphite forms [6]. New practical and scalable synthetic methods need to be developed in order to expand these applications and develop new ones.

The anions known to intercalate graphite are mostly fluoro-, oxo-, or chlorometallates with 4 – 6 highly electronegative ligands around a central metal. More recently, a few carbon-based anions have also been demonstrated to form GICs. These anions include perfluoroalkylsulfonates ($C_nF_{2n+1}SO_3^-$, n = 1 [7], 4, 6, or 8 [8-11]), trifluoroacetate ($CF_3COO^-$) [12], and formate ($HCOO^-$) [13]. These syntheses involved the electrooxidation of graphite in either the neat acid or a solution of the acid or related salt in an oxidatively stable organic solvent.

The electrochemical method for GIC synthesis has some advantages, particularly in the coulometric control over reaction rate and progress, and the ready preparation of intermediate phases. With larger anions or less stable electrolytes, however, this method is inherently limited by the large overpotential that develops at the carbon surface, which results in low charge efficiencies at high rate, and requires very low charge densities to prepare low stage compounds. In addition, the very high potential required for graphite

oxidation limits the selection of binders, electrolytes, and current collectors. For these reasons, scalable electrochemical reactions are unlikely to be realized for many GICs, and it is preferable to find chemical routes for their bulk preparation.

We have recently demonstrated [11] a convenient chemical method to obtain $C_xC_8F_{17}SO_3$, using a soluble Mn(IV) ion, $MnF_6^{2-}$, as the oxidant in hydrofluoric acid. This GIC contains a bilayer structure that leads to very expanded galleries, with approximately 30 Å between carbon sheets encasing the anions. At 20°C, a GIC between stage 2 and 3 is obtained in approximately 50 h, and the same product can be prepared in 1 h at 50°C.

The very strong electron-withdrawing nature of the perfluoroalkylsulfonyl group, due to a highly delocalized electronic structure, leads to the stabilization of the anions bis(trifluoromethanesulfonyl) imide $(CF_3SO_2)_2N^-$ and tris(trifluoromethanesulfonyl) methide $(CF_3SO_2)_3C^-$. The Li salts of these anions are very oxidatively stable, thermally stable above 200°C, and therefore readily dried, and form highly conductive solutions in organic solvents and polymer electrolytes. For these reasons, their application in lithium batteries has been evaluated by a number of groups [14,15]. Their oxidative stability and solubility also suggest that these anions can readily form GICs.

In this study, we report for the first time the chemical intercalation of these and the related fluoroanions, bis(pentafluoroethanesulfonyl) imide $(CF_3CF_2SO_2)_2N^-$, and trifluoromethanesulfonyl-*n*-nonafluorobutanesulfonyl imide $(CF_3SO_2)(CF_3(CF_2)_3SO_2)N^-$.

## 3.3 Experimental

Hydrofluoric acid (Mallinckrodt AR, 48% (w / o)) was used as received. Bright yellow $K_2MnF_6$ powder was synthesized according to a literature method [16] by reduction of $KMnO_4$ (EM Science GR) with $H_2O_2$ (Mallinckrodt AR, 30 % in aqueous solution). Two types of graphite reagent were used: SP-1 powder (Union Carbide, 100 μm average particle diameter) and natural graphite flakes (Aldrich, 1-2 μm).

Intercalant anion sources were the $LiN(SO_2CF_3)_2$ (3M), $LiC(SO_2CF_3)_3$ (Covalent Assoc., 99%), $LiN(SO_2CF_2CF_3)_2$, (3M), $LiN(SO_2CF_3)(SO_2(CF_2)_3CF_3)$ (Central Glass Co., Japan). All reagents were used as received.

In a typical reaction, the intercalant anion salt and $K_2MnF_6$ were dissolved in hydrofluoric acid, and graphite was added to give molar ratios of approximately 12:1:1::C:Mn:anion. For example, $LiN(SO_2CF_3)_2$ (200 mg, 0.70 mmol) and $K_2MnF_6$ (180 mg, 0.70 mmol) were dissolved in 20 mL of hydrofluoric acid, then graphite (100 mg, 8 mmol) was added. The reactants were stirred under ambient conditions for the specified time, and then immediately filtered and rinsed with hydrofluoric acid to stop the reaction. The filtrate was briefly washed with hexane and dried overnight under vacuum. Products were stored under an inert atmosphere.

For some reagents, reactions were also carried out at 50 and 70°C, with fresh oxidant added to the solutions periodically. *Caution – heating hydrofluoric acid produces dangerous vapors and must be carried out under controlled conditions in a fume hood.*

PXRD data were collected on a Siemens D5000 powder diffractometer, using Cu Kα radiation, with 0.02° 2θ steps, between 1.5° and 60°. Collection times varied from 0.1 s/step for routine analyses to 1 s/step for data used in structural modeling. PXRD peak widths were analyzed according to the Williamson-Hall relation [17]; a plot of the peak full widths (in radians) at half maxima vs. sin θ provided the coherent domain size by extrapolation to θ = 0. Thermal analyses of powdered samples were carried out at 5°C / min under flowing $N_2$ using a Shimadzu TGA-50. Elemental analyses (C, H, N) were performed by Desert Analytics (Tuscon, AZ).

Energy-minimized structural models for the $N(SO_2CF_3)_2^-$ anion were calculated using Gaussian 94 and full geometry optimizations were carried out using density functional theory. Becke's three parameter hybrid functional method was employed using the non-local correlation from Lee, Yang and Parr (B3LYP) [18] and the split valence basis set 6-31G(d). Final geometries were determined to be energy minima by frequency calculations.

One-dimensional electron density maps were generated for stage 2 $C_xN(SO_2CF_3)_2$ using both the experimental diffraction data and a proposed structural model. Observed intensity data were used to generate structure factors after correction by a Lorentz-polarization factor:

$$F_{obs} = \pm [I * (\sin^2\theta \cos\theta) / (1 + \cos^2 2\theta)]^{1/2} \qquad (3.1)$$

where I is the integrated peak intensity. Calculated structure factors, $F_{00l}$, were obtained using the angle-dependent atomic scattering factors.[19] Electron density maps were then generated for z = 0 – 1, at increments of 0.004, using:

$$\rho(z) = (1/c)[F_0 + 2 \Sigma F_{00l} \cos(2\pi l z)] \quad (3.2)$$

where z is the fractional coordinate of atoms along the *c* axis, c is the cell dimension, and $F_0$ is the zero-order structure factor. Structures were refined by minimizing the crystallographic R factor:

$$R = \Sigma |k| F_{obs}(00l)| - |F_{cal}(00l)|| / \Sigma k |F_{obs}(00l)| \quad (3.3)$$

Powder X-ray diffraction patterns for solid solutions were simulated by the Diffax program (v1.76) [20], which allows the introduction of probability into the stacking sequence of structural models.

## 3.4 Results and Discussion

After the reaction of SP-1 graphite in a hydrofluoric acid solution of $K_2MnF_6$ and $LiN(SO_2CF_3)_2$, PXRD patterns of the products showed that the graphite phase disappeared after only 15 s, and a new pattern appeared consisting of 3 main reflections (Fig. 3.1). In each case, the new PXRD pattern indicated a GIC containing the bis-(trifluoromethanesulfonyl) imide anion, denoted $C_xN(SO_2CF_3)_2$, with $d_i \cong 8.1$ Å. Graphite intercalation compounds (GICs) usually display well-defined stages, i.e., phases with

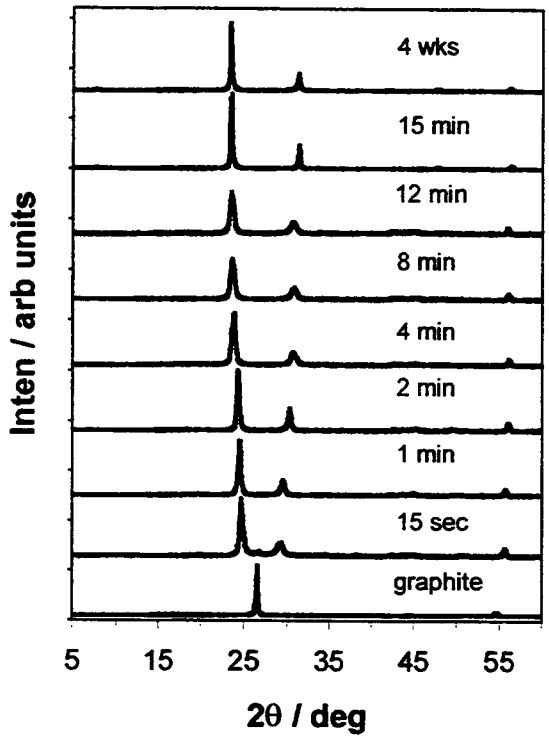


**Figure 3.1** Powder X-ray diffraction patterns for products described in Table 1.

ordered arrangements of occupied and unoccupied galleries. The relationship between the basal repeat length ($I_c$), gallery height ($d_i$), and stage (n) can be expressed as

$$I_c = d_i + (n - 1)(3.354\ \text{Å}) \qquad (3.4)$$

The two strongest peaks in the product, between 20° and 35° 2θ, were indexed for each pattern as (00*l*) reflections with $l = n + 1$ or $n + 2$. The intensity pattern observed, I $(0,0,n+1) >$ I $(0,0,n+2) >$ I (all other peaks), is common for GICs where $d_i$ is close to the unit cell c parameter for graphite (6.708 Å). After a 15 s reaction, the pattern was indexed as a solid solution of stage 4 and 5 GIC on the basis of the ratio of these two strong peak positions, which at 1.179 is between the theoretical values for stage 5 (1.117) and stage 4 (1.200). The products were best modeled as solid solutions of phases, because the reflections arising from physical mixtures of the stages would be sufficiently separated to form distinct peaks.

The changing peak position ratios (Table 3.1) indicated that the solid evolved to lower stages during the first several minutes in the solution. The diffraction peaks were notably sharper when the product by the above analysis consisted predominantly of a single stage GIC, as seen after 2 min reaction where a stage 3 GIC was obtained. After 15 min reaction or longer, the PXRD pattern was indexed to be nearly entirely stage 2, and the peaks were again sharper than for the intermediate stage products. The very small content of stage 3 was never entirely removed according to the best fit of peak positions, as is indicated by the fits of the PXRD pattern indicated in Figure 3.2. For this compound, analysis of peak widths by the Williamson-Hall relation gave a coherent

**Table 3.1** Peak position ratios, stage assignments and graphitic carbon / anion mole ratios ($x$) in $C_xN(CF_3SO_2)_2$ for products obtained after reaction of graphite with $K_2MnF_6$ and $LiN(CF_3SO_2)_2$ in hydrofluoric acid for the specified time at 20 °C.

| **Reaction time** | **d (00 *l*) / d (00 *l+1*)** | **assignment stage (fraction)** | | **x in $C_xN(CF_3SO_2)_2$** |
|---|---|---|---|---|
| | | | | |
| 15 sec. | 1.179 | 5 (0.63) | 4 (0.37) | 101 |
| 1 min. | 1.200 | 4 (1.00) | - | 78 |
| 2 min. | 1.241 | 3 (0.82) | 4 (0.18) | 60 |
| 4 min. | 1.284 | 3 (0.59) | 2 (0.41) | 45 |
| 8 min. | 1.296 | 2 (0.55) | 3 (0.45) | 44 |
| 12 min. | 1.297 | 2 (0.57) | 3 (0.43) | 43 |
| 15 min. | 1.329 | 2 (0.95) | 3 (0.05) | 37 |
| 48 h. | 1.331 | 2 (0.98) | 3 (0.02) | 32 |

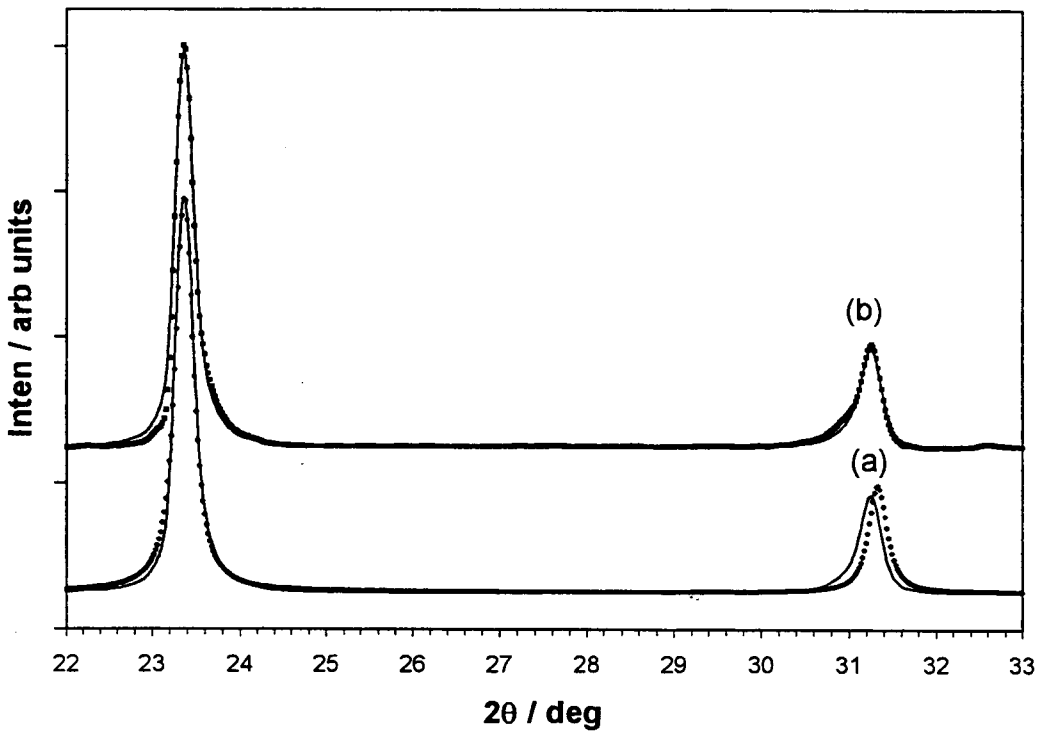


**Figure 3.2** (a) Observed (solid line) and calculated best-fit (dotted) PXRD patterns for stage 2 $C_{34}N(CF_3SO_2)_2$, and (b) is the difference obtained for the best-fit pattern using 5% stage 3 character in the structure model.

domain length along the stacking direction of 1000 Å, or approximately 80 cell repeats. After 15 min reaction, the $C_xN(CF_3SO_2)_2$ did not subsequently change in stage, and the PXRD remained unchanged even after several months, so long as the yellow color of dissolved $MnF_6^{2-}$ remained in solution.

Our previous investigation [11] of the formation of $C_xC_8F_{17}SO_3$ in hydrofluoric acid indicated that the stage 2 compound could not be obtained and that a solid solution of stage 2 and 3, with approximately 70% stage 2 character, was the limit of intercalant content in hydrofluoric acid at 20 and 50°C. For $C_xN(CF_3SO_2)_2$, however, 96% stage 2 was obtained rapidly under the same conditions. Anions with different volumes and geometries can have very different steric requirements for graphene basal surface; thus the same stage GIC of different anions may have a different intercalant content and charge density on the graphene layers. Stage 2 GICs will thus display a range of chemical potential, depending on the charge density attained for the intercalated anion. As will be indicated below, the $C_xN(CF_3SO_2)_2$ contains about one-half of the intercalant content for stage 2, compared to $C_xC_8F_{17}SO_3$ ($x \cong 18$). It follows that a lower oxidation potential is required for its preparation, and this is seen by the present results to be accessible in hydrofluoric acid.

Thermal analyses of the products by TGA and DSC showed that the total mass loss increased with longer reaction time and lower stage assignment. Three major regions of mass loss were observed: (1) a sharp endothermic event near 120°C, (2) a complex exothermic region between 150 and 300°C, and (3) the complete volatilization of the residual between 550 and 800°C. (Fig. 3.3) The product obtained after 15 s also showed a significant mass decrease between 300 and 500°C.

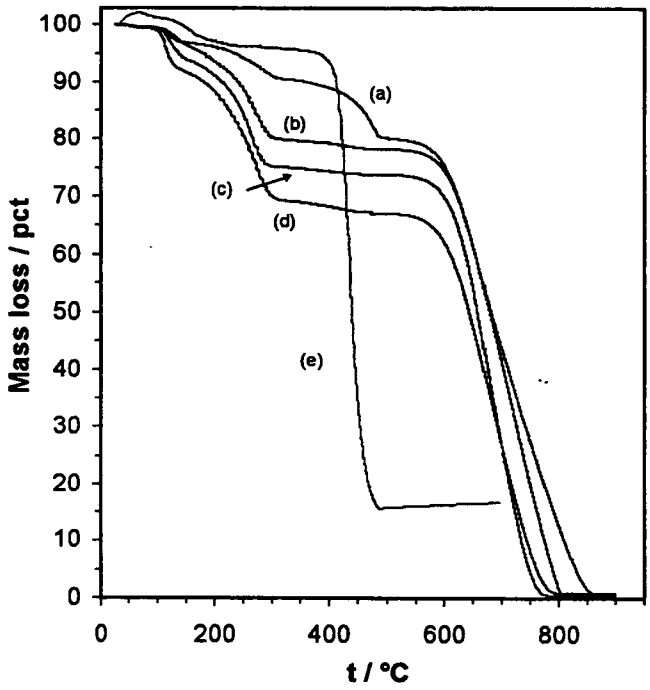


**Figure 3.3** TGA data for several products described in Table 1, reaction times are (a) 15 s, (b) 1 min, (c) 2 min, and (d) 4 min; (e) is the trace for $LiN(CF_3SO_2)_2$.

The GICs were dried *in vacuo* prior to analysis, and the mass losses below 100°C (< 0.5%) indicated little adsorbed water or HF at particle surfaces or within the intercalated galleries. Losses in regions 1 and 2 were attributed to the anion decomposition into volatile fragments. For comparison, the lithium imide salt showed one sharp mass decrease from 400 to 500°C (Fig 3.3e), thus the anion was less thermally stable in the GIC than in the Li salt. PXRD patterns of the materials heated at 300°C showed an amorphous structure, with only a broad reflection near 3.4 Å. After annealing under inert atmosphere at 300°C, the materials showed the pattern of sharp reflections due to a crystalline graphite structure, indicating that the graphene layers remained largely intact after heating at this temperature. Under the same conditions, graphite starts to lose mass at 700°C.

The molar ratio of graphite to imide anion, i.e., $x$ in $C_xN(CF_3SO_2)_2$, was calculated from the sum of losses below 500°C, and these values were plotted against reaction time in Figure 3.4. By this analysis, the stage 2 $C_xN(CF_3SO_2)_2$ had a final stoichiometry of x = 32. Elemental analysis provided a similar anion content (mass % observed (calculated) for $C_{30}N(CF_3SO_2)_2$; C, 60.4 (60.0); N, 2.7 (2.2): H, 0.00 (0.07)). Using $d_i$ = 8.07 Å and a volume of 198 Å for the anion (obtained from Gaussian calculations) yielded an occupied volume fraction of 0.52 for the intercalated galleries. By comparison, the stage 2 $C_xC_8F_{17}SO_3$ has x = 18, $d_i$ = 29.6 Å, and an occupied volume fraction of 0.80 [11]. Although the $N(CF_3SO_2)_2^-$ anion volume was calculated to be less than that of $C_8F_{17}SO_3^-$, the more isometric shape of the former and its arrangement in a monolayer, rather than bilayer, within the galleries, tend to decrease its molar content for a given stage relative to $C_8F_{17}SO_3^-$. As noted above, this suggests a lower charge density

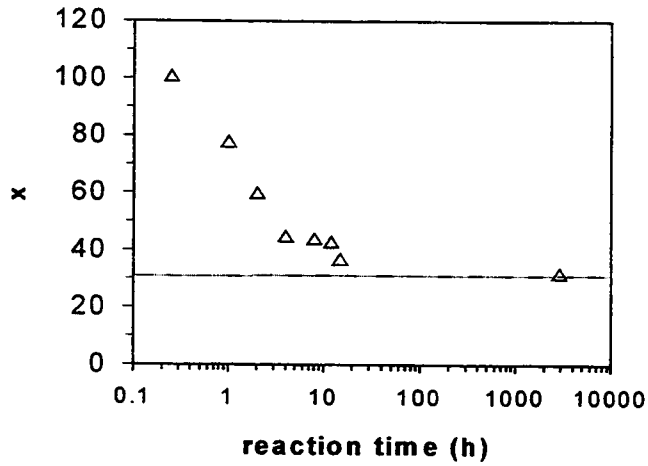


**Figure 3.4** $x$ in $C_xN(SO_2CF_3)_2$ vs. reaction time for $C_xN(SO_2CF_3)_2$ prepared in hydrofluoric acid. The mole ratio is determined by TGA mass loss below 500 °C.

on the graphene layers and therefore a lower oxidation potential for formation of the stage 2 GIC.

The steric requirements imposed by the gallery height, $d_i$ = 8.07 Å, allow only a single layer of intercalating anions in $C_xN(CF_3SO_2)_2$ galleries. Furthermore, the pseudo-cylindrical anions must be aligned with the long axis parallel to the graphene layers. We calculated the isolated $N(CF_3SO_2)_2^-$ anion to possess a minimum energy geometry similar to that reported previously by Johansson et al.[21], with the dihedral angle < C-S-N-S = 91.2°. An evaluation of transition state energies indicates that rotation about the dihedral angle has a barrier of only 3.9 kJ/mol [21], thus that the free anion has significant internal flexibility. At the calculated energy minimum geometry for the isolated anion, the $-CF_3$ substituents require a larger gallery dimension for the GIC than that observed. A rotation about each S-$CF_3$ bond, however, reduced the steric requirement sufficiently to give an acceptable dimension for the intercalant. The rotation was constrained to be identical for each $-CF_3$ to maintain $C_2$ symmetry, and the final position determined by PXRD refinement. Energy calculations indicated the resulting conformation is increased above the energy minimum by no more than 1.2 kJ/mol.

The electron density maps for the stage 2 GIC show a double maximum of electron density near the gallery center (Fig 3.5), which was modeled by adding equal occupancies of anions with N oriented towards each encasing graphene sheet. The structural refinement optimized two parameters, $x$ in $C_xN(CF_3SO_2)_2$ and the rotational angle of each S-$CF_3$ bond. The values obtained for the best fit are x = 34, with dihedral < O-S-C-F rotated by 60°. Calculated and observed PXRD patterns are compared in Figure 3.6.

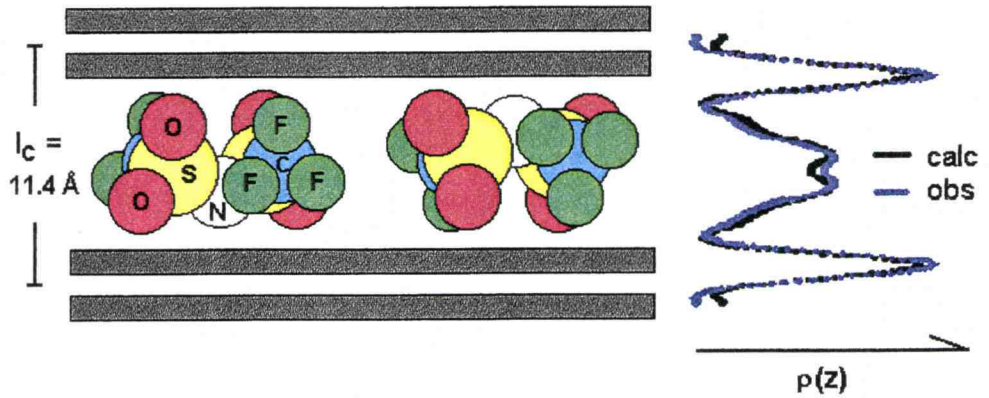


**Figure 3.5** 1D electron density maps derived from PXRD data and calculated for refined structural model of $C_{34}N(CF_3SO_2)_2$. The structure model indicates both possible orientations of the anion.

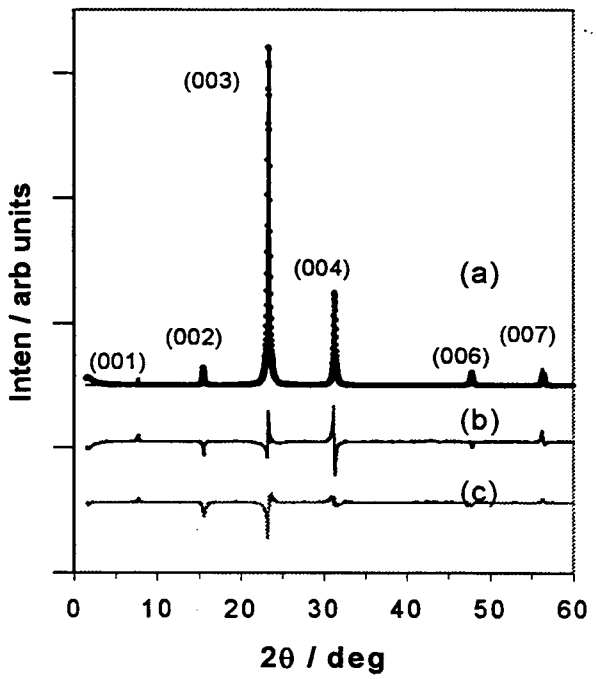


**Figure 3.6** (a) Observed (solid line) and calculated best-fit (dotted) PXRD patterns for stage 2 $C_{34}N(CF_3SO_2)_2$, and (b) difference pattern for these. Pattern (c) is the difference obtained for the best-fit pattern using 5% stage 3 character in the structure model.

This structure model for stage 2 $C_xN(CF_3SO_2)_2$ places the anionic nitrogen (Mulliken charge = - 0.71) approximately 3.0 Å and one O (charge = - 0.54) from each $SO_2$ group approximately 2.9 Å from one graphene surface, and the other two O a similar distance from the other graphene layer. The distances found are comparable to the graphene plane–oxygen distance of 3.2 Å for graphite nitrate (stage 2, $I_c$ = 9.9 Å).

When the chemical oxidation of graphite was carried out using $LiN(CF_2CF_3SO_2)_2$ in hydrofluoric acid, a GIC slowly develops, although the intercalation reaction was much slower than for the $N(CF_3SO_2)_2^-$ anion. Natural graphite, with a particle size 2 orders of magnitude less than SP-1 graphite, provides a reactive greater surface area, and was therefore used in these experiments. Even with the smaller particle size graphite, a mixed-phase product containing stage 3 and higher, as well as a strong reflection due to pristine (unreacted) graphite, was obtained after 3 weeks reaction at 20°C. (Fig 3.7) At 50°C, a similar product was obtained after 3 weeks, although the peak due to unreacted graphite was less intense. After 2 day reaction at 70°C, a solid solution of stage 2 and 3 GIC, along with graphite, was obtained. Higher reaction temperatures in hydrofluoric acid were not practical due to the increased rate of $K_2MnF_6$ decomposition. In these products, $d_i$ was determined to be 8.2 ± 0.1 Å.

For reactions using $LiN(CF_3SO_2)(CF_3(CF_2)_3SO_2)$, a stage 3 GIC ($d_i$ = 8.2 ± 0.1 Å) was obtained after 6 days at 70°C, with a strong reflection from unreacted graphite again present. Although the broad reflections provided a less accurate value for $d_i$ than for $C_xN(CF_3SO_2)_2$, it is clear that both the $N(CF_2CF_3SO_2)_2^-$ and $N(CF_3SO_2)(CF_3(CF_2)_3SO_2)^-$ anions must be oriented within the galleries in a manner similar to the smaller anion, with extended chains directed parallel to the graphene layers. The low degree of ordering and

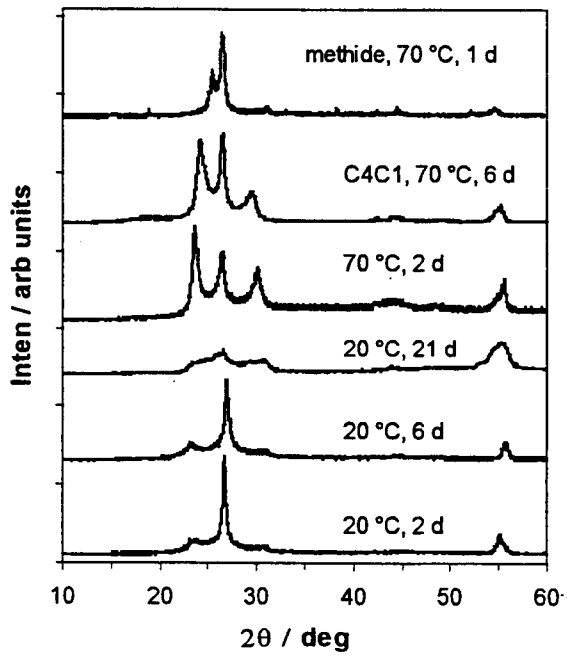


**Figure 3.7** Powder X-ray diffraction patterns for products obtained by reaction of graphite with $K_2MnF_6$ and $LiN(C_2F_5SO_2)_2$, or $LiN(CF_3SO_2)(CF_3(CF_2)_3SO_2)$ for the pattern at top. Reactions were in hydrofluoric acid at the specified temperature and times.

presence of multiple phases did not permit structural details of these products to be evaluated.

The $C(CF_3SO_2)_3^-$ anion had the lowest rate of intercalation of the anions studied. After reaction for weeks at 20 and 50°C, small reflections indicated the presence of a GIC, but the dominant reflection was from unreacted graphite. At 70°C, the GIC reflections became similar in intensity to the (002) reflection of the remaining unreacted graphite, and after 1 day a stage 4 GIC was obtained with $d_i = 10.6$ Å (Fig 3.7).

## 3.5 Acknowledgements

The authors gratefully acknowledge support from NSF grant DMR-9419481. The authors also thank 3M, Covalent, and Central Glass for supplying reagents, and Dr. Victor Koch for helpful discussions.

## 3.6 References


1. Bartlett, N; McQuillan, B. in *Intercalation Chemistry*; Whittingham, S.; Jacobson, A, Eds.; Academic Press: New York, **1982**.
2. Zable, H.; Solin, S. Eds., *Graphite Intercalation Compounds* I; Springer – Verlag: Berlin **1990**.
3. Watanabe, N.; Touhara, H.; Nakajima, T.; Bartlett, N.; Mallouk, T.; Selig, H. in *Inorganic Solid Fluorides Hagenmuller*, P., Ed. Academic Press: New York **1985**.
4. Ozawa, K. *Sol. St. Ionics* **1994**, *69*, 212.
5. Guerard, D.; Herold, A. *Carbon* **1975**, *13*, 337.
6. Markovsky, B.; Levi, M.; Aurback, D. *Electrochim. Acta* **1998**, *43*, 2287.
7. Buckley, J.; Edie, D. Eds., in *Carbon-carbon Materials and Composites*, Noyes Publ.: NJ **1993**.
8. Horn, D.; Boehm, H.P. *Mater. Sci. Eng.* **1977**, *31*, 87.
9. Ruisinger, B.; Boehm, H.P. *Angew. Chem. Int. Ed. Engl.* **1987**, *26*, 3, 253.
10. Boehm, H. P.; Helle, W.; Ruisinger, B. *Synth. Met.* **1988**, *23*, 395.
11. Zhang, Z.; Lerner, M. *Chem. Mater.* **1996**, *8*, 257.
12. Zhang, X.; Lerner, M. *Chem. Mater.* in Press, **1999**.
13. Bourelle, E.; Douglade, J.; Metrot, A. *Mol. Cryst. Liq. Cryst.* **1994**, *244*, 227.
14. Kang, F.; Leng, Y. *Carbon* **1997**, *35*, 8, 1089.
15. Armand, M.; Gorecki, W.; Andreani, R. in *Proceedings of Second International Symposium on Polymer Eectrolytes*, Scrosati, B. Editor, P. 91, Elsevier, London **1990**; M. Armand and R.E.K.C.E. Moursli, Fr. Pat. 82-09540, **1983**.

16. Dominey, L. A.in *Proceedings of the Fifth International Seminar on Lithium Battery Technology and Applications*. Florida (1991); Dominey, L., U.S. Pat. 5,273,840 **1993**.

17. Bode, H.; Jenssen, H.; Bandte, F. *Angew. Chem.* **1953**, *65*, 304.

18. Williamson, G.; Hall, W. *Acta Metallurgica* **1953**, *1*, 22.

19. Hehre, W.J.; Shusterman, A.J.; Huang, W.W. *A Laboratory Book of Computational Organic Chemistry*, Wavefunction Inc. **1996**.

20. Su, Z.; Coppens, P. *Acta Crys. A* **1997**, *53*, 749.

21. Johansson, P.; Gejji, S.P.; Tegenfeldt, J.; Lindgren, J. *J. Electrochimica Acta* 1998, *43*, 1375.

# Chapter 4

## Air Stability and Surface Passivation of Acceptor-Type Graphite Intercalation Compounds Prepared in Hydrofluoric Acid

*Xuerong Zhang and Michael M. Lerner,**

*Department of Chemistry and Center for Advanced Materials Research,*

*Oregon State University,*

*Corvallis, OR 97331-4003, USA.*

**to be submitted to Carbon**

## 4.1 Abstract

The environmental stabilities of graphite intercalation compounds (GICs) containing the anions $HF_2^-$, $NO_3^-$, $HSO_4^-$, $C_8F_{17}SO_3^-$, $N(CF_3SO_2)_2^-$, or $N(CF_2CF_3SO_2)_2^-$ are determined under ambient conditions at 20 °C, at 50 °C and 100 % relative humidity, and in liquid water at 20°C. The GICs are prepared as stage 2 – 3 products from SP-1 or natural graphite powder in 48 % hydrofluoric acid. The large perfluoroanions form far more stable materials than GICs with bifluoride, nitrate, or sulfate, with $C_{17}C_8F_{17}SO_3 \cdot 4F$ losing 16 % of intercalant content over 1000 h. The stabilities of graphite $C_xNO_3 \cdot \delta HNO_3$ and $C_xHSO_4 \cdot \delta H_2SO_4$ (prepared in the corresponding mineral acids) are less than those for $C_xHSO_4 \cdot \delta HF$ and $C_xNO_3 \cdot \delta HF$ (prepared in hydrofluoric acid). Evacuation of these GICs reduces the content of neutral species, decreasing gallery heights and increasing air stability. The stability of $C_xHF_2 \cdot \delta HF$ can be increased significantly by reacting the powder with dilute solutions containing large perfluoroanions under oxidizing conditions to generate a passive surface layer. The GICs derived from natural graphite (1 μm particle diameter) show decomposition rates 1 to 2 orders of magnitude higher than those derived from SP-1 graphite (100 μm).

## 4.2 Introduction

Considerable research interest has focused on the technological applications of graphite intercalation compounds (GICs). [1,2] The excellent electrochemical reversibility of the lithium intercalation in certain electrolytes, combined with a practical energy density above 300 mAh/g, permit the use of a $C_x$ / $LiC_x$ redox couple as the electroactive component in lithium-ion battery anodes. [3] Thermally exfoliated graphite (TEG) is an important commercial material prepared by hydration and thermolysis of GICs, with the unique ability to serve as high-temperature sealants under ambient conditions. [5] GICs have also been proposed for and used as reagents and catalysts for organic synthesis and polymerization initiators. [1, 4]

Since the reduction and oxidation potentials of the graphene layers lie, respectively, below and above the potential stability limits for aqueous solutions (except for oxidation of highly concentrated acids), most GICs decompose rapidly under environmental conditions. A typical example for acceptor-type GICs is the spontaneous reduction of graphite bifluoride in air. This GIC can be prepared by reaction of graphite with an oxidant in anhydrous liquid hydrogen fluoride, as in:

$$C_x + K_2MnF_6 + (1+\delta)\,HF \xrightarrow{\text{anhyd. HF}} C_xHF_2\cdot\delta HF + 2KF + MnF_3 \quad (4.1)$$

Upon exposure to ambient conditions the GIC quickly decomposes, losing intercalant to reform graphite:

$$2\,C_xHF_2\cdot\delta HF + H_2O \xrightarrow{\text{air}} 2\,C_x + O_2 + (\delta + 4)\,HF \quad (4.2)$$

The short ambient lifetime of such GICs obviously eliminates many practical applications for these materials, for example in anti-static coatings that would have environment exposure during use. In other cases, however, such as the application to electroactive components in energy storage devices, the technological barriers to coating, storing, and processing electrodes with air-sensitive materials might be overcome by incremental improvements in environmental lifetimes.

Because of several factors, including reactive surface area of the graphite host, the environmental stability of the intercalant anions, and the relative values for solvation enthalpies of intercalated species and lattice enthalpies of the GICs, the air stabilities of acceptor-type GICs vary widely. Many investigations on the stability of GICs have involved the chlorometallate intercalants, especially $FeCl_{3+y}^{y-}$ [6-8] and $SbCl_{5+y}^{y-}$. [9-11] When prepared from highly-oriented pyrolytic graphite (HOPG), these GICs can be very stable under ambient conditions. $C_xSbCl_{5+y}$, prepared from HOPG, showed only approx. 6 % weight decrease after exposure to air for one year. [9] Most likely, the stability derives from the low surface area of the starting graphite and the formation of a relatively inert surface layer via anion decomposition.

Schlogl et al. reported the studies on the mechanisms for decomposition of stage 1 $C_xSbCl_{5+y}$ and $C_xFeCl_{3+}$ from. [6,9,10] The initial reaction step in each case was determined to be desorption of HCl, followed by the slow conversion of stage 1 to higher stage. It has also been demonstrated, in the case of $C_xSbCl_{5+y}$, that the method of preparation can greatly affect the air stability of the GIC. For example, GICs prepared

using a solution method were found to co-intercalate neutral solvent molecules and also to be far more air stable than GICs prepared by direct reaction of graphite with $SbCl_5$ vapor. [9]

The influence on GIC stability arising from the graphite host type, particle size, and structural perfection has been reported for chlorometallate intercalants, and larger particle size hosts were found to have greater stability in air and liquid water. The degradation of graphite fibers intercalated with $TaCl_5$ was found to be slower for samples with higher structural perfection, [12] however, particle size was concluded to be a more important factor for stability.

Different proposals have been put forward for improving the environmental stability of GICs; many involve the intentional formation of a passivation layer on the reactive graphite surface. [1] This approach is currently employed to prevent the mechanical degradation of graphite anodes in Li-ion cells, because the formation of a protective surface layer is required to prevent electrode delamination that arises upon co-intercalation of the neutral polar solvent. By use of an appropriate solvent combination, the products from oxidative decomposition of the electrolyte form a compact, passive layer covering the graphite electrode. The surface layer allows rapid and reversible transport of $Li^+$ ions, but not solvent molecules, thus preventing delamination of the graphite electrode. Extensive studies have been done on the nature of the passivating film, the effect of different electrolyte compositions, and the role of additives such as $CO_2$, $SO_2$ and S in forming protective surfaces. [3] Much less research has been reported on forming passive surfaces on acceptor-type GICs.

Our group has previously reported the chemical synthesis of the GICs graphite perfluorooctanesulfonate, $C_{17}C_8F_{17}SO_3 \cdot 4F$ [13], and graphite bis(trifluoromethane-sulfonyl)imide, $C_xN(CF_3SO_2)_2$, in 48 % hydrofluoric acid. [14] It was noted briefly that these GICs show unusually high air stabilities compared with other GICs containing fluoroanions. In this report, we compare the stability for these and related materials to those for GICs containing bifluoride or small oxoanions, and evaluate the effects of evacuation, surface species, and surface area.

## 4.3 Experimental

### 4.3.1 Reagents:

Fuming $H_2SO_4$ (Baker, 30 – 33 oleum %), conc. $HNO_3$ (Mallinckrodt, 69.2 %) and hydrofluoric acid (Mallinckrodt AR, 48 % (w / o)) were used as received. $C_8F_{17}SO_2F$ (3M, experimental product) was treated with excess 20 % KOH solution and refluxed at 120 °C overnight. The white precipitate $KC_8F_{17}SO_3$ was washed with distilled water and dried under vacuum at room temperature. $KC_6F_5SO_3$ was synthesized from $C_6F_5SO_2Cl$ (Aldrich, 99 %) by the same method. $NaC_4F_9SO_3$, (3M, 98 %), $LiN(CF_3SO_2)_2$ (3M), and $LiN(C_2F_5SO_2)_2$ (3M), and were used as received. Bright yellow $K_2MnF_6$ powder was synthesized according to a literature method by reduction of $KMnO_4$ (EM Science GR) using $H_2O_2$ (Mallinckrodt AR, 30 % in aqueous solution) in a KF / hydrofluoric acid solution [15]. Two types of graphite reagent were used; SP-1 powder (Union Carbide, 100 um avg. particle diameter) and natural graphite flakes

(Aldrich, 1 - 2 um). Unless otherwise indicated, SP-1 graphite was used to prepare the GICs.

### 4.3.2 Preparation of GICs

Graphite bifluoride ($C_xHF_2 \cdot \delta HF$) [16] was prepared by stirring graphite powder (100 mg, 8.3 mmole) in a solution of $K_2MnF_6$ (400 mg, 1.6 mmole) in hydrofluoric acid (15 ml) for 2 h. The product was collected by rapid filtration in air. Stage 2 graphite sulfate ($C_xHSO_4 \cdot \delta HF$) and graphite nitrate ($C_xNO_3 \cdot \delta HF$) were made by the same method, fumming $H_2SO_4$ or conc. $HNO_3$ was added to 48% aqu. HF to compose a 20 % (v / o) solution. $C_xNO_3 \cdot \delta HNO_3$ was also prepared by stirring graphite powder (100 mg, 8.3 mmole) in a solution of $KMnO_4$ (300 mg, 1.9 mmole) in conc. $HNO_3$ (10 mL) for 2 h. A similar reaction with fumming $H_2SO_4$ leads to a stage 1 graphite sulfate, of reported composition $C_{24}HSO_4 \cdot 2.5H_2SO_4$. [17] In order to obtain the desired stage 2 GIC ($C_xHSO_4 \cdot \delta H_2SO_4$), the Mn(VII) : C ratio was limited to give a maximum oxidation corresponding to $C_{48}^+$. By this method, the stage 2 GIC was obtained with $d_i$ = 7.85 Å, which is similar to a reported value of 7.98 Å for the stage 1 compound. [18] These stoichiometries and gallery heights are compatible with a single layer of sulfate, or hydrosulfate tetrahedra, in the intercalated galleries.

$C_xN(CF_3SO_2)_2$, $x \approx 35$, $C_{17}C_8F_{17}SO_3 \cdot 4F$, and $C_xN(C_2F_5SO_2)_2$, were prepared in hydrofluoric acid as reported previously. [13,14] Reactions proceeded for 1 h at 20 °, 72 h at 20 °C, or 48 h at 70 °C, respectively, to obtain the GICs.

Surface-treated $C_xHF_2 \cdot \delta HF$ was prepared by brief exposure of the GIC product to a dilute solution of either $LiC_4F_9SO_3$, $KC_8F_{17}SO_3$ or $LiN(CF_3SO_2)_2$, in hydrofluoric acid under oxidizing conditions. These products are labeled $C_xHF_2 \cdot \delta HF$ / $C_4F_9SO_3$, $C_xHF_2 \cdot \delta HF$ / $C_8F_{17}SO_3$, and $C_xHF_2 \cdot \delta HF$ / $N(C_2F_5SO_2)_2$. In a typical reaction, 100 mg of graphite was reacted to prepare $C_xHF_2 \cdot \delta HF$ as described above, then $KC_8F_{17}SO_3$ (20 mg, 0.037 mmole) was added to the reaction solution for the final 5 minutes. Reaction stoichiometries were limited to a maximum mole ratio of C / anion = 225. Stage 2 GICs were collected by filtration in air and washed briefly with hydrofluoric acid. PXRD data showed no change in gallery heights or phases other than $C_xHF_2 \cdot \delta HF$ in these products, indicating that the larger anions do not exchange for bifluoride anions in the graphite galleries. The enhanced stability of the products, however, allows the isolation of lower stage GICs for the initial diffraction samples.

Products described as evacuated in the text were dried under dynamic vacuum (0.1 torr) at ambient temperature for 24 h. immediately after preparation. GICs were evaluated immediately following preparation or evacuation. Table 4.1 summarizes the stage compositions and gallery heights of the GICs used in the study.

### 4.3.3 Analyses

Environmental stability tests were carried out either under ambient conditions at 20 °C, at 50 °C and 100 % relative humidity, or by reaction with liquid water at 20 °C.

**Table 4.1** Stage composition and gallery heights for GICs prior to air exposure.

| | as prepared | | after evacuation | |
|---|---|---|---|---|
| | stage | $d_i$ / Å | stage | $d_i$ /Å |
| in 48 % hydrofluoric acid: | | | | |
| $C_xNO_3 \cdot \delta HF$ | 2 | 6.5 | | |
| $C_xHSO_4 \cdot \delta HF$ | 2 | 7.63 | 2 | 7.72 |
| $C_xHF_2 \cdot \delta HF$ | 2 + 3 | 6.48 | 5 | 6.5 |
| $C_xN(CF_3SO_2)_2$ | 2 | 8.07 | | |
| $C_{17}C_8F_{17}SO_3 \cdot 4F$ | 2 + 3 | 29.6 | | |
| $C_xN(C_2F_5SO_2)_2$ | 3 + 2 | 8.2 | | |
| $C_xHF_2 \cdot \delta HF$ / $C_4F_9SO_3$ | 2 | 6.48 | | |
| $C_xHF_2 \cdot \delta HF$ / $C_8F_{17}SO_3$ | 2 | 6.48 | | |
| $C_xHF_2$ / $N(CF_3SO_2)_2$ | 2 | 6.48 | | |
| in conc. nitric acid: | | | | |
| $C_xNO_3 \cdot \delta HNO_3$ | 2 | 7.8 | 5 | 7.5 |
| in conc. sulfuric acid: | | | | |
| $C_xHSO_4 \cdot \delta H_2SO_4$ | 2 | 7.85 | 2 + 3 | 7.8 |

Conditions of 100 % relative humidity were obtained by maintaining the sample and water at 50 °C in a closed container such that the GIC powder did not directly contact the liquid. A single powder sample was analyzed under each condition at different reaction times. Powder X-ray diffraction (PXRD) data were collected using a Siemens D5000 powder diffractometer with Ni – filtered CuKα radiation: the angle was stepped at 0.02 ° 2θ between 1.5 and 60 °, at 0.1 s / step.

**4.4 Results and Discussions**

Similar synthetic methods and product stages are desirable in order to compare the effect of anion type on the stability of different graphite salts. Although graphite in the form of fibers or mesospheres can have very lower reactive surface areas (often < 1 $m^2$ / g) and thus lower reaction rates to moisture, this study used the crystalline powders of natural graphite and SP-1 grade to decrease the required observation times while permitting informative PXRD data to be obtained for general trends.

GICs containing the anions $NO_3^-$, $HSO_4^-$, $HF_2^-$, $C_8F_{17}SO_3^-$, $N(CF_3SO_2)_2^-$, or $N(C_2F_5SO_2)_2^-$, can all be readily prepared from graphite powder in 48 % hydrofluoric acid by the addition of the corresponding acid or salt along with $K_2MnF_6$ as an oxidant. Stage 2 GICs are obtained for $C_xNO_3 \cdot \delta HF$, $C_xHSO_4 \cdot \delta HF$ and $C_{35}N(CF_3SO_2)_2$. $C_xHF_2 \cdot \delta HF$, however, is highly unstable under ambient conditions and shows significant decomposition within minutes. For this reason, a pure stage 2 product was not served, the product as isolated by filtration is identified by PXRD as a solid solution containing 51 mole percent stage 2 and 49 mole % stage 3.

For $C_{17}C_8F_{17}SO_3 \cdot 4F$, the product obtained is a solid solution comprising 79 mole % stage 2 and 21 mole % stage 3, which is similar to the highest intercalant content reported previously to be obtained from 48 % hydrofluoric acid. [13] $C_xN(C_2F_5SO_2)_2$ is also limited to a maximum intercalant content of less than stage 2 in this solution, the GIC obtained is determined by peak position analysis to be a solid solution containing 31 mole % stage 2 and 69 mole % stage 3.

For starting GICs or decomposition intermediates that are indexed as a solid solution of two stages, or physical mixtures of two stages, a more general, non-integral, stage parameter, n', is employed:

$$\text{stage parameter} = n' = (m * p) / [(m * \text{mole fraction stage p}) + (p * \text{mole fraction stage m})] \quad (4.3)$$

where m and p denote the stage numbers for constituent phases. PXRD peak positions and intensities are used to determine the GIC stage(s) present and relative content of each stage during the decomposition reactions. In order to normalize conditions for comparisons, the relative intercalant content within the graphite galleries is determined using the usual approximation that all stages (2 and higher) of a GIC for a particular anion have similar intercalant densities within the occupied galleries. Then, if the relative intercalant content, *i*, for stage 2 is set to be 100 %, a stage 3 GIC for the same anion will have $i = 100\% * 2/3 = 67\%$. In general, *i* is therefore determined using the relation:

$$i = 100\% * (2 / n') \quad (4.4)$$

Thus, $C_xNO_3 \cdot \delta HF$, $C_xHSO_4 \cdot \delta HF$, and $C_xN(CF_3SO_2)_2$ are prepared as stage 2 GICs and have initial intercalant contents, $i_0$, of 100 %, but $i_0$ for $C_{17}C_8F_{17}SO_3 \cdot 4F$ is 90 % and for $C_xN(SO_2C_2F_5)_2$ is 83 %.

In reactions where the intermediate higher-stage GIC products are best indexed as a solid solution, mole fractions of the constituent stages are determined from (00*l*) peak positions and known cell parameter for single stage GICs. Methods for evaluating non-integral peak positions resulting from solid solutions in GICs have been described previously. [13] As an example of this method of data reduction, Figure 4.1a displays data obtained from the air stability test for $C_xHF_2 \cdot \delta HF$ / $N(C_2F_5SO_2)_2$ at 20 °C. The strongest PXRD reflection for the GIC remains as a single peak that broadens and shifts to lower angle with increasing air exposure time. Since the gallery height, $d_i$, for a given GIC is nearly independent of stage for $n \geq 2$, the phase components for the disordered stage products are determined from the relation:

$$n' = (d_i - d_{obs} - 3.354\ \text{Å}) / (d_{obs} - 3.354\ \text{Å}) \quad (4.5)$$

where $d_{obs}$ is the strong diffraction peak near 27 ° 2θ and corresponds to (00*l*) for a stage (*l* −1) GIC. For this GIC, $d_i$ can be set at 6.48 Å from the known gallery height for the stage 2 [21]. The derived values for *n'* and *i* from the PXRD data in Figure 4.1a are provided in Table 4.2a.

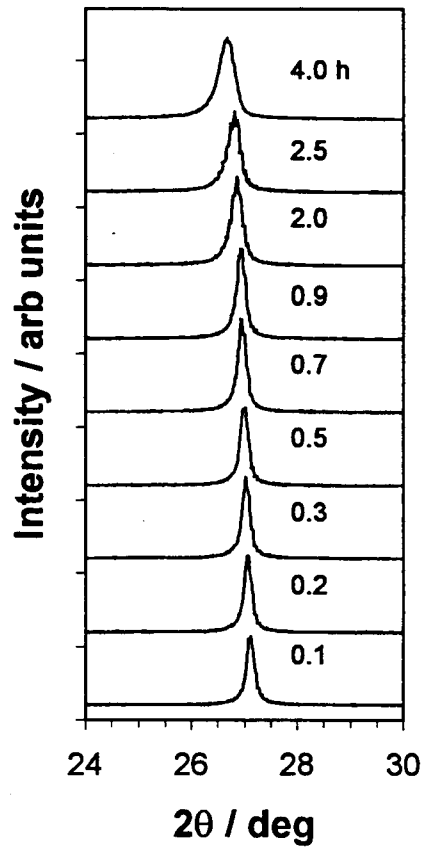


**Figure 4.1(a)** PXRD patterns at various air exposure times at 20 °C for (a) $C_xHF_2 \cdot \delta HF$ / $N(C_2F_5SO_2)_2$, and (b) for $C_xHSO_4 \cdot \delta HF$

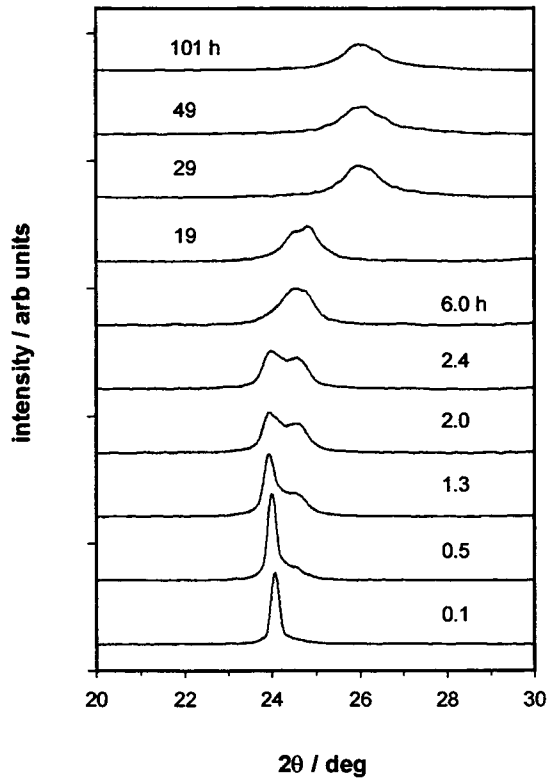
101 h
49
29
19
6.0 h
2.4
2.0
1.3
0.5
0.1
intensity / arb units
20
22
24
26
28
30
2θ / deg

**Figure 4.1(b)**

**Table 4.2** Peak diffraction position ($d_{obs}$) or stage mole fractions, and calculated stage parameter, n, and relative intercalant content, I, for samples as-prepared and after air exposure at 20 °C for (a) $C_xHF_2 \cdot \delta HF$ / $N(C_2F_5SO_2)_2$, and (b) $C_xHSO_4 \cdot \delta HF$.

**(a)**

| time | $d_{obs}$ | *n'* | *i* |
|---|---|---|---|
| h | Å | | pct |
| | | | |
| 0.1 | 3.285 | 2.30 | 87 |
| 0.2 | 3.291 | 2.62 | 76 |
| 0.3 | 3.297 | 3.00 | 67 |
| 0.5 | 3.300 | 3.22 | 62 |
| 0.7 | 3.306 | 3.71 | 54 |
| 0.9 | 3.309 | 4.08 | 49 |
| 2.0 | 3.319 | 5.51 | 36 |
| 2.5 | 3.324 | 6.60 | 30 |
| 4.0 | 3.330 | 8.50 | 24 |

**(b)**

| time | mole fraction | | $d_{obs}$ | *n'* | *i* |
|---|---|---|---|---|---|
| h | n = 2 | n = 3 | Å | | pct |
| | | | | | |
| 0.1 | 1.00 | 0.00 | - | 2.00 | 100 |
| 0.5 | 0.96 | 0.04 | - | 2.04 | 98 |
| 1.3 | 0.72 | 0.28 | - | 2.28 | 88 |
| 2.0 | 0.61 | 0.39 | - | 2.39 | 84 |
| 2.4 | 0.57 | 0.43 | - | 2.43 | 82 |
| 6.0 | 0.19 | 0.81 | - | 2.74 | 73 |
| 19 | - | - | 3.56 | 3.39 | 59 |
| 29 | - | - | 3.52 | 4.47 | 45 |
| 49 | - | - | 3.43 | 11 | 18 |
| 101 | - | - | 3.42 | 14 | 14 |

In reactions where the intermediate GICs include physical mixtures of different stages, the relative intensities of strongest diffraction peak intensities are used to approximate the mole fraction of stages present. The stage parameter is then calculated according to equation (4.5). As an example of the use of this method, the PXRD patterns in Figure 4.1b show the strongest peaks observed for $C_xHSO_4 \cdot HF$ at different air exposure times. For times between 0.5 and 2.4 h, the patterns are analyzed by fitting the data as two strong peaks; (*003*) for stage 2 (peak calculated at 24.12 ° 2θ) and (*004*) for stage 3 (24.66 °). At longer exposure times, multiple peaks are not easily resolved, and the peak maximum is used, as in the previous example, as $d_{obs}$ in equation (5) to calculate the stage parameter. In Table 2b, the stage parameters, *n'*, and *i* are provided for this example.

### 4.4.1 Environmental Stability of GICs as prepared from hydrofluoric acid

The stability data of the GICs at 20 °C in air are presented in Figure 4.2. As is consistent with the difficulty in obtaining a purely stage 2 product after handling briefly under ambient conditions, the decomposition of $C_xHF_2 \cdot \delta HF$ is found to be rapid. The intercalant content decreased by half in 0.2 h and the compound completely reduced to graphite within 1 h. $C_xNO_3 \cdot \delta HF$ and $C_xHSO_4 \cdot \delta HF$ also decompose fairly rapidly, with half the intercalant lost within 24 h. These latter reactions eventually slow to produce more stable high-stage materials with approximately 15 - 25 % of the original intercalant content. These decomposition products are high stage (n' ≥ 10) and show broad peaks indicative of poor ordering along the stacking direction.

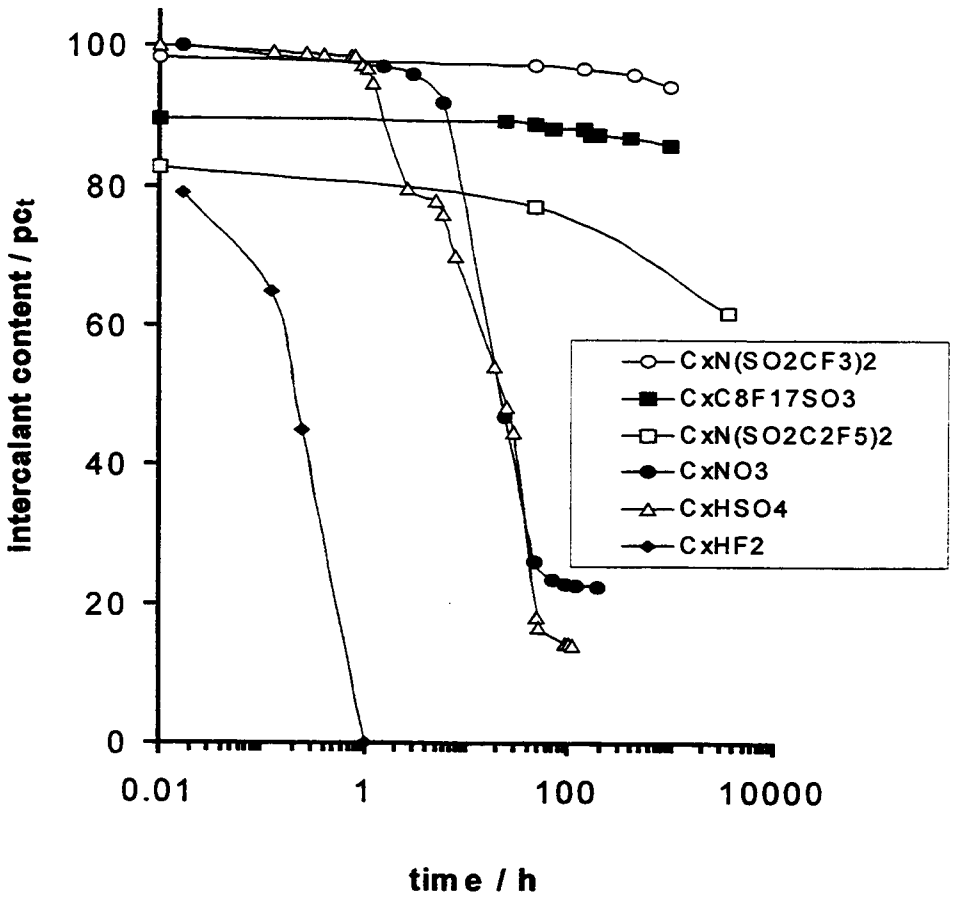


**Figure 4.2** Intercalant content vs. time in air at 20 °C for GICs prepared in hydrofluoric acid.

By comparison, $C_{17}C_8F_{17}SO_3 \cdot 4F$, $C_xN(CF_3SO_2)_2$, and $C_xN(C_2F_5SO_2)_2$ are much more stable, the first two GICs retain at least 95 % of their original intercalant contents for several hundred hours. The most stable GIC evaluated, $C_{17}C_8F_{17}SO_3 \cdot 4F$, is prepared originally as a solid solution with 79 : 21 :: mole % stage 2 : mole % stage 3, with n' = 2.15, and shows a slow increase in the stage 3 content with time of air exposure. After 3 months in air, the GIC is still a stage 2 : stage 3 solid solution, with a ratio of 33 % : 67 % of the respective constituent phases (n' = 2.58), corresponding to a decrease in intercalant content of 4%. After several hundred hours, the PXRD patterns for the sample show the layer structure of a solid acid phase $HC_8F_{17}SO_3$, which has a stacking repeat of approximately 27 Å.

As expected, the decomposition reaction rates for all samples increase at higher temperature and humidity, and are even more rapid in liquid water. (Figure 4.3) In water, $C_{17}C_8F_{17}SO_3 \cdot 4F$ and $C_xN(CF_3SO_2)_2$, are reduced back to graphite within 1 – 1.5 h. $C_xN(C_2F_5SO_2)_2$ is somewhat more stable in water, the intercalant content decreased from 67 % to 42 % in 2 h. The extended time required to prepare $C_xN(C_2F_5SO_2)_2$ (approximately 500 - 1000 h are required to obtain a solid solution of stage 2 and 3 at 20 °C, compared with 50 - 100 h for similar preparation of $C_xC_8F_{17}SO_3$ ) indicates a very slow anion diffusion rate within the graphite galleries, which may determine a limiting rate for decomposition in water.

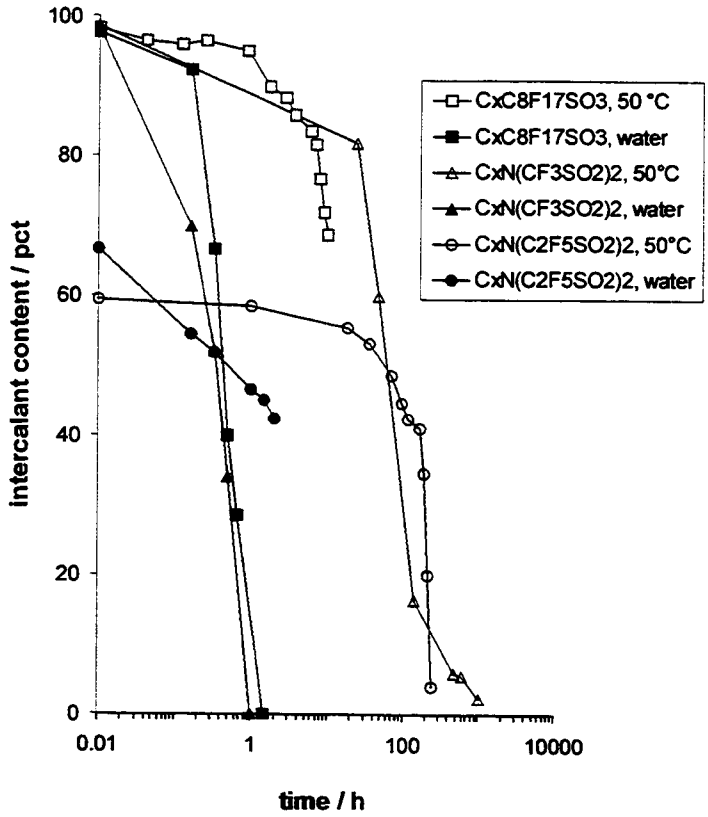


**Figure 4.3** Intercalant content vs. time for $C_{17}C_8F_{17}SO_3 \cdot 4F$, $C_xN(CF_3SO_2)_2$, and $C_xN(C_2F_5SO_2)_2$ exposed to air at 50 °C and 100 % relative humidity or in liquid water at 20 °C.

### 4.4.2 Effect of evacuation on GIC stabilities

As indicated above, $C_xHF_2 \cdot \delta HF$ is extremely air-sensitive and reverts to crystalline graphite within 1 h. The oxidative intercalation of graphite in the acid solutions results in the reversible incorporation of neutral acid along with anions within graphite galleries. The neutral acids act as dielectric spacers for intercalant ions, and can form hydrogen bonds within the intercalated galleries. [18] The neutral co-intercalants can be removed by evacuation, resulting in a decrease in intercalant volume and corresponding increase in the GIC stage. [19] After evacuation for 24 h, $C_xHF_2 \cdot \delta HF$ is stage 5, losing approximately 60 % of the intercalant volume from the as-prepared sample, but showing an increased air stability at 20 °C. After 1 h. the intercalant content decreases from 40 % to 35 %, and then after 8 h to 20 % (Figure 4.4a).

$C_xNO_3 \cdot \delta HNO_3$ (obtained in conc. $HNO_3$) has a gallery height, $d_i$, of 7.8 Å, which is reported by Touzain, et. al. as corresponding to a composition of $x = 26$, $\delta = 5$ [20]. Evacuation of the product reduces the $HNO_3$ content, and allows the planar $NO_3^-$ to align at the gallery centers in a parallel orientation to the graphene layers. The gallery height decreases significantly to 6.6 Å indicating the new anion orientation. The evacuated product is reported to $\delta < 1$. [18] Due to the reduced intercalant volume, the GIC change from stage 2 to stage 5 after evacuation, corresponding to a calculated decrease in the calculated intercalant content from 100 % to 39 %.

The stability curves for $C_xNO_3 \cdot \delta HNO_3$ before and after evacuation are provided in Figure 4.4a. As previously reported, the as-prepared sample decomposes rapidly. [6] The decomposition products contain a mixture of stages, with stage 4 predominating after 1 h. A wide range of gallery heights, from 6.8 – 7.8 Å, is observed in the decomposition

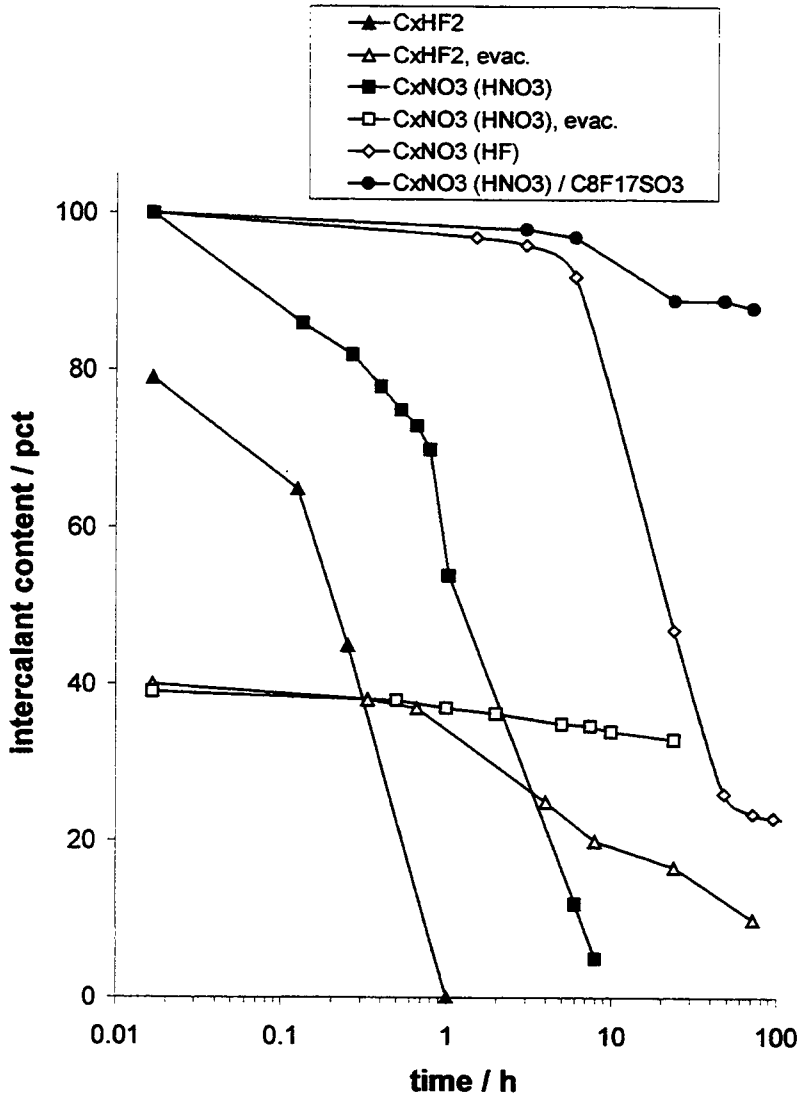


**Figure 4.4(a)** Intercalant content vs. time for GICs exposed to air at 20 °C either as-prepared or after evacuation at 0.1 torr for 24 h.

products, with a mean value close to 7.5 Å after 1 h. These data indicate partial elimination of $HNO_3$ from galleries prior to reductive deintercalation. The evacuated sample of $C_xNO_3 \cdot \delta HNO_3$ has a greater air stability. Although the initial intercalant content is much less (39 %), the loss of intercalant occurs more slowly than for the as-prepared GIC. After 24 h in air, the intercalant content is 33 %.

For comparison, the stage 2 $C_xNO_3 \cdot \delta HF$ (prepared from a hydrofluoric acid / conc. $HNO_3$ solution) has $d_i$ = 6.6 Å without evacuation, which is consistent with the presence of HF rather than $HNO_3$ as neutral co-intercalant. Since the linear bifluoride anion can reside in galleries with $d_i$ = 6.5 Å, the product could also contain some bifluoride anion intercalant. This GIC, however, is significantly more stable than as prepared $C_xHF_2 \cdot \delta HF$ and $C_xNO_3 \cdot \delta HNO_3$.

$C_xHSO_4 \cdot \delta H_2SO_4$ decomposes rapidly in air, losing 50 % of intercalants within 1.5 h. (Figure 4.4b) After 6 h. no GIC remains in the product. After evacuation, the $C_xHSO_4 \cdot \delta H_2SO_4$ remains stage 2, but the gallery height decreases slightly to 7.80 Å, some loss of $H_2SO_4$. Since the vapor pressure of $H_2SO_4$ is significantly less than that of $HNO_3$ and HF (<< 1 torr for $H_2SO_4$ at 20 °C, as compared with 50 torr for $HNO_3$ and 650 torr for HF), evacuation is less effective at removing the neutral co-intercalant from $C_xHSO_4 \cdot \delta H_2SO_4$. After evacuation, the decomposition reaction proceeds in a similar fashion, although at about half the rate as before.

$C_xHSO_4 \cdot \delta HF$ has a smaller gallery height (7.63 Å), even without evacuation, indicating that, as with $C_xNO_3 \cdot \delta HF$, the predominant neutral species for the GIC prepared in hydrofluoric acid is HF. Gallery heights less than 7.7 Å require, from steric

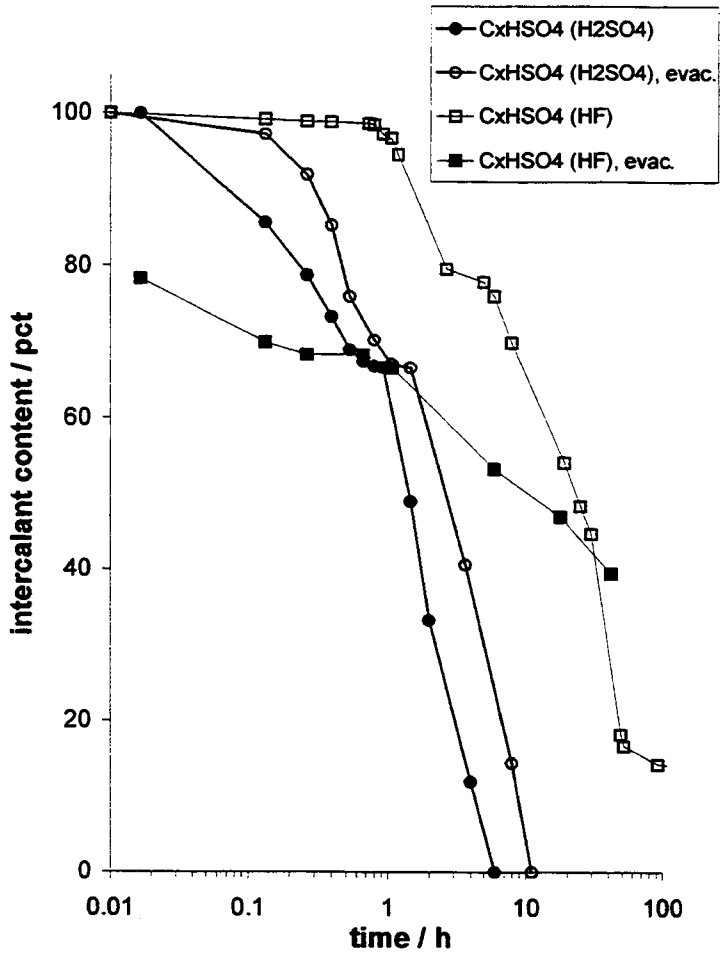


**Figure 4.4(b)** Intercalant content vs. time for GICs exposed to air at 20 °C either as-prepared or after evacuation at 0.1 torr for 24 h.

considerations, some nestling of sulfate anions into graphene layers, [18] and galleries of this dimension can only be achieved from $C_xHSO_4 \cdot \delta H_2SO_4$ by prolonged evacuation. $C_xHSO_4 \cdot \delta HF$, both as-prepared and following evacuation, has a greater environmental stability than $C_xHSO_4 \cdot \delta H_2SO_4$. (Figure 4.4b)

After evacuation of $C_xHSO_4 \cdot \delta HF$, a new, sharp PXRD reflection at 9.13 Å is observed, indicating the formation of a new phase. The peak position corresponds to the stage 2 graphite fluoride $C_xF$, basal repeat distance = 9.15 Å, reported by Bartlett, et. al. [25] Simultaneously, during evacuation the gallery height for $C_xHSO_4 \cdot \delta HF$ *increases* slightly to 7.72 Å. These unusual results can both be understood by an acid-base interaction of the hydrosulfate and neutral HF co-intercalants, leading to phase separation of graphite sulfate and graphite fluoride:

$$[HSO_4^- \cdot (r+s)HF] \rightarrow [(1 - r)HSO_4^- \cdot rH_2SO_4] + r\,[F^-] + s\,HF\,(g) \qquad (4.5)$$

(the brackets indicate intercalated species)

In a separate test of this hypothesis, $C_xHSO_4 \cdot \delta HF$ was maintained under an inert atmosphere for 24 h and periodically examined by PXRD. A new phase appeared again, although this time the greater basal repeat (9.8 Å) indicates that it is a stage 2 graphite bifluoride:

$$[HSO_4^- \cdot (2r)HF] \rightarrow [(1 - r)\,HSO_4^- \cdot rH_2SO_4] + r\,[HF_2^-] \qquad (4.6)$$

This phase separation may play some role in the stabilization of $C_xHSO_4 \cdot \delta HF$ against decomposition. Additionally, these reactions suggest a possible chemical route to obtain graphite fluorides using 48 % hydrofluoric acid. Further characterization of these phase transformations in the future would therefore be desirable.

In each set of reactions described above, it is found that evacuation leads to a decrease in gallery height and increased air stability for the GICs. Similarly, preparation in hydrofluoric acid rather than the parent mineral acid for nitrate and sulfate, again leads to a smaller gallery height and increase in air stability. The changes are least significant for $C_xHSO_4 \cdot \delta H_2SO_4$, where the low volatility of the neutral and the small observed change in gallery heights, indicate that less neutral being removed by evacuation.

A likely mechanism for the observed stabilization is the hydrophilic and even deliquescent nature of the GICs when neutral acidic species are present at higher levels. When $C_xHSO_4 \cdot \delta H_2SO_4$, prepared as a dry powder, is exposed to air for 4 h, ambient moisture adsorbs in sufficient quantity to form a visible liquid coating on the particle surfaces. In contrast, after evacuation $C_xHSO_4 \cdot \delta HF$ remains a free–flowing dry powder even after longer air exposure. Since water is the reducing agent for GICs, hydrophilic surfaces or galleries are not likely to form or provide a passive surface. Additionally, the decrease in gallery heights on removal of neutral species may decrease diffusion rates of ions and molecular species within the intercalated galleries, limiting the rate of exposure of gallery interiors to ambient moisture.

### 4.4.3 Stability of $C_xHF_2 \cdot \delta HF$ after surface protection

The gallery heights obtained for the $C_xHF_2 \cdot \delta HF$ treated with small quantities of large fluoroanions under oxidizing conditions are, at 6.5 Å, unchanged from that of the untreated graphite bifluoride. The stabilities of these GICs are all significantly higher than without surface treatment. In Figure 4.5, the stabilities of $C_xHF_2 \cdot \delta HF$, $C_xHF_2 \cdot \delta HF$ / $C_4F_9SO_3$, $C_xHF_2 \cdot \delta HF$ / $C_8F_{17}SO_3$, $C_xHF_2 \cdot \delta HF$ / $C_6F_5SO_3$, and $C_xHF_2 \cdot \delta HF$ / $N(C_2F_5SO_2)_2$ are compared. The greatest change is seen for $C_xHF_2 \cdot \delta HF$ / $C_8F_{17}SO_3$, where the time to 50 % intercalant loss increases to 6 h.

These reactions demonstrate that development of a hydrophobic surface layer can significantly improve the air stability of GICs. Since bifluoride is readily displaced by $C_8F_{17}SO_3^-$ or $N(C_2F_5SO_2)_2^-$, the passive layer thickness can be controlled by appropriate use of reaction time and stoichiometry. These parameters were not evaluated in this study, but their optimization might enhance the effect significantly. The $C_4F_9SO_3^-$ and $C_6F_5SO_3^-$ anions do not form bulk GICs in 48 % hydrofluoric acid, and the anions do not exchange bifluoride when reacted in excess with $C_xHF_2 \cdot \delta HF$. Nevertheless, the exposure of graphite bifluoride to these anions under oxidizing conditions produces a protective surface as demonstrated by the decreased rate of intercalant loss (Figure 4.5). These results emphasize that a thin surface layer without bulk anion exchange is sufficient to cause a significant change in stability.

### 4.4.4 Natural Graphite as Host Material

Graphite intercalation is a topotactic process and intercalants must enter at particle edges or defects, therefore, the edge surface area of the graphite host should

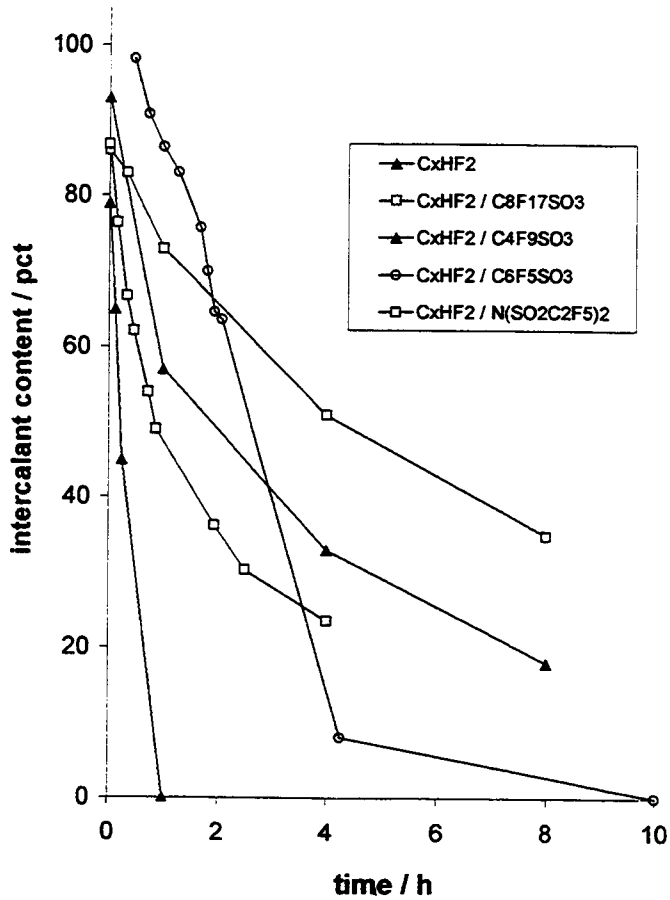


**Figure 4.5** Intercalant content vs. time for $C_xHF_2 \cdot \delta HF$ at 20 °C and these for samples treated with solutions containing large fluoroanions under oxidizing conditions.

affect the rate of intercalation and deintercalation. As was previously reported, intercalation to form $C_{17}C_8F_{17}SO_3 \cdot 4F$ is increased by 10 – 100 times by using natural graphite powder in place of SP-1. Natural graphite has a mean diameter of approx. 1 % of that for SP-1, and the edge surface areas for these platy particles will have a similar ratio. Figure 4.6 shows the relative stabilities of $C_{17}C_8F_{17}SO_3 \cdot 4F$ and $C_xNO_3 \cdot \delta HF$ prepared from the different graphite powders. In each case, GIC prepared from natural graphite decomposes more rapidly by 1 or 2 orders of magnitude than that prepared using SP-1 graphite.

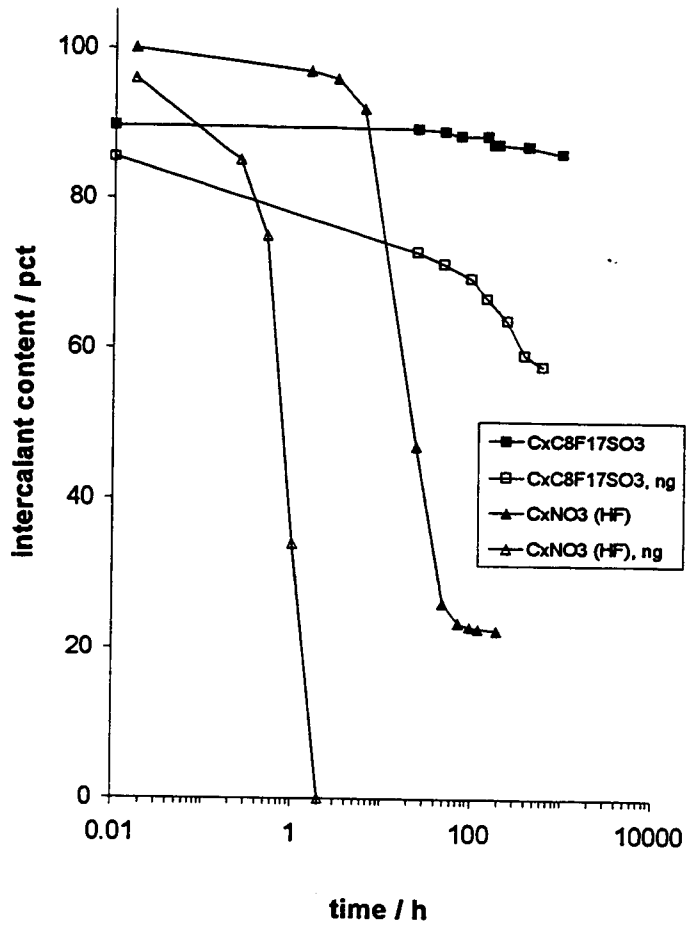


**Figure 4.6** Intercalant content vs. time for $C_xNO_3 \cdot \delta HF$ and $C_{17}C_8F_{17}SO_3 \cdot 4F$ at 20°C, comparing GICs prepared from SP-1 and natural graphite powders.

## 4.5 References


1. Inagaki, M. *J. Mater. Res.*; **1989**, *4*, 6.
2. Rashkov, I. *Mat. Sci. For.* **1992**, *91*, 829.
3. Winter, M.; Besenhard, J.O.; Spahr, M.E.; Novak, P. *Adv. Mater.* **1998**, *10*, 725.
4. Setton, R. *Synth. Met.* **1988**, *23*, 519.
5. Frackowiak, E.; Kaiser, W.; Krohn, H.; Beck, F. *Mol. Cryst. Liq. Cryst.* **1994**, *244*, 221.
6. Schlogl, R.; Bowen, P.; Millward, G. R.; Jones, W.; Boehm, H. P. *J. Chem. Soc., Faraday Trans.* **1983**, *1*, 79, 1793.
7. Endo, M.; Chieu, T.; Dresselhaus, M. *Synth. Met.* **1983**, *8*, 2251.
8. Shioya, J.; Matsubare, h.; murakami, S. *Synth. Met.* **1986**, *14*, 1131.
9. Scholgl, R.; Jones, W. *J. Chim. Physique*, **1984**, *81*, 877.
10. Scholgl. R. in *Progress in Intercalation Research*, Muller-Warmuth, W; Schollhorn, R., Kluwer Acad Publ., Netherlands, **1993**.
11. Yosida, Y.; Sato, K.; Suda, K.; Suematsu, H. *Synth. Met.* **1985**, *12*, 167.
12. Walter, J.; Shioyama, H. *Synth. Met.* **1998**, *92*, 91.
13. Zhang, X.; Lerner, M.M. *Chem. Mater.* in press.
14. Zhang, X.; Sukpirom, N.; Lerner, M.M. *Mater. Res. Bull.* in press.
15. Bode, H.; Jenssen, H.; Bandte, F. *Angew. Chem.* **1953**, *65*, 304.
16. The oxidation of graphite and consequent intercalation of anions often results in the co-intercalation of polar neutral species from the reactants, solvent, or electrolyte. Their role in the stability of the GICs will be discussed but the predominant neutral

species present during reaction is indicated in each case. Where more accurate compositions have been determined, these are provided.

17. Rudorff, W.; Hofmann, U. *Z. Phys. Chem.* **1938**, *238*, 1.

18. Bartlett, N.; McQuillan, B. in *Intercalation Chemistry*; Whittingham, S.; Jacobson, A., Eds.; Acad. Press: New York, **1982**.

19. Takenaka, H.; Kawaguchi, M.; Lerner, M.; Bartlett, N. *J. Chem. Soc., Chem. Commun.* **1987**, 1431.

20. Touzain, P. *Synth. Met.* **1979**, *1*, 3.

21. A stage 2 $C_xHF_2 \cdot \delta HF$ / $C_4F_9SO_3$ was obtained, and $d_i$ was found to be 6.48 Å.

# Chapter 5

## Structural Refinement of $C_xC_8F_{17}SO_3$ Prepared in Mixed Acids or 48% Aqueous HF

*Xuerong Zhang and Michael M. Lerner,**
*Department of Chemistry and Center for Advanced Materials Research,*
*Oregon State University,*
*Corvallis, OR 97331-4003, USA.*

**to be submitted**

## 5.1 Introduction

Graphite is a unique host that can undergo both oxidative and reductive intercalation. A broad range of anionic species have been intercalated into graphite by oxidation of the carbon layers, including oxoanions, fluoroanions, and chlorometallates. Unlike intercalation compounds from many layered metal oxides, oxyhalides, and sulfide, which can exhibit stacking repeat dimensions of 20 - 30Å or more, the gallery heights for most graphite compounds are less than 10 Å. [1] The smaller gallery heights, in combination with the strong preferred orientation, lead to relatively few observed diffraction peaks, which constitute an obstacle to detailed structural refinement of the graphite intercalation compounds (GICs).

Boehm, et al first reported electrochemical intercalation of perfluoroalkyl-sulfonate anions into graphite in the molten acids. [2-4] A dramatic expansion of the gallery height ($d_i$) was observed when graphite was intercalated with $C_nF_{2n+1}SO_3^-$ ($n \geq 4$), $d_i$ was found to be 17.7 Å for $C_xC_4F_9SO_3$, and 34 Å for $C_xC_8F_{17}SO_3$ ($C_x$PFOS). In these GICs, the large gallery dimensions indicate that a bilayer intercalant structure is the most reasonable model. The three oxygens in each anionic $-SO_3$ headgroup can be positioned in a plane parallel to graphite sheets, and the hydrophobic fluorocarbon chains oriented towards the center of the gallery. There was, however, very limited structural characterization presented in the original reports. PFOS anions were also intercalated into graphite by electrooxidation in a $LiC_8F_{17}SO_3/CH_3NO_2$ electrolyte. A stage 2 GIC was obtained with $d_i = 26 - 27$ Å, significantly lower than the previous values [5].

We recently reported the synthesis of $C_x$PFOS in 48% aqueous HF or a mixed acid solution containing aqu. HF and concentrated nitric or sulfuric acid, using $K_2MnF_6$ as an oxidant. The gallery heights were found to be approx. 29.6 Å. Some results of structural refinement were also included, using a linear anion geometry generated from semi-empirical PM3 calculations. Stage disorder was observed for the products prepared in aqu. HF and a solid solution model was found to provide a better fit to the data than a physical mixture of stages.

Stage disorder is a common phenomenon seen in graphite intercalation compounds (GICs), which can be described as frequent stacking faults in the ordered staging arrangement for graphene and intercalant layers. Stage disorder is most significant at high temperature and with higher stages due to the increase of entropy term relative to the enthalpy difference between stages. Hendricks-Teller's theory [6] on the effects of one-dimensional disorder in lattice diffraction interprets the diffraction peak shift and broadening in terms of a structural model that includes stage disorder. Fuerst, et al. observed that the *00l* peaks for a $C_xK$ containing 76% : 24% of stage 7: 8 shift from the ideal stage 7 positions in an oscillating manner as a function of the Bragg index *l*. [7,8] In a detailed modeling study on stage disorder in $C_xK$ done by Huster et al [9], two parameters were used to describe the probability distribution for component stages: one related to the overall stoichiometry and another, $\alpha$, related to the type of disorder present. In their study, $\alpha = 1$ represented a complete separation of all phases with different stages, $\alpha = 0$ was a truly random solution of the different types of staging, and $\alpha = -1$ indicated an ordered superlattice where the component stages alternated regularly. The stage 4-5

GICs were found to best fit a partially random mixture of two stages, while samples of stage 6 and higher were best fit as a mixture of many stages GICs.

Although studies have been done on stage disorder of donor-type GICs, such as alkaline metal compounds, there have been only two reports on stage disorder for acceptor-type compounds. Hohlwein and Metz reported peak broadening and the periodic shift of Bragg reflections due to stage disordering for $C_xFeCl_4 \cdot \delta FeCl_3$. [10] Suzuki, et. al. have studied stage disorder in $C_xCo_cM_{1-c}Cl_2$ GICs (M = Mn, Ni) and found that the stage-disorder-induced peak shifts and full width at half-maxima (FWHM) of the Bragg reflections oscillate as a function of the Bragg index. [11] The GICs were assumed to be a random solid solution and a physical mixture of stages was not considered in their model.

The PM3 optimized structure of PFOS predicted longer C-C bonds (1.6-1.65 Å) than the expected value (1.54 Å). In order to obtain a reliable starting geometry for further structural refinement, the hybrid density functional method (DFT) method was employed to perform full geometry optimization of the PFOS anion. A helical structure was obtained, with the C-C bond lengths were calculated to be 1.52-1.54 Å. We here report the detailed structural refinement of a chemically-synthesized stage 2 $C_x$PFOS using the new optimized anion structure. Stage disorder analysis of a random stage 2/3 GIC with the same anion will also be presented in more detail.

## 5.2 Experimental

A stage 2 $C_xC_8F_{17}SO_3$ was obtained by oxidizing SP-1 graphite powder (Union Carbide, 100 um avg. particle diameter) with $K_2MnF_6$ in a solution containing 83:17 (v/v)

of 48% aqu. HF and 69% $HNO_3$ under ambient conditions for 1 day. [12] The $C_xPFOS$ exhibiting stage disorder were prepared from a solution of SP-1 graphite powder and $K_2MnF_6$ in 48% aqu. HF at room temperature.

PXRD data were collected on a Siemens D5000 powder diffractometer, using CuKα radiation, with 0.02 ° 2θ steps, between 1.5 and 60 degrees. The data collection time was 1 s / step. Elemental analyses (C, H, N) were performed by Desert Analytics (Tuscon, AZ). Integration of $^{19}F$ NMR peaks for $-CF_3$ endgroup analysis indicated that the $C_8F_{17}SO_2F$ reagent used contained 70 % linear and 30 % branched isomers, with the predominant branched isomer being $(CF_3)_2C(F)(CF_2)_5SO_2F$. The same isomeric composition for the potassium salt and GICs was assumed.

Energy-minimized structural models for the PFOS anion were calculated using Gaussian 94 [13] and a full geometry optimization was carried out using density functional theory. The method employed was Becke's three parameter hybrid functional with the non-local correlation provided by Lee, Yang and Parr (B3LYP) [14] and the split valence basis set 3-21G*. The structural minima was characterized by frequency calculation.

The twist angle was used to measure the helical nature of the carbon backbones, therefore the twist angle is ~ 0° for a linear structure, and otherwise (180° – dihedral F2-C1-C2-F3). The twist angle for the PFOS anion in GICs was optimized in the structural refinement. The effect of twist angle on the atomic z values of all atoms in the unit cell was established as follows: all bond distances and angles were constrained as the minimum energy structure values, the twist angle was varied and subsequently optimized at the PM3 semi-empirical level using Spartan 4.0 [14]. The atomic z coordinates were

then obtained for each twist angle allowing the $-SO_3$ headgroup to lie flat on the graphite surface. The twist angles for linear and branched isomers were kept the same.

A centrosymmetric unit cell was generated for a simple stage 2 $C_xC_8F_{17}SO_3$ and one-dimensional electron density maps were generated for both the experimental diffraction data and the proposed structural model using equations 1.5 and 1.6. The structure model was then refined by minimizing the crystallographic R factor (defined in equ. 1.7). The refined parameters were used construct structural models for the stage 2-3 GICs.

PXRD pattern simulations were performed by DIFFaX (v. 1.76) [15], using pseudo-Voigt peak profiles. Data collected between 14 and 17.5 ° 2θ were excluded due to small, broad peaks at 5.8 and 5.4 Å, that are ascribed to a $C_xF$ impurity phase. The DIFFaX software allows the introduction of probability in the stacking sequence in structural models, and was described in more detail in Section 1.6.3.

## 5.3 Results and Discussion

### 5.3.1 Stage 2 Structure Model Refinement

The optimized geometry for the isolated PFOS anion shows a helical conformation of the carbon backbone with an average twist angle of 20°, smaller than that for polytetrafluoroethylene, which crystallizes with a 13 carbon atom helix (average twist angle = 360°/13 = 28°). [16] A comparison of the geometries of the helical and linear anions is provided in Fig. 5.1, and calculated structural parameters for the optimized anion geometry are listed in Table 5.1.

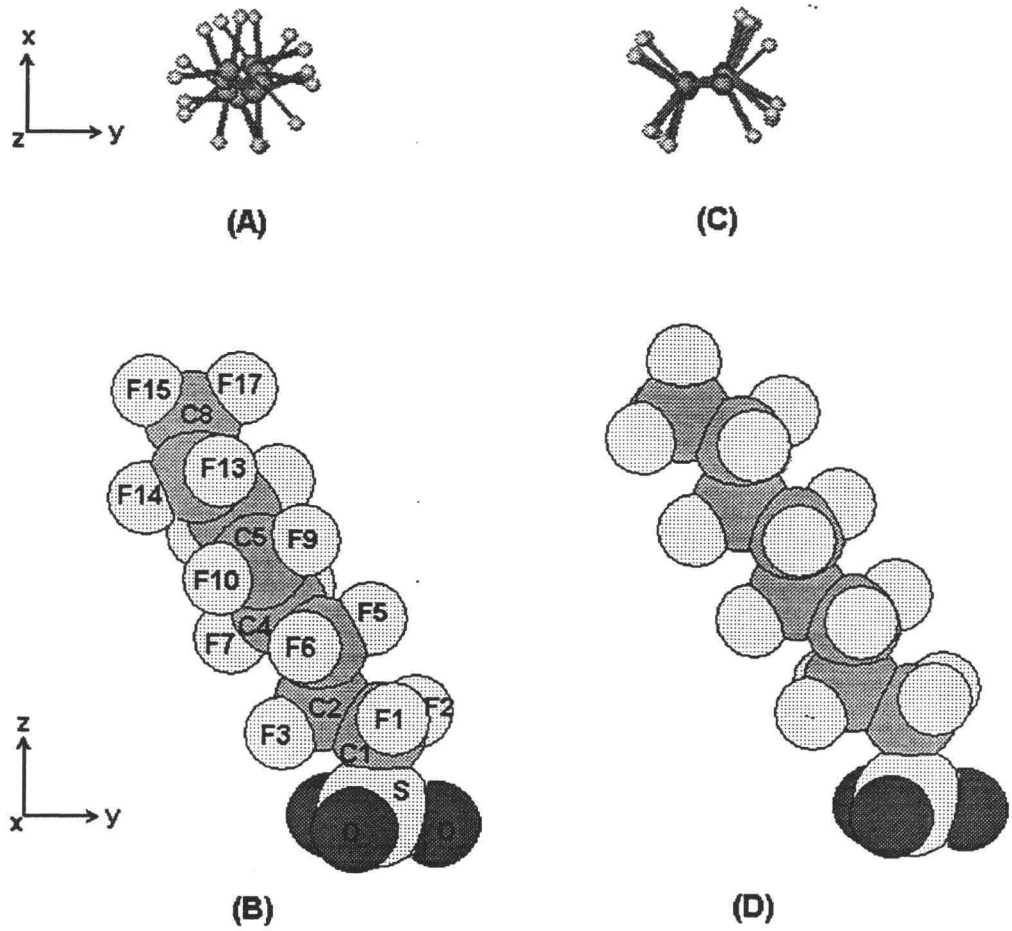


**Figure 5.1** Comparison of the twisted and linear geometries of PFOS anion. (A) and (B) are the view of twist structure obtained from ab initio calculations. (C) and (D) are the nearly linear structure provide by semi-empirical calculations. Axes and some atomic labels are included.

**Table 5.1** Selected calculated structure parameters for the PFOS anion obtained from the b3lyp calculation (3-21G* basis set). Bond lengths (r) in Å and angles (a) and dihedrals (d) in degrees.

| | | | |
|---|---|---|---|
| a(O1-S1-O2) | 116.6 | r(O1-S1) | 1.59 |
| a(O3-S1-O2) | 116.7 | r(O2-S1) | 1.59 |
| a(O1-S1-O3) | 116.2 | r(O3-S1) | 1.59 |
| a(F2-C1-F1) | 109.7 | r(C1-S1) | 1.97 |
| a(F4-C2-F3) | 110.5 | r(C1-C2) | 1.51 |
| a(F5-C3-F6) | 110.0 | r(C2-C3) | 1.54 |
| a(F8-C4-F7) | 110.4 | r(C3-C4) | 1.54 |
| a(F9-C5-F10) | 110.4 | r(C4-C5) | 1.54 |
| a(F12-C6-F11) | 110.0 | r(C5-C6) | 1.54 |
| a(F13-C7-F14) | 110.1 | r(C6-C7) | 1.54 |
| a(F17-C8-F16) | 109.5 | r(C7-C8) | 1.53 |
| a(F15-C8-F16) | 108.6 | r(C1-F2) | 1.38 |
| a(F15-C8-F17) | 108.5 | r(C1-F1) | 1.39 |
| | | r(C2-F4) | 1.39 |
| | | r(C2-F3) | 1.38 |
| | | r(C3-F5) | 1.38 |
| | | r(C3-F6) | 1.38 |
| | | r(C4-F7) | 1.38 |
| | | r(C4-F8) | 1.38 |
| | | r(C5-F9) | 1.38 |
| d(F2-C1-C2-F3) | 161.6 | r(C5-F10) | 1.38 |
| d(F3-C2-C3-F5) | 158.3 | r(C6-F11) | 1.38 |
| d(F5-C3-C4-F7) | 160.3 | r(C6-F12) | 1.38 |
| d(F7-C4-C5-F9) | 158.4 | r(C7-F13) | 1.38 |
| d(F9-C5-C6-F11) | 159.4 | r(C7-F14) | 1.37 |
| d(F11-C6-C7-F13) | 157.1 | r(C8-F15) | 1.37 |
| | | r(C8-F16) | 1.37 |
| | | r(C8-F17) | 1.36 |

Knochenhauer et al have demonstrated using diffraction data and molecular calculations that isolated molecules of perfluorododecanoic acid have a helical conformation, however, the molecules return to a linear conformation for the energy minimum when packed into a periodic structure. [17] In the structural refinement, the twist angle was allowed to vary between 0° (linear) and 20° (isolated anion value). The calculated correlation of atomic z coordinates in the unit cell and the twist angle is provided in Fig. 5.2. For a linear chain anion, the z values for C and F are clustered into four groups, each containing two adjacent $-CF_2-$ or $-CF_3$ groups. The four peaks in the calculated 1-D electron density map for the linear chain at z = 0.23, 0.30, 0.38, and 0.45 are consistent with the clusters (Figure 5.3). As the twist angle of the carbon backbone increases, these z coordinate clusters broaden and eventually merge, with the effect most pronounced for groups closest to the gallery center. With a twist angle of 20°, the clustering is only obvious for the first $-C_2F_4-$ group in the chain.

In previous refinement (chapter 2), four parameters were employed: the chain take-off angle (56.6°), the graphene plane to sulfonate oxygen plane distance (3.04 Å), the graphene plane to fluoride plane distance (3.8 Å), and the graphene carbon / intercalant molar ratio (x = 21.6). These results provide a reliability factor R = 0.082 for $C_{21.6}$PFOS·4F. However, the linear geometry of PFOS used was optimized using PM3 methods, which gives unusually long C-C bonds. The new refinement is carried out using the DFT-calculated PFOS structure. A fixed stoichiometry composition of $C_{20}C_8F_{17}SO_3$·5F is used in the refinement, based on the elemental analysis results reported previously [1], and is not further refined. A single plane of fluorines is placed at ~ 3 - 4 Å above the graphene layers (where additional electron density is observed) as in

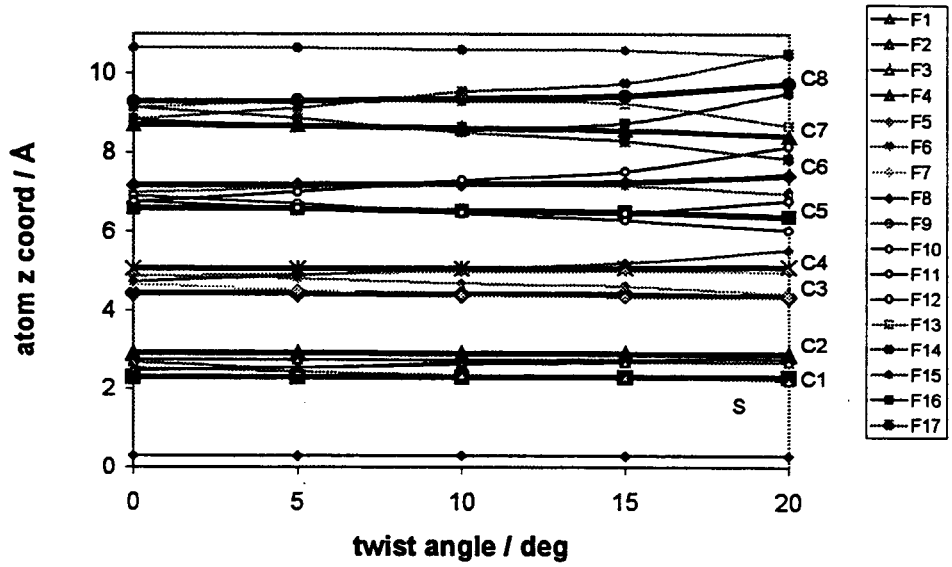


**Figure 5.2** The correlation of atom position along z with the twist angle of PFOS chain.

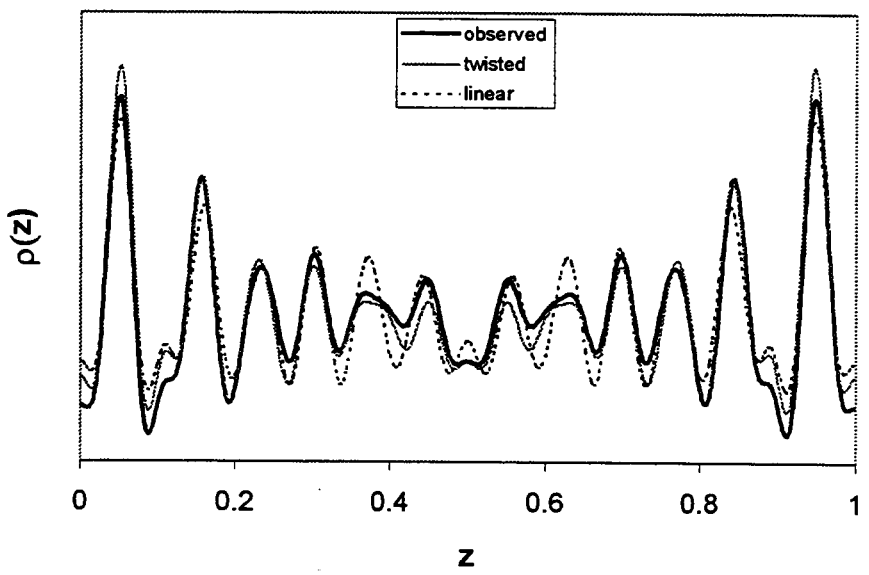


**Figure 5.3** Observed and calculated one-dimensional electron density maps for $C_{20}C_8F_{17}SO_3 \cdot 5F$.

previous work. [12]The electron density map calculated from the observed PXRD along with the best fit from the linear geometry is shown in Figure 5.3. The calculated electronic map for the linear anion geometry predicts relatively sharp electron density peaks, especially at z = 0.38, for the successive $-CF_2$ or $-CF_3$ groups when compared to the e-map derived from the observed data. The refined e-map incorporating a twisted angle for the carbon backbone provides an excellent match to the desired profile and the four refined parameters as well as the R values for the best-fit structures from both the helical and linear are provided in Table 5.2. Figure 5.4 shows the observed and calculated PXRD for the refined helical structure model of the stage 2 $C_{20}C_8F_{17}SO_3 \cdot 5F$.

### 5.3.2 Stage disordering in $C_x$PFOS

A simple stage model fails to provide reasonable fit in peak positions for majority of Bragg (*00l*) reflections from $C_xC_8F_{17}SO_3$ prepared in 48% aqu. HF. A better fit to the observed peak positions can be obtained using a weighted average of the calculated stage 2 and 3 positions (assuming the same gallery height for both stages). Figure 5.5 shows the calculated 00l reflections from stage 2 and 3 respectively of $C_xC_8F_{17}SO_3$ containing a gallery height of 29.6 Å.

In a physical mixture of stage 2 and 3 phases, the broadening due to overlapping reflections can be determined by considering the minimum separation, Δ, between the nearest calculated peak positions for the two phases and the intrinsic FWHM peak width. This function Δ for any two adjacent stages has minima at d = 3.354 Å / m, where m is an integer. In Figure 5.5, the function is plotted against 4sinθ and the minima can be seen

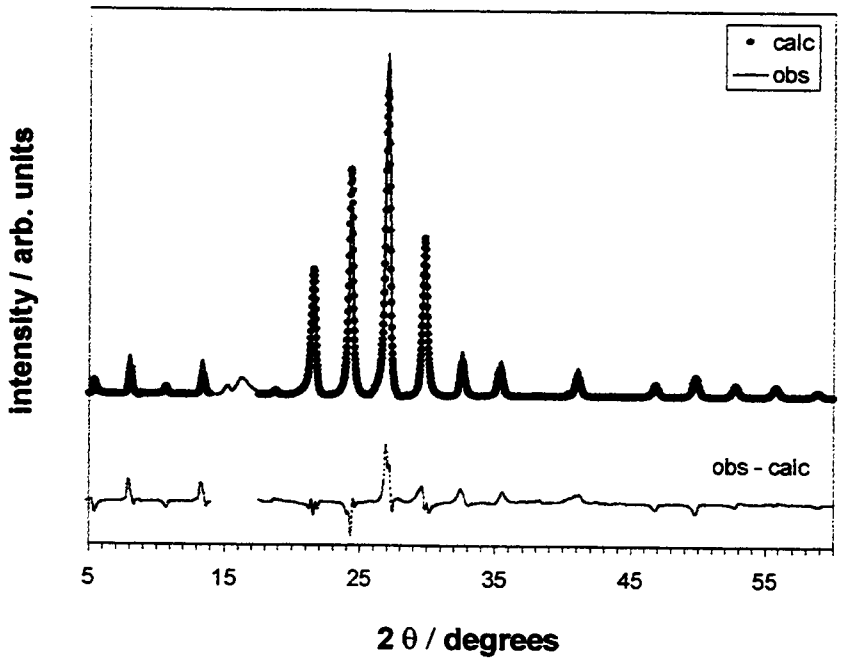


**Figure 5.4** Observed and calculated PXRD patterns for $C_xPFOS$ prepared by 24 hours reaction using $HNO_3$ 17% (v / v) in 48% aqu. HF. Data between 14 and 17.5° 2θ were excluded due to peaks ascribed to a $C_xF$ impurity phase.

**Table 5.2** Refined parameters for the best-fit helical and linear model:

| | Helical model | Linear model |
|---|---|---|
| Chain take-off angle (deg) | 60.0 | 58.8 |
| Graphene plane to sulfonate oxygen plane distance Å | 2.95 | 3.05 |
| Graphene plane to fluoride plane distance Å | 3.8 | 3.9 |
| Twist angle (deg) | 16.4 | 0 |
| R | 0.062 | 0.168 |

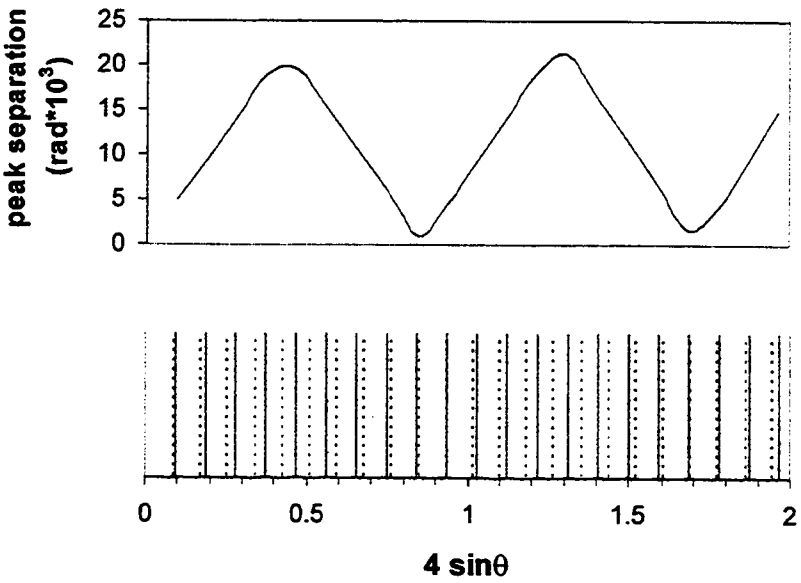


**Figure 5.5** Calculated positions for (*00l*) reflections from stage 2 and stage 3 phases and their minimum separation Δ function.

for n = 1 and n = 2. The first minimum close to d = 3.354 Å, corresponds to the near overlap of stage n *(0,0,l)* reflection with the stage n+1 *(0,0,l+1)* reflection, and the minima at 1.68Å is due to the near overlap of stage n *(0,0,l)* with stage n + 1 *(0,0,l+2)* reflections, respectively. For $C_x$PFOS, the stages are n = 2 or 3 and the reflections are (0, 0, 10) and (0, 0, 11) for first minimum, and (0,0,18) and (0,0, 20) for the next minimum. The Δ function will be greatest at ≈ 5 – 15 ° and ≈ 35 - 40° 2θ, where peakwidths of approx. 1.5° 2θ are predicted (or separate peaks will be resolved for sharper reflections).

The experimental data show single peaks for each *(00l)* reflection with much smaller peakwidths than those predicted value by a physical mixture. For example, the observed *(003)* reflection for the GIC prepared in aqu. HF has a single peak at 2θ = 8.0° with a peakwidth of 0.43° 2θ which should be easily resolved as three distinct peaks for a physical mixture of stages 2 and 3. For these reasons, the patterns were instead evaluated using the model of a best fit as solid solution resulting from stage disorder between two stages.

Two factors contribute to peak broadening in solid solution material of $C_x$PFOS. One is the strain – domain size broadening that relates peakwidth to the finite coherent domain size and lattice strain in the stacking direction, and predicts a linear relationship between full-width at half-maximum (FWHM) and tanθ [18]. The other effect is due to the disordered presence of the two component sequences (in this case, stage 2 and stage 3), which is will result in an oscillating peakwidth similar generally to the Δ function predicted from the physical mixture model. The magnitude of peakwidth oscillation, however, as determined from calculations, is much smaller and closely related to the extent of stage disorder. Figure 5.6 shows calculated peak broadening for random solid

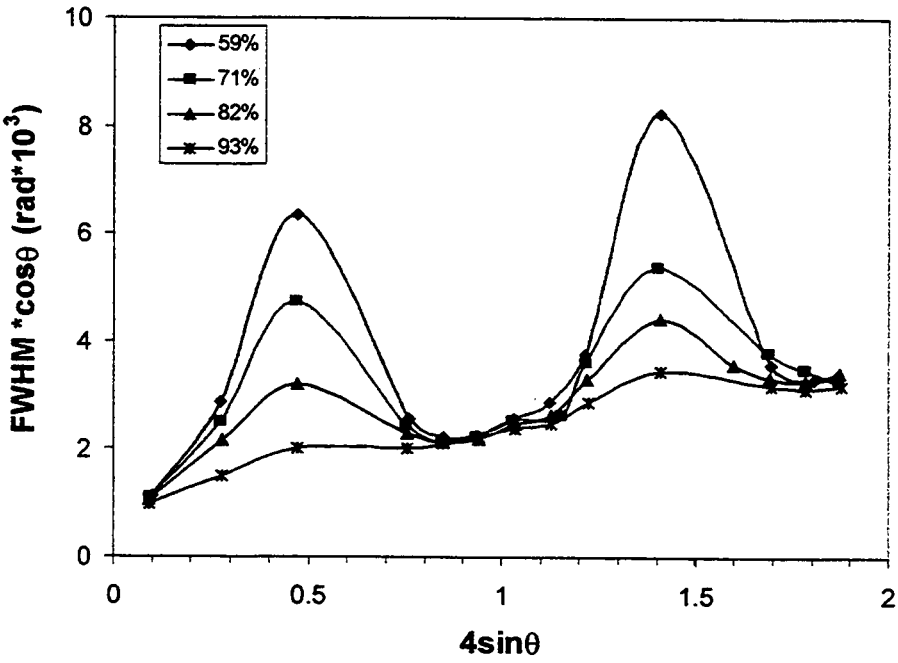


**Figure 5.6** Williamson-Hall plot for $C_x$PFOS calculated using the random solid solution model for stage 2-3. The percentage of 2nd staging component for the structural models is indicated in the legend.

solutions of $2^{nd}$ and $3^{rd}$ staging with different compositions. When the GIC has fewer defects and is close to stage 2 (93%), the magnitude of oscillation in peakwidth is very small, the strain - domain broadening is dominant, resulting in a nearly linear plot. The magnitude of oscillation increases as more $3^{rd}$ staging component is introduced. These observations agree with the experimental data (Table 5.3) from $C_xPFOS$ prepared in 48% aqu. HF with various reaction time and temperature (Figure 5.7). Both observed and calculated peakwidth have similar magnitudes for peakwidth and sa imilar trend of decreasing peak width with increasing $2^{nd}$ staging content (Figure 5.8). As a result, a random solid solution model due to stage disorder is concluded to be a better model for these products than a physical mixture.

The PXRD of the observed 71%: 29% of $2^{nd}$: $3^{rd}$ staging components as well as the calculated patterns using solid solution model is shown in Figure 5.9. All structural parameters are maintained the same as the stage 2 model and not further refined. A reasonable fit to the data is obtained.

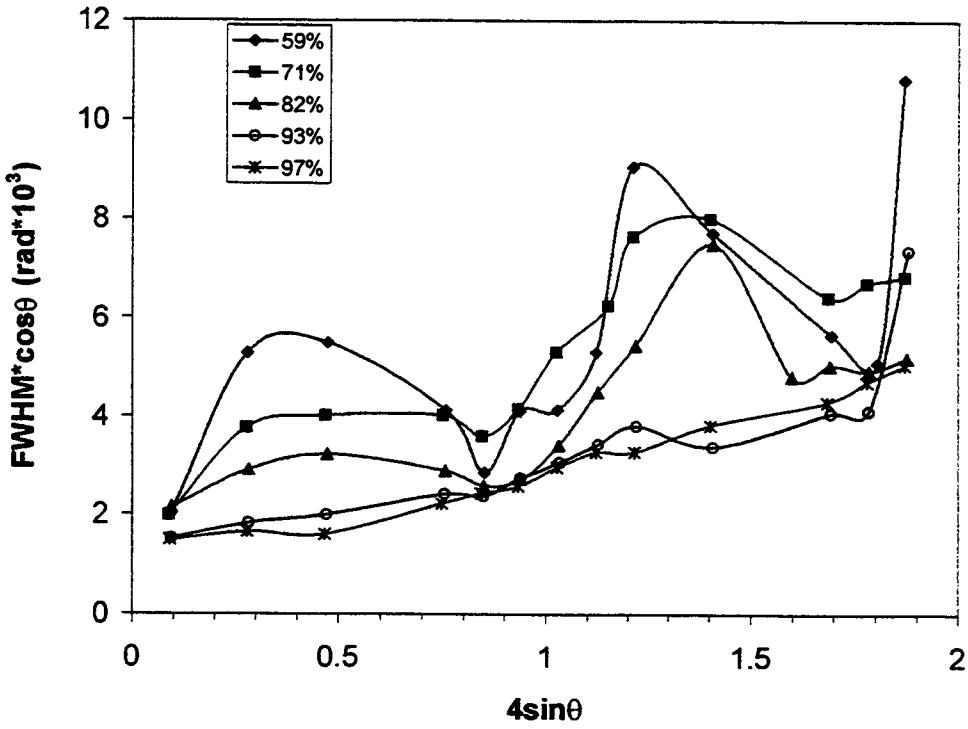


**Figure 5.7** Williamson-Hall plot for different compositions of 2nd and 3rd staging of $C_x$PFOS obtained from 48% aqu. HF. The percentage of 2nd staging is as indicated in the legend.

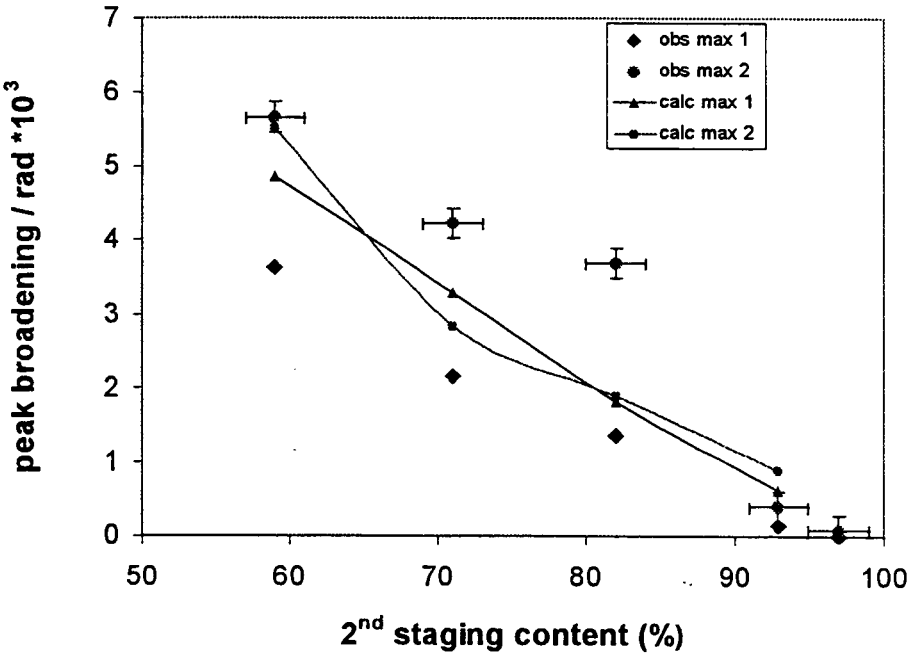


**Figure 5.8** The observed and calculated correlation of peak broadening with the percent 2nd staging present using a random stage disorder model. The oscillation maxima are derived from the disorder induced peak broadening, i. e. the maximum observed or calculated FWHM*cosθ less that predicted from strain-domain effects.

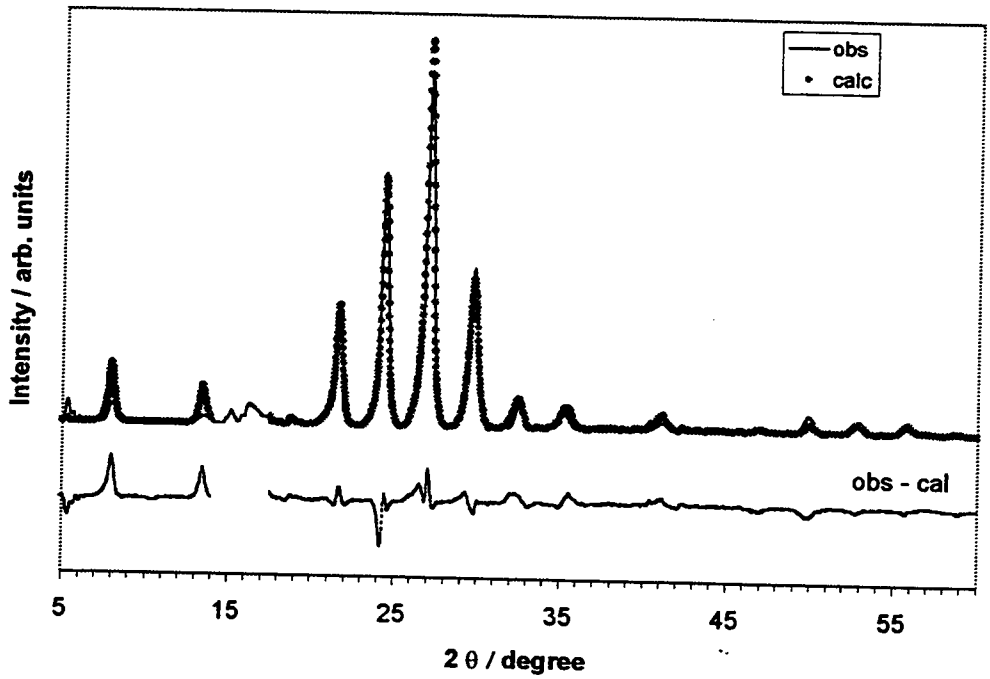


**Figure 5.9** Observed and calculated PXRD patterns for $C_xPFOS$ prepared by 72 hour reaction in 48% aqu.HF. Data between 14 and 17.5° 2θ were excluded due to peaks ascribed to a CxF impurity phase.

**Table 5.3** $C_x$PFOS obtained from 48% aqu. HF.

| Reaction | Reaction time at 20°C (h) | Reaction time at 70°C (min) | % 2nd staging | % 3rd staging |
|---|---|---|---|---|
| 1 | 48 | | 59 | 41 |
| 2 | 72 | | 71 | 29 |
| 3 | 96 | | 82 | 18 |
| 4 | | 30 | 93 | 7 |
| 5 | 24* | | 97 | 3 |

1. In this reaction, 83:17 v/v of 48% aqu. HF and 69% $HNO_3$ was used.

## 5.4 Reference


1 Bartlett, N.; McQuillan, B. in *Intercalation Chemistry*; Whittingham, S.; Jacobson, A., Eds.; Acad. Press: New York, **1982**.

2 Ruisinger, B; Boehm, H. P. *Angew. Chem. Int. Ed. Engl.* **1987**, *26*, 253

3 Boehm, H.P.; Helle, W.; Ruisinger, B. *Synth. Met.* **1988**, *23*, 395

4 Ruisinger, B.; Boehm, H.P. *Carbon* **1993**, *31*, 1131.

5 Zhang, Z.; Lerner, M. *Chem. Mater.* **1996**, *8*, 257.

6 Hendricks, S.; Teller, E. *J. Chem. Phys.* **1942**, *10*, 147.

7 Fuerst, C.; Fischer, J.; Axe, J.; Hastings, J.; McWhan, D. *Phys. Rev. Lett.* **1983**, *50*, 357.

8 Fischer, J.E.; Fuerst, C.D; Woo, K. C. *Phys. Rev. B* **1989**, *39*, 4374.

9 Huster, M.E.; Heiney, P.A.; Cajipe, V.B.; Fischer, J.E. *Phys. Rev. B* **1987**, *35*, 3311.

10 Hohlwein, D.; Metz, W. *Z. Kristallogr.* **1974**, *139*, 279.

11 Suzuki, I. S.; Suzuki, M. *J. Phys. Condens. Matter.* **1991**, *3*, 8825.

12 Zhang, X.; Lerner, M. *Chem. Mater.* **1999**, in press.

13 Frisch, M. J. et. al. *Gaussian 94*, Revision E.1, Gaussian, Inc., Pittsburgh PA, **1995**.

14 Hehre, W.J.; Shusterman, A.J.; Huang, W.W *A Laboratory Book of Computational Organic Chemistry*, Wavefunction Inc., Irvine, CA, **1996**.

15 Treacy, M. M; Newsam, J. M.; Deem, M. W. *Proc. R. Soc. Lond. A* **1991**, *433*, 499.

16 Bunn, C.W.; Howells, E.R. *Nature* **1954**, *4429*, 549.

17 Knochenhauer, G.; Reiche, J.; Brehmer, L; Barberka, T.; Woolley, M; Tredgold, R.; Hodge, P. *J. Chem. Soc., Chem., Commun.* **1995**, 1619.

18 Williamson, G.; Hall, W. *Acta Metallurgica* **1953**, *1*, 22.

# Chapter 6

## Ab initio Studies of Some Fluoroanion Intercalants of Graphite

*Xuerong Zhang, James K. Pugh and Michael M. Lerner,**
*Department of Chemistry and Center for Advanced Materials Research,*
*Oregon State University,*
*Corvallis, OR 97331-4003, USA.*

**to be submitted**

## 6.1 Introduction

The high electronegativity of the trifluoromethanesulfonyl group, $\chi_p = 2.49(9)$ [1], $CF_3SO_2$-, lead to bis(trifluoromethanesulfonyl) imide $N(CF_3SO_2)_2^-$ and tris(trifluoromethanesulfonyl) methide $C(CF_3SO_2)_3^-$ anions that form salts with a high extent of dissociation in polar solvent and excellent oxidative stability. The lithium salts have high ionic conductivities in organic and polymer solutions and there have been demonstrated to have electrochemical stabilities as high as 5.2 V [2]. They have been studied for use in lithium ion batteries and related applications. [3,4] The crystal structures for $HN(CF_3SO_2)_2$ [5,8], $KN(CF_3SO_2)_2$ [5], $Mg(H_2O)_6[N(CF_3SO_2)_2]_2 \cdot 2H_2O$ [8] and $HC(CF_3SO_2)_3$ [9] have been determined and ab initio calculations on molecular structures have been done for the isolated anions $N(CF_3SO_2)_2^-$ [6,7] and $HC(CF_3SO_2)_2^-$ [6].

Lindgren et. al [7] performed ab initio self-consistent-field Hartree-Fock (HF) calculations on $N(CF_3SO_2)_2^-$. In the study, a one-dimensional potential energy surface was generated through rotation of the C-S-N-S dihedral angle in steps of 30°. Two minimum energy anion geometries were found and then each was optimized using 6-31G* basis set. The energy difference between the minima was calculated to be 2.3kJ $mol^{-1}$, with a rotational barrier of only 3.9 $kJmol^{-1}$. These results were thus used to explain the known plasticizing effect observed for the lithium imide salt when dissolved in crystalline organic polymer such as poly(ethylene oxide).

We have recently reported the chemical intercalation of these and related fluoroanions into graphite in 48% aqu. HF. [10] Graphite intercalation compounds (GICs) were prepared with $N(CF_3SO_2)_2^-$, bis(pentafluoroethanesulfonyl) imide

$N(CF_3CF_2SO_2)_2^-$, (trifluromethanesulfonyl-n-nonafluorobutanesulfonyl imide $N(CF_3SO_2)(CF_3(CF_2)_3SO_2)^-$ and $C(CF_3SO_2)_3^-$. Dramatic differences in reaction kinetics were observed for these fluoroanions. The $N(CF_3SO_2)_2^-$ anion intercalates graphite rapidly, the graphite phase disappears in 15 seconds and a stage 2 GIC is formed in 15 minutes. In contrast, under these conditions, it takes weeks for the other three fluoroanions to form stage 3 or higher GICs. The reaction conditions and the resulting GICs from these anions are compared in Table 6.1. The reaction rates for these anions can be summarized as follow:

$$N(CF_3SO_2)_2^- >> N(CF_3CF_2SO_2)_2^- > N(CF_3SO_2)(CF_3(CF_2)_3SO_2)^- > C(CF_3SO_2)_3^- \quad (6.1)$$

Although the rate of GIC formation can be increased in all cases by use of a smaller particle size graphite reagent or higher reaction temperatures, the very large difference in inherent insertion rates for these anions suggested some further study of the anion structures themselves. In order to achieve better understanding of the graphite intercalation kinetics and the nature of the GICs obtained, semi-empirical and ab initio calculations have been performed for these fluoroanions. The optimized geometries will be reported below for all anions listed in equ. 6.1. The energy potential surface maps and rotational energy barriers for $N(CF_3SO_2)_2^-$, $N(CF_3CF_2SO_2)_2^-$ and $N(CF_3SO_2)(CF_3(CF_2)_3SO_2)^-$ are reported below, and these results discussed in terms of anion structure and mobility in GICs.

**Table 6.1** Reaction rates and gallery heights for different fluoroanion intercalants in GICs:

| Intercalant | Reaction temperature | | $d_i$ (Å) |
|---|---|---|---|
| | 20°C | 70°C | |
| $N(CF_3SO_2)_2^-$ | 15 minutes to stage 2 | Seconds to stage 2 | 8.07(4) |
| $N(CF_3CF_2SO_2)_2^-$ | 1 month to a mixture of stage 3 and higher | 2 days to stage 2-3 mix + graphite[a] | 8.2(1) |
| $N(CF_3SO_2)(CF_3(CF_2)_3SO_2)^-$ | 1 month to high stage + graphite | 6 days to a 3rd and 4th stage mixed + graphite[a] | 8.2(1) |
| $C(CF_3SO_2)_3^-$ | 1 month to high stage + graphite | 24 days to stage 4 + graphite[a] | 10.6(3) |

a. Natural graphite powder (1-2μm particle diameter) was used in place of Sp-1 graphite (100 μm particle diameter) for these reactions.

## 6.2 Computation Methodology

In order to obtain an initial probe of the energy profile, PM3 semi-empirical calculations were performed. The coordinate driving procedure included in the Spartan 5.1 suite of program [11] was utilized to map the potential energy surface for dihedral rotation angle C1-S1-S2-C2 (this dihedral will be abbreviated as C-S-S-C here on) for $N(CF_3SO_2)_2^-$, $N(CF_3CF_2SO_2)_2^-$, and $N(CF_3SO_2)(CF_3(CF_2)_3SO_2)^-$. The dihedral C-S-S-C was rotated counter clockwise by 360° in 40 equal steps of 9°, beginning with an initial optimized minimum. Once a plot of relative energy versus structure was generated, each found energy minimum and maximum was fully optimized and characterized as a minima or transition structure by a frequency calculation at the PM3 level. Geometry optimizations at the Hartree Fock (HF) level combined with the 3-21G* basis set were then performed on each minima using the Gaussian 94 and Gaussian 94W suite of programs [12], which also provided the Mulliken charges for all atoms. The hybrid density functional method (DFT) of Becke and Purdew (b3lyp) [11] with the split valence 6-31G* basis set included in the Gaussian programs were conducted on the $N(CF_3SO_2)_2^-$ and $C(CF_3SO_2)_3^-$ anions. As it provides electron correlation, the b3lyp gives more accurate values for energies than the other methods employed (the HF calculations tend to overestimate the energies when compared with the experimental values). The DFT structures were also characterized as energy minima by subsequent frequency calculations.

The minimum energy geometries labeled as conformations 1 – 5 denote the structure found by PM3 calculations, corresponding to the minima shown in Figure 6.1.

Conformations denoted 1'- 5' represent the structures found by HF calculations, the starting geometry of which are conformations 1 – 5. Conformations 1''- 5'' are the energy minima obtained by b3lyp calculations. The ' – ' sign for C-S-S-C dihedral indicates the rotation is counter-clockwise from the geometry with both S-C bonds eclipsed.

## 6.3 Results and Discussions

### 6.3.1 Computational Results

#### *6.3.1.1 PM3 Calculations*

The one dimensional potential energy maps for $N(CF_3SO_2)_2^-$, $N(CF_3CF_2SO_2)_2^-$, $N(CF_3SO_2)(CF_3(CF_2)_3SO_2)^-$ have significant similarities (Figure 6.1). There are approximately five energy minima observed for each anion, where conformations 1 and 3 are enantiomers (nonsuperposable mirror images), as are conformations 4 and 5. Therefore only a total of three unique minimum energy geometries were located. The C-S-S-C dihedrals and energy of the minima, along with values for some transition structures, are provided in Table 6.2.

Three factors are observed to relate energy with conformation. Firstly, in all species the electrostatic charge on oxygen was approximately –0.7. This negative charge affects the conformation energies in that the oxygens prefer a staggered arrangement about the S-S axis, due to electrostatic repulsion. For example, the energy maximum of $N(CF_3SO_2)_2^-$ between conformations 3 and 4 has eclipsing geometries for both S1-O1,

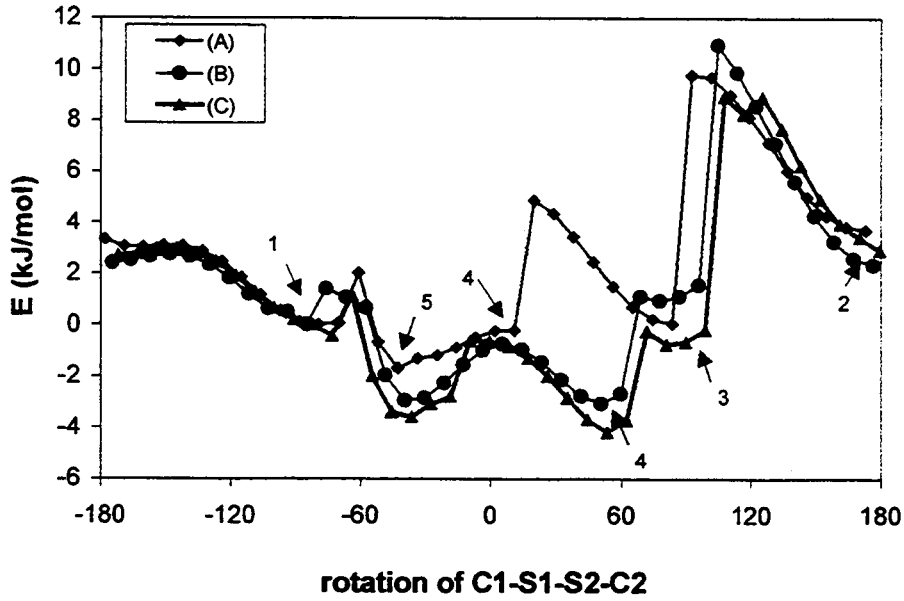


**Figure 6.1** One dimensional potential surface for (A)$N(CF_3SO_2)_2^-$, (B) $N(CF_3CF_2SO_2)_2^-$ (C) $N(CF_3SO_2)(CF_3(CF_2)_3SO_2)^-$. The '-' sign of dihedral denotes counter clockwise rotation.

**Table 6.2** Energy difference (ΔE) of five minima and two transition states of the potential surface generated with rotation of C1-S1-S2-C2 dihedral for $N(CF_3SO_2)_2^-$, $N(CF_3CF_2SO_2)_2^-$, and $N(CF_3SO_2)(CF_3(CF_2)_3SO_2)^-$ and the corresponding dihedrals values.

| | $N(CF_3SO_2)_2^-$ | | | $N(CF_3CF_2SO_2)_2^-$ | | | $N(CF_3SO_2)(CF_3(CF_2)_3SO_2)^-$ | | |
|---|---|---|---|---|---|---|---|---|---|
| | C-S-S-C[c] | ΔE[c] | $\Delta E_{trans}$ | C-S-S-C | ΔE | $\Delta E_{trans}$ | C-S-S-C | ΔE | $\Delta E_{trans}$ |
| conformation 1 | -78.91[b] | 0 | | -84.56 | 3.1 | | -81.66 | 4.2 | |
| Transition 1-2[a] | -145.08 | | 3.1 | -147.72 | | 8.1 | -169.5 | | 6.9 |
| conformation 2 | -161.98 | 3.0 | | 173.91 | 5.4 | | -173.97 | 6.8 | |
| conformation 3 | 78.02 | 0.05 | | 72.37 | 4.0 | | 84.49 | 3.5 | |
| conformation 4 | 68.79 | 0.2 | | 44.67 | 0 | | 47.57 | 0 | |
| conformation 5 | -51.21 | 1.7 | | -47.63 | 0.1 | | -44.74 | 0.6 | |
| Transition 5-1 | 60.02 | | 1.8 | -78.09 | | 5.0 | -41.63 | | 2.6 |

a. The transition state from minimum 1 to 2 is listed as transition 1-2, likewise for transition 5-1, and the energy difference from the lowest minimum is $\Delta E_{trans}$.

b. The '-' sign of dihedral denotes the counter clockwise rotation from the 0° conformation with 2 S-C bonds eclipsed.

c. The energies are given in kJ/mol and the dihedrals are given in degree.

S2-O3 and S1-O2, S1-O4. The electrostatic repulsion of the negatively charged oxygens causes an increase in energy.

Secondly, the non-polar $-CF_3$ (or in general $-C_nF_{2n+1}$) substituents favorably interact with one another. Conformation 4 also has all oxygen atoms eclipsed, but surprisingly is still low in energy. It is observed that the fluorines from each of the $-CF_3$ substituents are oriented towards eachother. This through space interaction of the fluorines has a stabilizing effect. In conformation 4, the two fluorines are separated by 2.72Å, compared with 3.63Å at the energy maximum between 3 and 4. Another interesting feature of this interaction is that the two fluorines will remain as close as is possible through the dihedral rotations until required to separate by large strain energies. This interaction also explains the determination that $N(CF_3SO_2)_2^-$ has a higher maxima between conformation 3 and 4 than the other two imide anions. Calculations show that both $N(CF_3CF_2SO_2)_2^-$ and $N(CF_3SO_2)(CF_3(CF_2)_3SO_2)^-$ allow greater interaction between $-C_nF_{2n+1}$ groups than for $N(CF_3SO_2)_2^-$ at that maximum, therefore, lower energies are obtained.

The conformation for either $HN(SO_2R)_2$ acids or their salts were found to be mostly *trans* (with the two $-CF_3$ groups are on opposing sides of the S-N-S plane), and only 9 of 77 experimental determined geometries of the $R\text{-}SO_2\text{-}N\text{-}SO_2\text{-}R'$ have the *cis* configuration (with both $-CF_3$ groups on the same side of the S-N-S plane). [5] It was only recently that both computational [7] and crystallographic studies [5] showed the existence of a *cis* conformation for the $N(CF_3SO_2)_2^-$ anion. Zak, et al observed that when structures exhibit intermolecular or cation-anion interactions involving oxygen atoms of the $N(SO_2R)_2$ moiety, they are more likely to display the *cis* configuration. [5] For

example, alkali metal cations coordinate to the oxygens in $N(CF_3SO_2)_2^-$, and therefore their salts may *cis* configuration. This is true for $KN(CF_3SO_2)_2$ [5], however, $LiN(CF_3SO_2)_2$ was found to adopt a *trans* configuration regardless of the strong coordination found between $Li^+$ and the anion oxygens. [13]

A third factor observed to affect conformational stability is the energy decrease when nitrogen and oxygen atoms remove electron density from sulfur. This is evidenced by the largest energy maximum in each potential surface (the maxima between conformations 2 and 3). At the maximum energy conformation, the electrostatic charge of sulfur is less positive and that of nitrogen less negative than at all other points (the S-N distance is also shorter at this point).

The rotational barriers obtained are very small (Table 6.2). For conformations 1 to 2, the energy of rotation is $\Delta E_{1\text{-}2} = 3.1$ kJ/mol, and $\Delta E_{5\text{-}1}$ is calculated to be 1.8 kJ/mol, close to the previously calculated value of 3.9 kJ/mol [7]. The transition states for $N(CF_3CF_2SO_2)_2^-$ and $N(CF_3SO_2)(CF_3(CF_2)_3SO_2)^-$ present C-S-S-C dihedrals similar to $(CF_3SO_2)_2N^-$ and the rotational barriers obtained are slightly larger. The energies calculated are all within a range of ~ 8 kJ/mol. These results show that the isolated $R'SO_2NSO_2R$ anions are extremely flexible and should rotate freely even at room temperature.

#### *6.3.1.2 Ab initio Calculation Results*

The HF/ 3-21(G)* calculation results of the minima for $N(CF_3SO_2)_2^-$, $N(CF_3CF_2SO_2)_2^-$, $N(CF_3SO_2)(CF_3(CF_2)_3SO_2)^-$ are shown in Figures 6.2, 6.3, and 6.4, and

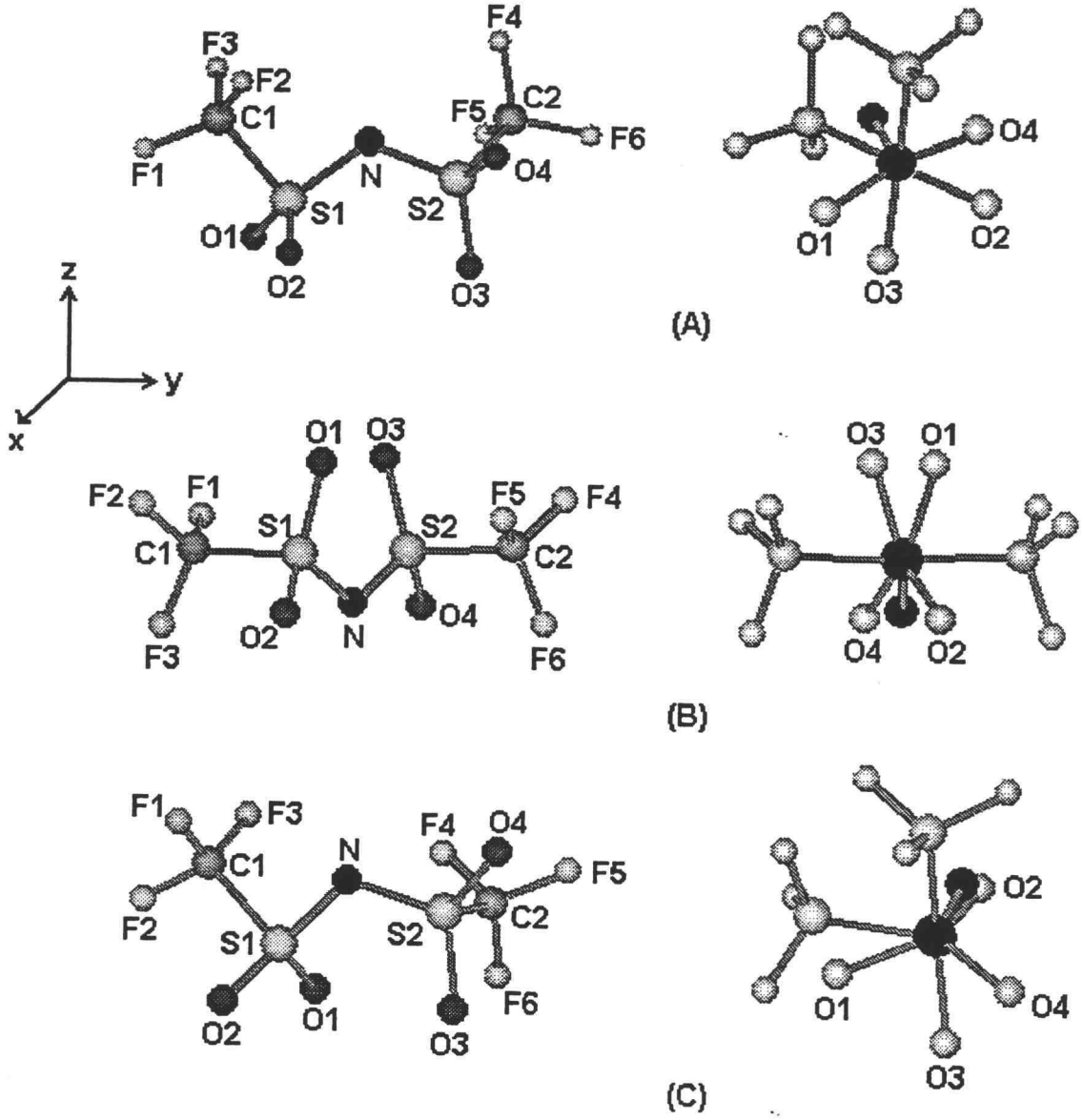


**Figure 6.2** Energy minima calculated for $N(CF_3SO_2)_2^-$ by HF method: (A) conformation 1' (B) conformation 2' (C) conformation 5'. The representations on the right-hand side are looking down the S1-S2 bond, and the atoms are colored differently from the left. S is the larger and N is the smaller dark sphere.

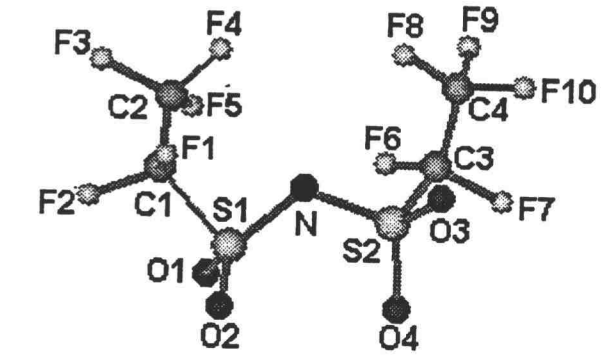


(A)

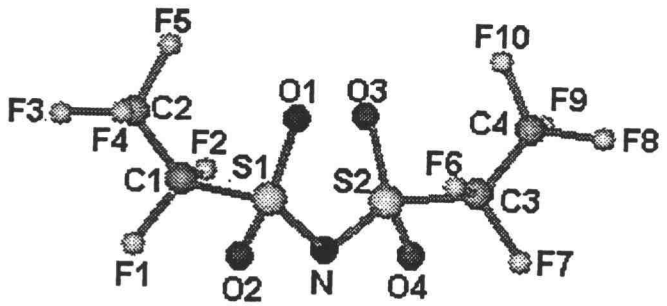


(B)

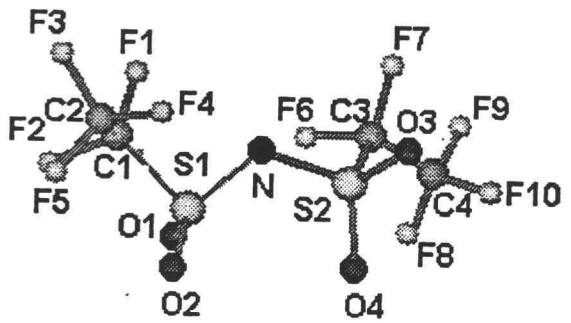


(C)

**Figure 6.3** Energy minima calculated for $N(CF_3CF_2SO_2)_2^-$ by HF method: (A) conformation 1' (B) conformation 2' (C) conformation 5'.

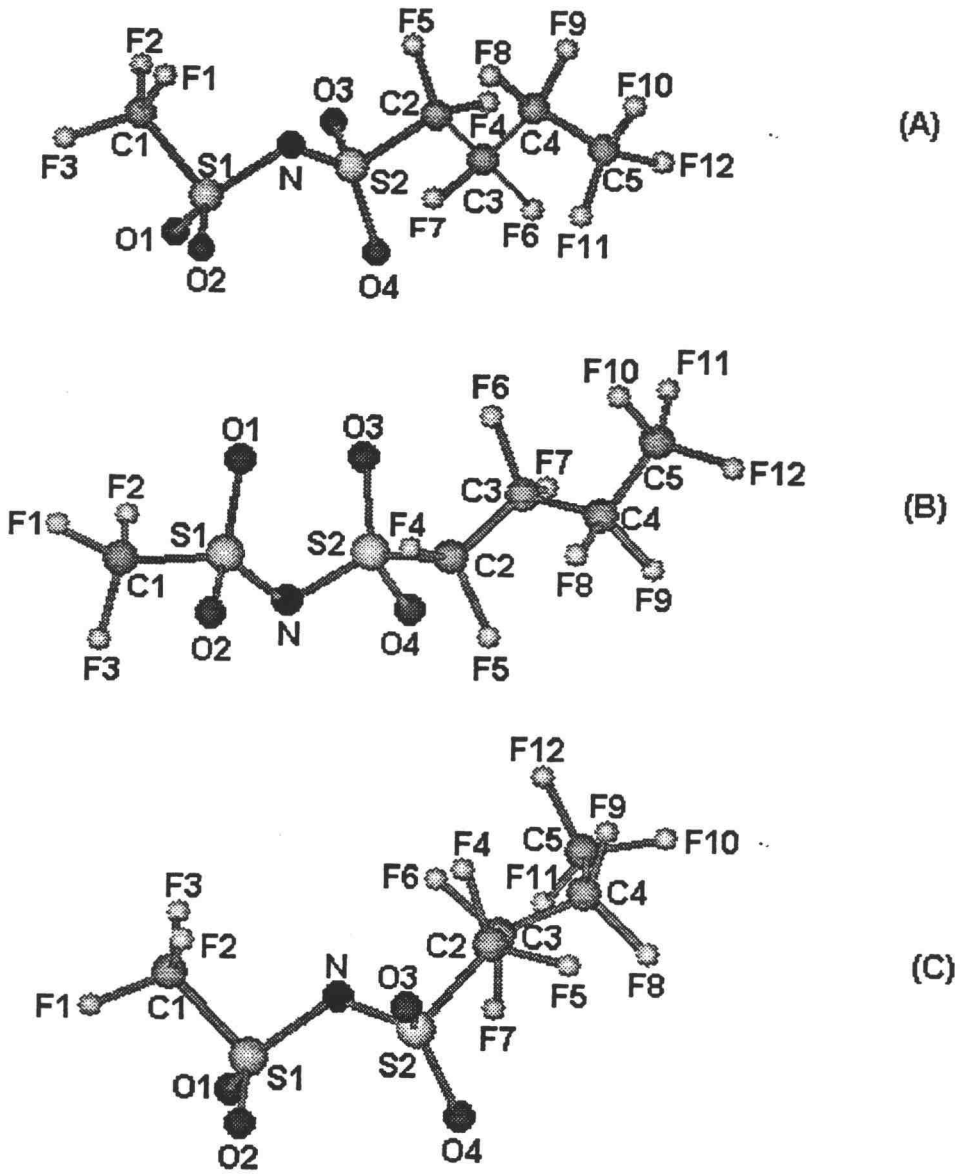


**Figure 6.4** Energy minima of calculated for $N(CF_3SO_2)(CF_3(CF_2)_3SO_2)^-$ by HF method: (A) conformation 1' (B) conformation 2' (C) conformation 5'.

the selected structural parameters are listed in Tables 6.3, 6.4, and 6.5 respectively. For $N(CF_3SO_2)_2^-$, the lowest energy conformation is 1', containing a dihedral C-S-S-C of –70.06°. Conformation 2' (C-S-S-C = 176.07°) and 5' (C-S-S-C = -77.6°) are higher in energy by 18.8 and 12.4 kJ/mol respectively. All of the minima found have C1 symmetry. The results from b3lyp calculations with 6-31G* basis set are tabulated in Table 6.3. Conformation 2'', which has C2 symmetry, is lower in energy (C-S-S-C = 169.98°). Conformation 1' and 5', given by HF calculations, converge to the same minimum energy conformation 1'' (C-S-S-C = 37.9°) and ΔE is 3.3 kJ/mol. The C-S-S-C dihedral from conformation 1''is much smaller than 1', while close values are obtained for conformations 2' and 2''.

Conformation 2'' is consistent with the recent computation of $N(CF_3SO_2)_2^-$ [7] and crystallographic study of $HN(CF_3SO_2)_2$ (C-S-S-C = 174°) [5]. All have C2 symmetry with *trans* configuration. Although 2' from HF calculation has a C1 symmetry, it also takes a *trans* conformation. Conformations 1', 5' and 1'' have a *cis* configuration, similar to the previous computational study on $N(CF_3SO_2)_2^-$ anion [7] and crystallographic data on $KN(CF_3SO_2)_2$ [5]. In the latter case, 2 anion geometries were found in the unit cell and the C-S-S-C dihedrals were determined to be 17° and 14°.

The S-O bond length calculated is hightly dependent on the computational method and basis set employed. The value obtained from HF calculation is ~ 0.11Å higher than results from b3lyp. The anion is expected to have longer S-O bonds but shorter N-S bonds than the molecular acid, since the nitrogen lone pair can delocalize onto the adjacent N-S bond. The above findings agree well with the experimental values from both $HN(CF_3SO_2)_2$ and $KN(CF_3SO_2)_2$. [5]

**Table 6.3** Calculated structural parameters and energies for $N(CF_3SO_2)_2^-$ calculated using the HF and b3lyp methods. Bond lengths are in Å, and bond angles are in degrees.

| | HF | | | B3lyp | | Experimental data [a] |
|---|---|---|---|---|---|---|
| | conformation 1' | conformation 2' | conformation 5' | conformation 1'' (5'') | conformation 2'' | |
| N-S1 | 1.682 | 1.689 | 1.68 | 1.620 | 1.620 | 1.644(1) |
| N-S2 | 1.681 | 1.684 | 1.680 | 1.613 | 1.620 | |
| S1-O1 | 1.574 | 1.581 | 1.577 | 1.470 | 1.468 | 1.401(2) |
| S1-O2 | 1.579 | 1.575 | 1.576 | 1.468 | 1.467 | 1.417(2) |
| S2-O3 | 1.579 | 1.575 | 1.578 | 1.468 | 1.469 | |
| S2-O4 | 1.574 | 1.575 | 1.575 | 1.468 | 1.468 | |
| S1-C1 | 1.844 | 1.843 | 1.852 | 1.871 | 1.873 | 1.840(3) |
| S2-C2 | 1.844 | 1.888 | 1.851 | 1.875 | 1.873 | |
| C1-F1 | 1.344 | 1.334 | 1.335 | 1.342 | 1.340 | 1.298(4) |
| C1-F2 | 1.333 | 1.343 | 1.340 | 1.346 | 1.346 | 1.307(3) |
| C1-F3 | 1.334 | 1.334 | 1.337 | 1.340 | 1.342 | 1.330(3) |
| C2-F4 | 1.335 | 1.334 | 1.34 | 1.340 | 1.339 | |
| C2-F5 | 1.334 | 1.342 | 1.336 | 1.346 | 1.346 | |
| C2-F6 | 1.343 | 1.330 | 1.336 | 1.343 | 1.342 | |
| O1-S1-O2 | 117.2 | 117.5 | 116.9 | 118.8 | 118.9 | 123.9(1) |
| O3-S2-O4 | 117.2 | 118.3 | 116.8 | 119.2 | 118.9 | |
| O1-S1-C1 | 104.5 | 105.9 | 105.3 | 104.2 | 104.3 | |
| O1-S1-N | 116.2 | 112.6 | 117.6 | 117.3 | 117.0 | 109.1(1) |
| O3-S2-C2 | 104.6 | 104.3 | 105.2 | 104.1 | 104.3 | |
| O3-S2-N | 114.4 | 114.7 | 117.5 | 116.1 | 117.0 | |
| O2-S1-C1 | 105.8 | 104.5 | 104.5 | 103.5 | 103.5 | |
| O2-S1-N | 114.6 | 110.2 | 117.8 | 110.3 | 108.1 | 106.9(1) |
| O4-S2-C2 | 104.5 | 104.3 | 104.5 | 103.0 | 103.6 | |
| O4-S2-N | 116.1 | 109.6 | 110.2 | 107.5 | 108.1 | |
| S1-N-S2 | 118.4 | 116.5 | 122.0 | 125.1 | 123.9 | 128.4(2) |
| C-S-S-C | -70.1 | 37.9 | 176.1 | 66.9 | 170.0 | |
| O1-S1-N-S2 | -99.8 | -45.7 | -20.5 | 8.9 | -22.2 | |
| O2-S1-N-S2 | 41.9 | 96.0 | -157.6 | -131.4 | -159.8 | |
| O3-S2-N-S1 | 39.3 | -35.5 | -19.1 | 33.1 | -22.4 | |
| O4-S2-N-S1 | -102.1 | -171.3 | -156.3 | 169.5 | -159.8 | |
| C1-S1-N-S2 | 151.6 | -155.0 | 92.8 | 120.3 | 91.2 | |
| C2-S2-N-S1 | 149.2 | 77.8 | 94.1 | -81.3 | 91.1 | |
| Relative energy (kJ/mol) | 0 | 18.8 | 11.8 | 3.3 | 0 | |

a. The experimental data comes from crystallographic study on $HN(CF_3SO_2)_2$ [8].

**Table 6.4** Structural parameters and energy for three minimum energy conformations of $N(CF_3CF_2SO_2)_2^-$ calculated using the HF method. Bond lengths are in Å, and bond angles are in degrees.

| | Conformation 1' | Conformation 2' | Conformation 5' |
|---|---|---|---|
| N-S1 | 1.682 | 1.680 | 1.686 |
| N-S2 | 1.670 | 1.682 | 1.674 |
| S1-O1 | 1.575 | 1.576 | 1.574 |
| S1-O2 | 1.571 | 1.574 | 1.575 |
| S2-O3 | 1.572 | 1.576 | 1.572 |
| S2-O4 | 1.578 | 1.573 | 1.579 |
| S1-C1 | 1.855 | 1.875 | 1.860 |
| S2-C3 | 1.866 | 1.876 | 1.870 |
| C1-F1 | 1.350 | 1.354 | 1.347 |
| C1-F2 | 1.361 | 1.352 | 1.361 |
| C2-F3 | 1.352 | 1.35 | 1.350 |
| C2-F4 | 1.333 | 1.333 | 1.333 |
| C2-F5 | 1.337 | 1.352 | 1.337 |
| C3-F6 | 1.348 | 1.352 | 1.349 |
| C3-F7 | 1.359 | 1.354 | 1.354 |
| C4-F8 | 1.335 | 1.350 | 1.333 |
| C4-F9 | 1.348 | 1.341 | 1.349 |
| C4-F10 | 1.337 | 1.333 | 1.340 |
| C1-C2 | 1.511 | 1.503 | 1.509 |
| C3-C4 | 1.507 | 1.503 | 1.507 |
| C2-C1-S1 | 117.0 | 113.8 | 114.9 |
| C4-C3-S2 | 114.6 | 113.7 | 113.5 |
| O1-S1-O2 | 116.9 | 117.2 | 117.4 |
| O3-S2-O4 | 118.3 | 117.3 | 118.2 |
| O1-S1-C1 | 106.2 | 103.7 | 104.9 |
| O1-S1-N | 116.4 | 117.5 | 116.7 |
| O3-S2-C3 | 103.1 | 103.7 | 105.4 |
| O3-S2-N | 114.4 | 117.4 | 112.8 |
| O2-S1-C1 | 104.7 | 105.1 | 103.3 |
| O4-S2-C3 | 105.5 | 105.1 | 103.4 |
| O4-S2-N | 113.6 | 110.3 | 114.3 |
| S1-N-S2 | 119.8 | 120.1 | 118.5 |
| C1-S1-S2-C3 | -75.4 | 166.0 | -75.4 |
| O1-S1-N-S2 | -84.4 | -23.6 | -65.5 |
| O2-S1-N-S2 | 59.1 | -161.4 | 79.0 |
| O3-S2-N-S1 | -122.8 | -23.5 | -143.6 |
| O4-S2-N-S1 | 17.2 | -161.4 | -4.9 |
| C1-S1-N-S2 | 166.5 | 88.0 | -174.3 |
| C3-S2-N-S1 | 128.4 | 88.0 | 105.0 |
| Relative energy (kJ/mol) | 5.2 | 12.2 | 0 |

**Table 6.5** Calculated structural parameters and energy for $N(CF_3SO_2)(CF_3(CF_2)_3SO_2)^-$ using the HF method. Bond lengths are in Å, and bond angles are in degrees.

| | Conformation 1' | Conformation 2' | Conformation 5' |
|---|---|---|---|
| N-S1 | 1.681 | 1.684 | 1.678 |
| N-S2 | 1.682 | 1.671 | 1.681 |
| S1-O1 | 1.581 | 1.579 | 1.574 |
| S1-O2 | 1.574 | 1.575 | 1.581 |
| S2-O3 | 1.572 | 1.574 | 1.573 |
| S2-O4 | 1.577 | 1.573 | 1.572 |
| S1-C1 | 1.846 | 1.845 | 1.846 |
| S2-C2 | 1.866 | 1.882 | 1.861 |
| C1-F1 | 1.334 | 1.342 | 1.341 |
| C1-F2 | 1.333 | 1.334 | 1.333 |
| C1-F3 | 1.343 | 1.334 | 1.335 |
| C2-F4 | 1.357 | 1.354 | 1.348 |
| C2-F5 | 1.351 | 1.355 | 1.365 |
| C3-F6 | 1.359 | 1.353 | 1.355 |
| C3-F7 | 1.348 | 1.355 | 1.353 |
| C4-F8 | 1.359 | 1.354 | 1.353 |
| C4-F9 | 1.353 | 1.358 | 1.359 |
| C5-F10 | 1.343 | 1.336 | 1.339 |
| C5-F11 | 1.339 | 1.340 | 1.337 |
| C5-F12 | 1.337 | 1.344 | 1.344 |
| C2-C3 | 1.513 | 1.507 | 1.512 |
| C3-C4 | 1.521 | 1.523 | 1.525 |
| C4-C5 | 1.516 | 1.515 | 1.516 |
| O1-S1-O2 | 117.6 | 117.1 | 117.7 |
| O3-S2-O4 | 117.5 | 116.8 | 116.7 |
| O1-S1-C1 | 106.2 | 105.2 | 104.8 |
| O1-S1-N | 113.3 | 116.8 | 114.8 |
| O3-S2-C2 | 104.1 | 103.6 | 103.1 |
| O3-S2-N | 116.6 | 118.6 | 116.9 |
| O2-S1-N | 115.4 | 112.6 | 113.0 |
| O2-S1-C1 | 104.8 | 104.7 | 106.2 |
| O4-S2-C2 | 104.1 | 105.0 | 107.0 |
| O4-S2-N | 116.6 | 109.2 | 116.1 |
| S1-N-S2 | 118.1 | 122.8 | 119.2 |
| F4-C2-C3-F7 | -157.8 | -162.0 | -157.9 |
| F7-C3-C4-F8 | -160.9 | -157.5 | -160.7 |
| C1-S1-S2-C2 | 71.4 | -175.2 | -68.1 |
| O1-S1-N-S2 | -24.6 | 9.6 | -120.2 |
| O2-S1-N-S2 | 115.1 | -130.0 | 18.7 |
| O3-S2-N-S1 | 87.9 | -38.6 | -83.0 |
| O4-S2-N-S1 | -56.3 | -175.8 | 60.9 |
| C1-S1-N-S2 | -135.2 | 120.7 | 129.8 |
| C2-S2-N-S1 | -164.0 | 73.9 | 171.1 |
| F4-C2-S2-O3 | -41.5 | 86.8 | 43.7 |
| Relative energy (kJ/mol) | 5.2 | 13.7 | 0 |

As with $N(CF_3SO_2)_2^-$, there are three minima found for $N(CF_3CF_2SO_2)_2^-$ by HF calculations. Conformation 1' (C-S-S-C = -75.4°) (*cis*) is the lowest energy among the three. Conformation 2' (C-S-S-C = 166.0°) (*trans*) and 5' (C-S-S-C = -68.1°) (*cis*) are higher in energy with $\Delta E$ = 12.2 and 5.2 kJ/mol respectively. Three minimas were also found for $N(CF_3SO_2)(CF_3(CF_2)_3SO_2)^-$: conformation 5' (-68.123°) (*cis*) is lower in energy than the other two geometries, $\Delta E$ for conformation 1' (71.35°) (*cis*) and 2' (-175.17°) (*trans*) are 5.2 and 13.7 kJ/mol respectively. The butyl chains are distorted with a F-C-C-F twist angle of approximately 20°, similar to the results calculated for $C_8F_{17}SO_3^-$ anion using b3lyp combined 3-21G* basis set. [11] The HF calculations show that the three energy minima for all these anions are similar in energy.

There was only one energy minimum located for tris(trifluoromethanesulfonyl) methide $C(CF_3SO_2)_3^-$ using b3lyp calculations (Figure 6.5). The structure determined from crystallographic data on $HC(CF_3SO_2)_3$ [9] gives values of S-C bondlengths in the range of 1.693 – 1.727Å, C-F bondlengths from 1.301 – 1.336Å, S-O bondlengths from 1.428 – 1.437Å, and SCS angle of 121.0 – 122.2°, OSO angle of 119.3 - 120.7° and CSC angle of 105.4 – 106.1°. Although the structure was not fully specified in the report, these data generally agree with the values reported in Table 6.6.

### 6.3.2. GICs with these fluoroanions

#### *6.3.2.1 Orientation of fluoroanions*

Two main factors influence how the intercalating anions orient inside the graphite galleries, the steric effect and coulumbic interactions between the positive charged host and the anions. $C_xN(CF_3SO_2)_2$ has an experimentally determined gallery height of

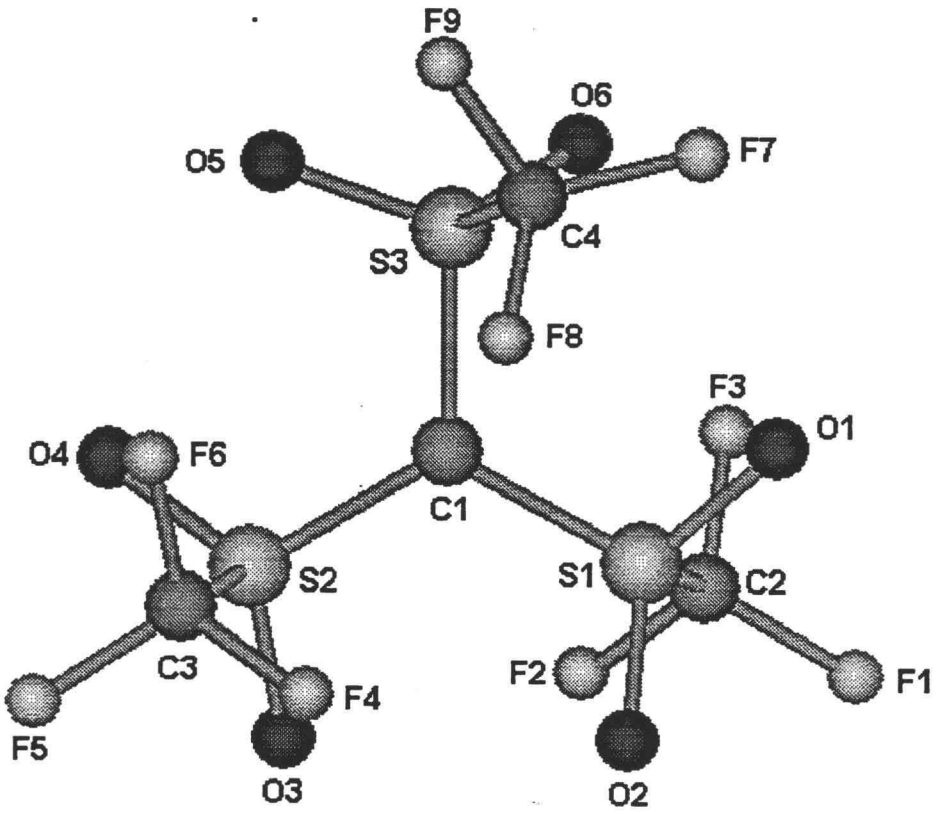


**Figure 6.5** Calculated minimum energy conformation for $C(CF_3SO_2)_3^-$ using the b3lyp method combined 6-31G* basis set.

**Table 6.6** Calculated structural parameters for $C(CF_3SO_2)_3^-$ using DFT computational method and the experimental values. Bond lengths are in Å, and bond angles are in degrees.

| | Calculated value (b3lyp) |
|---|---|
| C1-S1 | 1.741 |
| C1-S2 | 1.745 |
| C1-S3 | 1.755 |
| C2-S1 | 1.879 |
| C3-S2 | 1.879 |
| C4-S3 | 1.907 |
| S1-O1 | 1.469 |
| S1-O2 | 1.464 |
| S2-O3 | 1.466 |
| S2-O4 | 1.463 |
| S3-O5 | 1.466 |
| S3-O6 | 1.466 |
| C2-F1 | 1.344 |
| C2-F2 | 1.334 |
| C2-F3 | 1.336 |
| C3-F4 | 1.336 |
| C3-F5 | 1.343 |
| C3-F6 | 1.341 |
| C4-F7 | 1.331 |
| C4-F8 | 1.340 |
| C4-F9 | 1.343 |
| S1-C1-S2 | 121.8 |
| S2-C1-S3 | 118.1 |
| S3-C1-S1 | 120.0 |
| O1-S1-O2 | 120.0 |
| O3-S2-O4 | 120.3 |
| O5-S3-O6 | 120.0 |
| C1-S1-C2 | 105.6 |
| C1-S1-C2 | 104.7 |
| C1-S1-C3 | 105.7 |
| C1-S1-O1 | 108.3 |
| C1-S1-O2 | 112.9 |
| C1-S2-O3 | 109.9 |
| C1-S2-O4 | 112.5 |
| C1-S3-O5 | 109.5 |
| C1-S3-O6 | 112.1 |
| O1-S1-C-S3 | 14.5 |
| O1-S1-C-S2 | -161.9 |
| O3-S2-C-S3 | 164.7 |
| O3-S2-C-S1 | -19.05 |
| O5-S3-C-S2 | -176.64 |
| O5-S3-C-S2 | -0.35 |
| O1-S1-S3-O6 | 56.83 |
| O1-S1-S2-O4 | 61.48 |
| O4-S2-S3-O6 | -96.04 |

8.07(4) Å, which is only consistent with a single layer of intercalating anions in the galleries. Furthermore, the anions must be aligned with the longest dimension (along the y axis in Figure 6.2), parallel to the graphene planes (see Figure 3.5). The separating distance of these anions from the carbon layers can be estimated from other GICs. In well-evacuated graphite nitrate, where only planar $NO_3^-$ anions are present in the galleries, the observed value for $d_i$, 6.5 Å, indicates a carbon plane – O separation along the c axis of 3.2 Å. This value can be taken as close to a minimum value for other GICs where oxygen bears a similar charge. None of the minimum energy conformations obtained above can be fit into this known gallery height and with a reasonable oxygen to graphene plane distance. With a rotation of each S-$CF_3$ bond about 60°, however, conformation 2'' gives a distance of 2.9 Å and ~ 3 Å for the separation with the 2 oxygen atoms and the nitrogen atom oriented towards the graphene planes (Figure 3.5). PM3 calculations show that the resulting geometry from rotation of S-$CF_3$ bond 60° is increased in energy by no more than 1.2 kJ/mol. No other conformations are found that fit the 8.07 Å gallery with reasonable graphite to oxygen distance, even after low energy modification.

The orientation of the conformation 2'' mentioned above allows close interactions of the two negatively charged oxygens (Mulliken charge = -0.71) and the nitrogen atom (charge = 0.54) with the positive graphene sheets. The 1-D electron density map for the stage 2 $C_xN(CF_3SO_2)_2$ incorporating conformation 2'' with a rotation of S-$CF_3$ about 60°, show double maximum electron density peak near the gallery center (Figure 3.5), which is natural result from assuming equal populations of both possible orientations (up and

down). The structural refinement indicates a reasonable fit to the experimental data, see Chapter 3.

When $N(CF_3CF_2SO_2)_2^-$ and $N(CF_3SO_2)(CF_3(CF_2)_3SO_2)^-$ are intercalated into graphite the resulting gallery heights are 8.2 (1) Å. As with $N(CF_3SO_2)_2^-$, only the trans conformation 2 for these two anions can be arranged in graphite gallery to achieve the desirable gallery dimension, as shown in Figure 6.6 for $C_xN(CF_3CF_2SO_2)_2$. Rotations of S-$CF_3$ and C-$CF_3$ are again required for the anions to fit within the gallery. The resulting structures are then calculated to be ~ 0.2 Å larger along the z direction than the $N(CF_3SO_2)_2^-$ anion, which agrees with the observed difference in gallery heights.

Since the rotational barriers for both C-S-N-S [7] and C-S-S-C dihedrals are very small for $N(CF_3SO_2)_2^-$, starting geometries other than found minima could be considered. The number of possibilities will increase for the larger anions. However, minimum energy conformation 2' (or 2'') is a reasonable model for all intercalating anions as it provides the obserevd gallery height for the GICs and allows strong coulombic interactions between the graphene layers and the intercalants.

The $C(CF_3SO_2)_3^-$ anion has a pseudo-spherical geometry, with approximately a 5.2 Å diameter. This anion was observed to result in a GIC with gallery height of ~10.6(3) Å in a stage 4 or higher GIC [10]. This is consistent with the value derived from the calculated minimum energy conformation with an oxygen to carbon plane distance of ~ 2.9 Å.

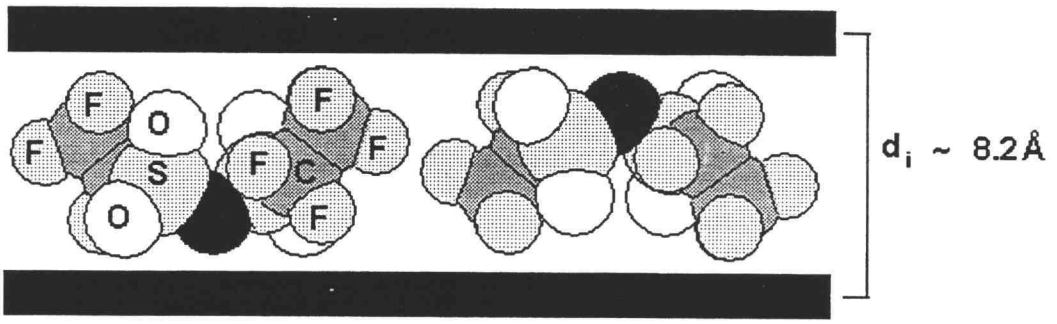


**Figure 6.6** Structural model of $C_xN(CF_3CF_2SO_2)_2$ including both possible anion orientations.

### *6.3.2.2 Intercalation Kinetics*

The graphite intercalation reaction is topotatic and the anions are intercalated into graphite by two-dimensional diffusion. The initial step in the intercalation process is the chemisorption of the anions onto the charged graphite surface, which modifies the graphene layer electronic structure and therefore allows an easier separation of the van der Waals gap. This step is not rate limiting, even for large anions. Chapter 4 shows that the $HF_2^-$ anions on the $C_xHF_2$ particle surface can be exchanged by the large anions such as $N(CF_3CF_2SO_2)_2^-$ in five minutes, which passivates the graphite surface and results in a much increased air stability. The solid state diffusion step is in all cases rate-determining. According to Beck, et. al. [14], the diffusion coefficient ($D_s$) for the intercalated anions in the graphite can be directly derived from the Stokes – Einstein relation:

$$\eta D_s = k T / (6\pi r) \qquad (6.2)$$

where $\eta$ is specific viscosity, and r is the anion radius. For pseudo – spherical anions, the radius will be directly related to the gallery height, $d_i$. Even for lower symmetry anions, the gallery height provides a first approximation for the effective value of r. The viscosity is proportional to $m^{1/2}$, where m is the molar mass. $D_s$ is, therefore, in a simple kinetic model approximately proportional to $1 / (m^{1/2} r)$. For larger anions, $D_s$ should be smaller and the intercalation is expected to be slower. The same research group also reported $D_s$ to approximately $10^{-6}$ $cm^2s^{-1}$ for both sulfate and perchlorate anions using

electrochemical method and single flake graphite (2 x 1.5 x 0.05 mm particle dimensions). The diffusion process should be considerably faster in a chemical intercalation using graphite powder with smaller particle diameter.

The observed intercalation rate ratio for the three imide anions is approximate 3000 : 3: 1 for $N(CF_3SO_2)_2^-$ : $N(CF_3CF_2SO_2)_2^-$ : $N(CF_3SO_2)(CF_3(CF_2)_3SO_2)^-$. These anions have molar masses of 280, 380, and 430 D, respectively, and their effective radii are 4.71, 4.85 and 4.85 Å respectively, as calculated from $d_i$ – 3.354Å. The ratio of $D_s$ according to a simple diffusion model, is therefore calculated to be 1.3 : 1.1 : 1. Clearly, the decrease in reaction rate with anion size is far more dramatic than the predicted effect from simple diffusion kinetics. Even though equ. 6.2 is based on the assumption that anions are spherical, all these three imide anions have a pseudo-cylindrical shape and it does not therefore seem reasonable to contribute the large kinetic differences to shape effects.

The charge on the anions affects the intercalation kinetics as well. It is well known that fluoride cannot be intercalated into graphite by direct reaction at room temperature. In contrast, the larger anion $HF_2^-$ can rapidly form low stage GICs under similar conditions. Hooley [15] suggested that due to their small size and high charge density, $F^-$ ions adsorbed at the opening to a gallery become fixed at edge sites and cannot move forward into the galleries. Thus strong electrostatic interactions due to high charge densities can effect changes in intercalation rates. The Mulliken charges for O, S, and N atoms of these imide anions, however, are very similar, and therefore their electrostatic interactions with graphene layers should be comparable.

The molar mass of $C(CF_3SO_2)_3^-$ anion is comparable to $N(CF_3CF_2SO_2)_2^-$, however, it's effective radius in the graphite galleries is much larger than any of the three imide anions. The diffusion model therefore predicts a slower intercalation rate. Although the reaction rate for $C(CF_3SO_2)_3^-$ cannot be obtained accurately due to the mixtures of phases present in the product, the intercalation rate for $N(CF_3SO_2)_2^-$ is observed to be approx. $10^4$ times faster than the $C(CF_3SO_2)_3^-$ anion,. According to equ. 6.2, the ratio of $D_s$ for these two anions should be only approx. 1.9 : 1, the calculated values again predict dramatically smaller rate changes than those observed.

The much slower intercalation kinetics for $N(CF_3CF_2SO_2)_2^-$ and $N(CF_3SO_2)(CF_3(CF_2)_3SO_2)^-$ and $C(CF_3SO_2)_3^-$ demonstrate that intercalation kinetics cannot be adequately explained using a classical diffusion model. Earlier in this chapter, we found that only a few specific anion conformations can fit within the known gallery dimension. The rotational barriers for all three selective imide anions are very small ($\leq$ 8 kJ/mol) , which should allow for nearly free conversion between the conformations in solution. However, as mentioned earlier, the first step of graphite intercalation is the adsorption of anions onto the positively charged graphite surface, which might significantly change the dihedral rotational barriers. The slow interconversion of adsorbed conformers might provide a rate-limiting step for the intercalation process.

Alternatively, intercalation rates might be limited by the passivation of the graphite surface. For example, perflurobenzenesulfonate anions were observed to create a passive graphite surface in 48% aqu. HF and prevent the formation of graphite bifluoride [10]. Therefore this anion was found to be an effective surface protection agent for graphite bifluoride, see Chapter 4. To provide further evidence for passivation,

additional experiments need to be undertaken. Graphite should be exposed to the larger anions first, followed by addition of small anions such as $N(CF_3SO_2)_2^-$. If the passivation theory is valid, there will be a decrease in subsequent intercalation rates relative to those previously obtained. Additional investigation will be useful in identifying the kinetic limits to graphite intercalation.

## 6.4 Reference


1. This experimental value is provided by Jan True, master thesis, 1999. The unit is standard Pauling unit, which is $eV^{1/2}$.

2. Koch, V.R.; Dominey, L.A.; Nanjundiah, C.; Ondrechen, M.J. *J. Electrochem. Soc.* **1996**, *143*, 799.

3. Armand. M.; Gorecki, W.; Andreani, R. in *Proceedings of Second International Symposium on Polymer Electrolytes*, B. Scrosati, Editor, P. 91, elsevier, London (1990); M. Armand and R.E.K.C.E. Moursli, Fr. Pat. 82-09540 (1983).

4. Dominey, in *Proceedings of the Fifth International Seminar on Lithium Battery Technology and Applications*. P. 1, Florida (1991); Dominey, L. A. U.S. Pat. 5,273,840, **1993**.

5. Zak, Z.; Ruzicka, A. *Z. Kristallogr.* **1998**, *213*, 217.

6. Benrabah, D.; Arnaud, R.; Sanchez, J-Y. *Electrochim. Acta* **1995**, *40*, 2437.

7. Johansson, P.; Gejji, S.P.; Tegenfeldt, J.; Lindgren, J. *J. Electrochim. Acta* **1998**, *43*, p.1375 (1998).

8. Haas, A.; Klare, Ch.; Betz, P.; Bruchkmann, J.; Kruger, C.; Tsay, Y.-H.; Aubke, F. *Inorg. Chem.* **1996**, *35*, 1918.

9. Turowsky, L.; Seppelt, K. *Inorg. Chem.* **1988**, *27*, 2135.

10. Zhang, X.; Lerner, M. *Mater. Res. Bull.* in press.

11. Hehre, W. J.; Shusterman, A. J.; Huang, W.W. *A Laboratory Book of Computational Organic Chemistry*, Wavefunction Inc. (1996).

12. Frisch, M. J. et. al. *Gaussian 94*, Revision E.1, Gaussian, Inc., Pittsburgh PA, **1995**.

13. Nowinski, J.L.; Lighnoor, P.; Bruce, P.G. *J. Mater. Chem.* **1991**, *4*, 1579.

14. Tormin, U.; Beck, F. *Electrochim. Acta*, **1995**, *40*, 1955.

15. Hooley, J.G.; in "*Preparation and Crystal Growth of Materials with Layered Structures*: (Lieth, R.M.A.ed.), Reidel Publ., Dordrecht, Netherlands, **1977**, pp. 1-33.

# Chapter 7

## Conclusion

First time chemical synthesis of GICs with large fluoroanions is achieved by a rapid and scalable method. $C_xC_8F_{17}SO_3$ and $C_xN(CF_3SO_2)_2$ are readily prepared using this method. Intercalation reactions with the larger fluoroanions $(CF_3CF_2SO_2)_2N^-$, $(CF_3SO_2)(CF_3(CF_2)_3SO_2)N^-$, and $(CF_3SO_2)_3C^-$ occurred but are dramatically slower. Stage disorder presents for all GICs prepared in 48% aq. HF. 1-D structural characterizations are done on $C_xC_8F_{17}SO_3$ and $C_xN(CF_3SO_2)_2$ and the anion conformation and orientation are discussed.

Potential maps for perfluoroalkyl sulfonyl imides are generated and ab initio calculations are performed for found minima.

Surface protections of air sensitive GICs with large fluoroanions are carried out and the stability of $C_xHF_2$ increases up to 10 times.

## Bibliography

Armand, M.; Gorecki, W.; Andreani, R. in *Proceedings of Second International Symposium on polymer Eectrolytes*, Scrosati, B. Editor, P. 91, elsevier, London **1990**; M. Armand and R.E.K.C.E. Moursli, Fr. Pat. 82-09540, **1983**.

Aubke, F.; Karunanithy, S. *J. Chim. Phys.* **1984**, *81*, 827.

Avdeev, V.; Sorokina, N.; Nikolskaya, I.; Monyakina, L.; Voronkina, A. *Inorg. Mater.* **1997**, *33*, 699.

Avdeev, V.V.; Monyakina, L.A.; Nikolskaya, I.V.; Sorokina, N.E.; Semenenko, K.N. *Carbon* **1992**, *30*, 819.

Bach, B.; Ubbelohde, A.R. *J. Chem. Soc. A* **1971**, 3669.

Bartlett, N.; McQuillan, B. in *Intercalation Chemistry*; Whittingham, S.; Jacobson, A., Eds.; Academic Press: New York, **1982**.

Beguin, F.; Frackowiak, E. *J. Phys. Chem. Solids* **1996**, *57*, 841.

Bell, R.; Bascombe, K.; McCoubrey, J. *J. Chem. Soc.* **1956**, 1286.

Benrabah, D.; Arnaud, R.; Sanchez, J-Y. *Electrochim. Acta* **1995**, *40*, 13, 2437.

Bode, H.; Jenssen, H.; Bandte, F. *Angew. Chem.* **1953**, *65*, 304.

Boehm, H. P.; Helle, W.; Ruisinger, B. *Synth. Met.* **1988**, *23*, 395.

Bourelle, E.; Douglade, J.; Metrot, A. *Mol. Cryst. Liq. Cryst.* **1994**, *244*, 227.

Brodie, B.C. *Ann. Chim. Phys.* **1855**, *45*, 351.

Buckley, J.; Edie, D. Eds., in *Carbon-carbon Materials and Composites*, Noyes Publ.: NJ **1993**.

Bunn, C.W.; Howells, E.R. *Nature* **1954**, *4429*, 549.

Daumas, N.; Herold, A. *C.R. Acad. Sci., Ser. C* **1969**, *268*, 373.

Dekany, I; Kruger-Grasser; Weiss, A. *Colloid Polym. Sci.* **1998**, *276*, 570.

Dominey, L. A.in *Proceedings of the Fifth International Seminar on Lithium Battery Technology and Applications*. P. 1, Florida (1991); Dominey, L., U.S. Pat. 5,273,840 **1993**.

Endo, M.; Chieu, T.; Dresselhaus, M. *Synth. Met.* **1983**, *8*, 2251.

Fischer, J.E.; Fuerst, C.D; Woo, K. C. *Phys. Rev. B* **1989**, *39*, 4374.

Frackowiak, E.; Kaiser, W.; Krohn, H.; Beck, F. *Mol. Cryst. Liq. Cryst.* **1994**, *244*, 221.

Freeman, A.J. J.C. S. *Chem. Commun.* **1968**, 193.

Frisch, M. J. et. al. *Gaussian 94*, Revision E.1, Gaussian, Inc., Pittsburgh PA, **1995**.

Fuerst, C.; Fischer, J.; Axe, J.; Hastings, J.; McWhan, D. *Phys. Rev. Lett.* **1983**, *50*, 357.

Furdin, G. *Fuel* **1998**, *77*, 6 479.

Guerard, D.; Herold, A. *Carbon* **1975**, *13*, 337.

Haas, A.; Klare, Ch.; Betz, P.; Bruchkmann, J.; Kruger, C.; Tsay, Y.-H.; Aubke, F. *Inorg. Chem.* **1996**, *35*, 1918.

Hagiwara, R.; Lerner, M.; Bartlett, N. *J. Chem. Soc., Chem. Commun.* **1989**, 573.

Hamwi, A.; Marchand, V. *J. Phys. Chem. Solids* **1996**, *57*, 867.

Hauw, C.; Gaultier, J.; Flandrois, S.; Gonzalez, O.; Dorignac, D.; Jagut, R. *Synth. Met.* **1983**, *7*, 313.

He, H.; Klinowski, J.; Forster, M.; Lerf, A. *Chem. Phys. Let.* **1998**, *287*, 53.

Hehre, W. J.; Shusterman, A. J.; Huang, W.W. *A Laboratory Book of Computational Organic Chemistry*, Wavefunction Inc. (1996).

Hendricks, S.; Teller, E. *J. Chem. Phys.* **1942**, *10*, 147.

Hohlwein, D.; Metz, W. *Z. Kristallogr.* **1974**, *139*, 279.

Hooley, G.G.; Bartlett, M.W.; Liengone, B.V; Sams, J.R. *Carbon* **1968**, *6*, 681.

Hooley, J.G.; in "*Preparation and Crystal Growth of Materials with Layered Structures*:(R.M.A.Lieth, ed.), Reidel Publ., Dordrecht, Netherlands, **1977**, pp. 1-33.

Horn, D.; Boehm, H.P. *Mater. Sci. Eng.* **1977**, *31*, 87.

Hummers, W.S. *U.S. Patent No. 2,798,878*, **1957**.

Huster, M.E.; Heiney, P.A.; Cajipe, V.B.; Fischer, J.E. *Phys. Rev. B* **1987**, *35*, 3311.

Inagake, M.; Shiwachi, Y. Maeda, Y. *J. Chimie. Phys.* **1984**, *81*, 847.

Inagaki, M. *J. Mater. Res.* **1989**, *4*, 1560.

Inagaki, M.; Iwashita, N.; Kouno, E. *Carbon* **1990**, *28*, 49.

Inagaki, M.; Wang, Z.D.; Okamoto, Y.; Ohira, M. *Synth. Met.* **1987**, *20*, 9.

Jacobson, A. in *Intercalation Chemistry*; Whittingham, S.; Jacobsen, A., Eds.; Academic Press: New York, **1982**.

Johansson, P.; Gejji, S.P.; Tegenfeldt, J.; Lindgren, J. *J. Electrochim. Acta* **1998**, *43*, p.1375.

Kang, F.; Leng, Y.; Zhang, T.-Y. *Carbon* **1997**, *35*, 1089.

Kang, F.; Leng, Y.; Zhang, T.-Y. *J. Phys. Chem. Solids* **1996**, *57*, 889.

Knochenhauer, G.; Reiche, J.; Brehmer, L; Barberka, T.; Woolley, M; Tredgold, R.; Hodge, P. *J. Chem. Soc., Chem., Commun.* **1995**, 1619.

Koch, V.R.; Dominey, L.A.; Nanjundiah, C.; Ondrechen, M.J. *J. Electrochem. Soc.* **1996**, *143*, 799.

Kuzina, T.A.; Shempel, N.A.; Golipad, P.N.; Kurnevich, G.I. *Zh. Prikladnoi Khim.* **1993**, *66*, 2, 271.

Lamont, R.; Ducker, W. *J. Coll. Inter. Sci.* **1997**, *191*, 303.

Lemmon, J.; Lerner, M. ACS National Meeting, San Diego, March, **1994**.

Lemmon, J.; Lerner, M. *Carbon* **1993**, *31*, 437.

Lerner, M. Ph.D. thesis, UC Berkeley, **1988**.

Mallouk, T. Bartlett, N. *Phil Trans. R.. Soc. Lond.* **1985**, *A314*, 179.

Mallouk, T.; Bartlett, N. *J. Chem. Soc. Chem. Commun.* **1983**, 103.

Mallouk, T.; Hawkins, B.L.; Conrad, M.P.; Zilm, K.; Maciel, G.E.; Bartlett, N. *Phil. Tran. R. Soc. Lond* A **1985**, *314*, 179.

Marcus, B.; Touzain, P. *Synth. Met.* **1988**, *23*, 13.

Markovsky, B.; Levi, M.; Aurbach, D. *Electrochim. Acta* **1998**, *43*, 2287.

Matsuo, Y.; Hatase, K.; Sugie, Y. *Chem. Mater.* **1998**, *10*, 2266.

Matsuo, Y.; Segawa, M.; Sugie, M. *J. Fluo. Chem.* **1998**, *87*, 145.

Matsuo, Y.; Tahara, K.; Sugie, Y. *Carbon* **1997**, *35*, 113.

Nakajima, T.; Matsuo, Y. *Carbon* **1994**, *32*, 469.

Nilol'skaya, I.V.; Fadeeva, V.A.; Semenenko, K.N. *Zh. Obshch. Khim.* **1989**, *59*, 2653.

Nowinski, J.L.; Lighnoor, P.; Bruce, P.G. *J. Mater. Chem.* **1991**, *4*, 1579.

Ozawa, K. *Sol. St. Ionics* **1994**, *69*, 212.

Pinnavaia, T. *Science* **1983**, *220*, 365.

Rashkov, I. *Mat. Sci. For.* **1992**, *91*, 829.

Rochester, C.H. in *Acidity Functions*, Blomquist, A.T. Ed.; Acad. Press: London, New York, **1970**, pp.21-71.

Rudorff, W.; Hofmann, U. *Z. Phys. Chem.***1938**, *238*, 1.

Ruff, O.; Bretschneider, O.; Ebert, F. *Z. Anorg, Allg. Chem.* **1934**, *217*, 1.

Ruisinger, B.; Boehm, H.P. *Angew. Chem. Int. Ed. Engl.* **1987**, *26*, 3, 253.

Ruisinger, B.; Boehm, H.P. *Carbon* **1993**, *31*, 7, 1131.

Salib, M.S.; Petrou, A.; Chung, D. *Carbon* **1997**, *35*, 5, 709.

Scharff, P. *GFECI 89*, Nantes, France, Mars **1989**, Ext. Abstracts, p81.

Scharff, P.; Xu, Z-Y.; Stumpp, E.; Barteczko, *Carbon* **1991**, *29*, 31.

Schlogl, R.; Bowen, P.; Millward, G. R.; Jones, W.; Boehm, H. P. *J. Chem. Soc., Faraday Trans.* **1983**, *1*, 1793.

Scholgl, R.; Jones, W. *J. Chim. Physique*, **1984**, *81*, 877.

Scholgl. R. in *Progress in Intercalation Research*, Muller-Warmuth, W; Schollhorn, R., Kluwer Acad Publ., Netherlands, **1993**.

Scholz, W.; Boehm, H.B. *Z. Anorg. Allg. Chem.* **1969**, *369*, 327.

Setton, R. *Synth. Met.* **1988**, *23*, 519.

Shioya, J.; Matsubare, H.; Murakami, S. *Synth. Met.* **1986**, *14*, 1131.

Staudenmaier, L. *Ber. Deut. Chem. Ges.* **1898**, *31*, 1481.

Su, Z.; Coppens, P. *Acta Crys.* **1997**, *A53*, 749.

Suzuki, I. S.; Suzuki, M. *J. Phys. Condens. Matter*. **1991**, *3*, 8825.

Takenaka, H.; Kawaguchi, M.; Lerner, M.; Bartlett, N. *J. Chem. Soc., Chem. Commun.* **1987**, 1431.

Thomas, J.; Millward, G.; Schlogl, R.; Boehm, H. *Mat. Res. Bull.* **1980**, *15*, 671.

Tormin, U.; Beck, F. *Electrochim. Acta*, **1995**, *40*, 1955.

Touzain, P. *Synth. Met.* **1979**, *1*, 3.

Treacy, M. M; Newsam, J. M.; Deem, M. W. *Proc. R. Soc. Lond. A* **1991**, *433*, 499.
Tredgold, R.; Hodge, P. *J. Chem. Soc., Chem. Commun.* **1995**, 1619.

True, J. Ph.D Thesis, 1999.

Turowsky, L.; Seppelt, K. *Inorg. Chem.* **1988**, *27*, 2135.

Ubbelohde, A. *Proc. R. Soc. London A* **1968**, *304*, 25.

Walter, J.; Shioyama, H. *Synth. Met.* **1998**, *92*, 91.

Watanabe, N.; Touhara, H.; Nakajima T.; Bartlett, N.; Mallouk, T.; Selig, H. In *Inorganic Solid Fluorides*, Hagenmuller, P. Ed.; Academic Press: New York, **1985**, (pp331-369) and references contained therein.

Williamson, G.; Hall, W. *Acta Metallurgica* **1953**, *1*, 22.

Winter, M.; Besenhard, J.O.; Spahr, M.E.; Novak, P. *Adv. Mater.* **1998**, *10*, 725.

Yosida, Y.; Sato, K.; Suda, K.; Suematsu, H. *Synth. Met.* **1985**, *12*, 167.

Zabel, H.; Solin, S. Eds. *Graphite Intercalation Compounds I*; Springer-Verlag: Berlin, **1990**.

Zak, Z.; Ruzicka, A. *Z. Kristallogr.* **1998**, *213*, 217.

Zhang, X.; Lerner, M. *Chem. Mater.* **1999**, in press.

Zhang, X.; Sukpirom, N.; Lerner, M.M. *Mater. Res. Bull.* in press.

Zhang, Z.; Lerner, M. *Chem. Mater.* **1996**, *8*, 257.

Zhang, Z.W. *Ph.D Thesis*, Oregon State Univ. **1995**, 11.

Zhang, Z.W.; Lerner, M.M. *J. Electrochem. Soc.* **1993**, *140*, 742.

# Appendices

# Appendix A

Sample DIFFaX Input File for a Solid Solution Structure of 71% 2nd and 29% 3rd Staging $C_xPFOS$.

```
{file name}
INSTRUMENTAL
X-RAY
1.5418
PSEUDO-VOIGT 1.154 0.289 0.025 0.7 TRIM

STRUCTURAL
0.5     0.5     32.953  120
UNKNOWN
2

LAYER 1
none
C       1       0       0       0.220181    5    0.037433
C       2       0       0       0.240046    5    0.037433
C       3       0       0       0.288784    5    0.037433
C       4       0       0       0.311794    5    0.037433
C       5       0       0       0.356576    5    0.037433
C       6       0       0       0.382908    5    0.037433
C       7       0       0       0.423562    5    0.037433
C       8       0       0       0.453449    5    0.037433
F       9       0       0       0.235107    5    0.037433
F       10      0       0       0.233151    5    0.037433
F       11      0       0       0.220371    5    0.037433
F       12      0       0       0.233894    5    0.037433
F       13      0       0       0.308717    5    0.037433
F       14      0       0       0.295079    5    0.037433
F       15      0       0       0.286734    5    0.037433
F       16      0       0       0.317429    5    0.037433
F       17      0       0       0.378047    5    0.037433
F       18      0       0       0.349837    5    0.037433
F       19      0       0       0.357965    5    0.037433
F       20      0       0       0.394214    5    0.037433
F       21      0       0       0.443619    5    0.037433
F       22      0       0       0.412594    5    0.037433
F       23      0       0       0.489596    5    0.037433
F       24      0       0       0.43397     5    0.037433
F       25      0       0       0.466249    5    0.037433
C       26      0       0       0.220181    5    0.016043
C       27      0       0       0.240046    5    0.016043
C       28      0       0       0.288784    5    0.016043
C       29      0       0       0.311794    5    0.016043
C       30      0       0       0.356576    5    0.016043
C       31      0       0       0.382908    5    0.016043
C       32      0       0       0.441033    5    0.016043
C       33      0       0       0.380372    5    0.016043
F       34      0       0       0.235107    5    0.016043
```

| | | | | | | |
|---|---|---|---|---|---|---|
| F | 35 | 0 | 0 | 0.233151 | 5 | 0.016043 |
| F | 36 | 0 | 0 | 0.220371 | 5 | 0.016043 |
| F | 37 | 0 | 0 | 0.233894 | 5 | 0.016043 |
| F | 38 | 0 | 0 | 0.308717 | 5 | 0.016043 |
| F | 39 | 0 | 0 | 0.295079 | 5 | 0.016043 |
| F | 40 | 0 | 0 | 0.286734 | 5 | 0.016043 |
| F | 41 | 0 | 0 | 0.317429 | 5 | 0.016043 |
| F | 42 | 0 | 0 | 0.378047 | 5 | 0.016043 |
| F | 43 | 0 | 0 | 0.349837 | 5 | 0.016043 |
| F | 44 | 0 | 0 | 0.377991 | 5 | 0.016043 |
| F | 45 | 0 | 0 | 0.455749 | 5 | 0.016043 |
| F | 46 | 0 | 0 | 0.458709 | 5 | 0.016043 |
| F | 47 | 0 | 0 | 0.456856 | 5 | 0.016043 |
| F | 48 | 0 | 0 | 0.380474 | 5 | 0.016043 |
| F | 49 | 0 | 0 | 0.405105 | 5 | 0.016043 |
| F | 50 | 0 | 0 | 0.319002 | 5 | 0.016043 |
| C | 51 | 0 | 0 | 0.779819 | 5 | 0.037433 |
| C | 52 | 0 | 0 | 0.759954 | 5 | 0.037433 |
| C | 53 | 0 | 0 | 0.711216 | 5 | 0.037433 |
| C | 54 | 0 | 0 | 0.688206 | 5 | 0.037433 |
| C | 55 | 0 | 0 | 0.643424 | 5 | 0.037433 |
| C | 56 | 0 | 0 | 0.617092 | 5 | 0.037433 |
| C | 57 | 0 | 0 | 0.576438 | 5 | 0.037433 |
| C | 58 | 0 | 0 | 0.546551 | 5 | 0.037433 |
| F | 59 | 0 | 0 | 0.764893 | 5 | 0.037433 |
| F | 60 | 0 | 0 | 0.766849 | 5 | 0.037433 |
| F | 61 | 0 | 0 | 0.779629 | 5 | 0.037433 |
| F | 62 | 0 | 0 | 0.766106 | 5 | 0.037433 |
| F | 63 | 0 | 0 | 0.691283 | 5 | 0.037433 |
| F | 64 | 0 | 0 | 0.704921 | 5 | 0.037433 |
| F | 65 | 0 | 0 | 0.713266 | 5 | 0.037433 |
| F | 66 | 0 | 0 | 0.682571 | 5 | 0.037433 |
| F | 67 | 0 | 0 | 0.621953 | 5 | 0.037433 |
| F | 68 | 0 | 0 | 0.650163 | 5 | 0.037433 |
| F | 69 | 0 | 0 | 0.642035 | 5 | 0.037433 |
| F | 70 | 0 | 0 | 0.605786 | 5 | 0.037433 |
| F | 71 | 0 | 0 | 0.556381 | 5 | 0.037433 |
| F | 72 | 0 | 0 | 0.587406 | 5 | 0.037433 |
| F | 73 | 0 | 0 | 0.510404 | 5 | 0.037433 |
| F | 74 | 0 | 0 | 0.56603 | 5 | 0.037433 |
| F | 75 | 0 | 0 | 0.533751 | 5 | 0.037433 |
| C | 76 | 0 | 0 | 0.779819 | 5 | 0.016043 |
| C | 77 | 0 | 0 | 0.759954 | 5 | 0.016043 |
| C | 78 | 0 | 0 | 0.711216 | 5 | 0.016043 |
| C | 79 | 0 | 0 | 0.688206 | 5 | 0.016043 |
| C | 80 | 0 | 0 | 0.643424 | 5 | 0.016043 |
| C | 81 | 0 | 0 | 0.617092 | 5 | 0.016043 |
| C | 82 | 0 | 0 | 0.558967 | 5 | 0.016043 |
| C | 83 | 0 | 0 | 0.619628 | 5 | 0.016043 |
| F | 84 | 0 | 0 | 0.764893 | 5 | 0.016043 |
| F | 85 | 0 | 0 | 0.766849 | 5 | 0.016043 |
| F | 86 | 0 | 0 | 0.779629 | 5 | 0.016043 |
| F | 87 | 0 | 0 | 0.766106 | 5 | 0.016043 |
| F | 88 | 0 | 0 | 0.691283 | 5 | 0.016043 |
| F | 89 | 0 | 0 | 0.704921 | 5 | 0.016043 |
| F | 90 | 0 | 0 | 0.713266 | 5 | 0.016043 |
| F | 91 | 0 | 0 | 0.682571 | 5 | 0.016043 |

```
F       92      0       0       0.621953    5     0.016043
F       93      0       0       0.650163    5     0.016043
F       94      0       0       0.622009    5     0.016043
F       95      0       0       0.544251    5     0.016043
F       96      0       0       0.541291    5     0.016043
F       97      0       0       0.543144    5     0.016043
F       98      0       0       0.619526    5     0.016043
F       99      0       0       0.594895    5     0.016043
F       100     0       0       0.680998    5     0.016043
S       101     0       0       0.149136    1     0.037433
S       102     0       0       0.149136    1     0.016043
O       103     0       0       0.140032    1     0.160428
O       104     0       0       0.859968    1     0.160428
S       105     0       0       0.850864    1     0.037433
S       106     0       0       0.850864    1     0.016043
C       107     0       0       0.050889    1           1
C       108     0       0       0.949111    1           1
F       109     0       0       0.16516     1     0.29
F       110     0       0       0.83484     1     0.29

LAYER   2
none
C        1      0       0       0.050922    1           1


STACKING
recursive
10

transitions

0.71    0       0       1
0.29    0       0       1

1       0       0       0.101778
0       0       0       0
```

# Appendix B

The xyz coordinates of energy minimum conformation 2′ of $N(CF_3SO_2)_2^-$.

| | | | | |
|---|---|---|---|---|
| 1 | 6 | 2.522322 | -.440517 | .000392 |
| 2 | 16 | 1.200271 | .854787 | -.062703 |
| 3 | 7 | -.001858 | .009921 | -.877350 |
| 4 | 8 | 1.794814 | 1.980065 | -.991938 |
| 5 | 8 | .927953 | 1.243633 | 1.440893 |
| 6 | 16 | -1.194683 | -.847800 | -.062041 |
| 7 | 6 | -2.528455 | .434647 | -.000611 |
| 8 | 8 | -1.778174 | -1.981024 | -.988519 |
| 9 | 8 | -.918344 | -1.230093 | 1.442696 |
| 10 | 9 | -2.041235 | 1.562894 | .523645 |
| 11 | 9 | -3.542830 | -.002442 | .758884 |
| 12 | 9 | -2.982588 | .679188 | -1.233209 |
| 13 | 9 | 3.535284 | -.017905 | .769663 |
| 14 | 9 | 2.982500 | -.681146 | -1.230793 |
| 15 | 9 | 2.021138 | -1.567998 | .513324 |

# Appendix C

The xyz coordinates of energy minimum conformation 2' of $N(CF_3CF_2SO_2)_2^-$.

| | | | | |
|---|---|---|---|---|
| 1 | 6 | -2.492287 | -.360831 | -.380522 |
| 2 | 16 | -1.143101 | -.581583 | .904264 |
| 3 | 7 | -.000046 | -1.424711 | .005083 |
| 4 | 8 | -1.771630 | -1.516715 | 2.002484 |
| 5 | 8 | -.788221 | .893945 | 1.330116 |
| 6 | 16 | 1.143426 | -.588735 | -.900212 |
| 7 | 6 | 2.492186 | -.357888 | .383315 |
| 8 | 8 | 1.772368 | -1.532602 | -1.990703 |
| 9 | 8 | .788762 | .883342 | -1.337977 |
| 10 | 9 | 1.915145 | -.206063 | 1.596137 |
| 11 | 6 | 3.382783 | .824164 | .118947 |
| 12 | 9 | 3.257535 | -1.474654 | .374928 |
| 13 | 6 | -3.383099 | .822984 | -.124858 |
| 14 | 9 | -3.257349 | -1.477694 | -.363462 |
| 15 | 9 | -1.915623 | -.218013 | -1.594611 |
| 16 | 9 | 4.501515 | .723896 | .867691 |
| 17 | 9 | 2.784519 | 1.974407 | .425895 |
| 18 | 9 | 3.754711 | .841108 | -1.168948 |
| 19 | 9 | -2.785334 | 1.970972 | -.441103 |
| 20 | 9 | -3.754298 | .849888 | 1.163076 |
| 21 | 9 | -4.502219 | .716567 | -.872164 |

# Appendix D

The xyz coordinates of energy minimum conformation 2' of $N(CF_3SO_2)(CF_3(CF_2)_3SO_2)^-$.

| | | | | |
|---|---|---|---|---|
| 1 | 6 | -0.600867 | 0.325083 | 0.580833 |
| 2 | 16 | 0.799476 | 1.378606 | -0.106052 |
| 3 | 7 | 2.122371 | 0.692594 | 0.649397 |
| 4 | 8 | 0.553930 | 2.815546 | 0.485834 |
| 5 | 8 | 0.655015 | 1.217601 | -1.664557 |
| 6 | 16 | 2.750675 | -0.805116 | 0.205803 |
| 7 | 6 | 4.448397 | -0.226335 | -0.226672 |
| 8 | 8 | 2.956974 | -1.763942 | 1.437633 |
| 9 | 8 | 2.184027 | -1.449392 | -1.119511 |
| 10 | 9 | 4.378372 | 0.673739 | -1.209651 |
| 11 | 9 | 5.176104 | -1.273589 | -0.644445 |
| 12 | 9 | 5.041219 | 0.314588 | 0.839428 |
| 13 | 9 | -0.926824 | 0.810017 | 1.802898 |
| 14 | 9 | -0.141964 | -0.943262 | 0.697053 |
| 15 | 6 | -1.839670 | 0.321025 | -0.276587 |
| 16 | 9 | -2.081150 | 1.575766 | -0.728392 |
| 17 | 6 | -3.075592 | -0.123772 | 0.494012 |
| 18 | 9 | -1.681646 | -0.526538 | -1.319644 |
| 19 | 6 | -4.168173 | -0.667311 | -0.403616 |
| 20 | 9 | -3.589697 | 0.929049 | 1.172923 |
| 21 | 9 | -2.747658 | -1.110035 | 1.367439 |
| 22 | 9 | -4.354964 | 0.141751 | -1.455046 |
| 23 | 9 | -5.319194 | -0.736434 | 0.286209 |
| 24 | 9 | -3.868502 | -1.894455 | -0.838193 |

# Appendix E

The xyz coordinates of energy minimum conformation $C(CF_3SO_2)_3^-$.

| | | | |
|---|---|---|---|
| 9 | .472503 | 3.273763 | -.954683 |
| 6 | -.133685 | -.102730 | .323902 |
| 16 | -1.440311 | -.017030 | -.823870 |
| 8 | -.314441 | -2.721338 | .317537 |
| 16 | .596269 | -1.640499 | .705971 |
| 6 | -3.007418 | -.316626 | .169989 |
| 8 | 1.616371 | 1.120147 | 1.869483 |
| 8 | -.605742 | 2.280303 | 1.445602 |
| 8 | -1.413941 | -1.107325 | -1.801111 |
| 8 | -1.564250 | 1.374644 | -1.278308 |
| 16 | .475676 | 1.400088 | .993835 |
| 6 | 1.274335 | 2.329698 | -.468558 |
| 8 | 1.219815 | -1.651587 | 2.029604 |
| 6 | 2.041652 | -1.791823 | -.485539 |
| 9 | 1.628044 | -1.711113 | -1.753237 |
| 9 | 2.640413 | -2.979861 | -.303529 |
| 9 | 2.941860 | -.823955 | -.265534 |
| 9 | -4.057432 | -.288971 | -.668773 |
| 9 | -3.172200 | .634880 | 1.091893 |
| 9 | -2.976402 | -1.506202 | .775953 |
| 9 | 1.614116 | 1.485341 | -1.452183 |
| 9 | 2.391549 | 2.921583 | -.016151 |